The Dissertation Committee for Sirirat Kasemset Certifies that this is the approved version of the following dissertation:

Surface Modification of Water Purification Membranes to Improve Fouling Resistance in Oily Water Filtration

Committee:

Benny D. Freeman, Supervisor

Mukul M. Sharma, Co-Supervisor

Donald R. Paul

Isaac C. Sanchez

Christopher J. Ellison

Todd S. Emrick

Surface Modification of Water Purification Membranes to Improve Fouling Resistance in Oily Water Filtration

by

Sirirat Kasemset, B.E.; M.S.E.

Dissertation

Presented to the Faculty of the Graduate School of

The University of Texas at Austin

in Partial Fulfillment

of the Requirements

for the Degree of

Doctor of Philosophy

The University of Texas at Austin

December 2015

Dedication

To my family

Acknowledgements

A completion of research work presented in this dissertation has been enabled by continuous supports from a great number of people and resources. First and most importantly, I would like to express my deep gratitude to Dr. Benny Freeman, my research supervisor, who has been guiding me throughout my Ph.D. research. His in-depth perspective on research work and his excellent graduate mentorship has allowed me to become a more professional researcher over the course of my Ph.D. I have learned and improved tremendously from his teachings, including my critical and analytical skills, presentation and writing skills, as well as working and living ethics. His kindness, generosity, and consideration of his students have set an example for me as a great leader. I need to specifically thank to his extreme patience in teaching me all the important skills to do good research and thank to his belief in me that I can learn, improve, and achieve research work with important contributions. I have always been thankful to his forgiveness to any mistakes or delays I have made unintentionally due to challenges of research work, and I am grateful for opportunities to relearn and stand up to make research progress once again from all lessons learned. I have always recognized his perseverance and dedication to the research, driving me to respect and believe in the values of my research work. His encouragement has always been valuable and appreciated. His devotion and emphasis on the quality of work have driven me to keep learning and improving, and to become more professional. The overall training has equipped me with an idea that "Although perfection is hard to reach, one should always keep learning and improving (and trying)". I am in debt of all learning opportunities for both professional and personal development, having him as my advisor.

I would also like to thank my research co-supervisor, Dr. Mukul Sharma, for his advice throughout my Ph.D., including directions of research work and his broad perspectives beyond a mindset of chemical engineers (i.e., those from research applications in Petroleum Engineering). His advice on pursuing and finishing my Ph.D. as well as his encouragement has always been very helpful. In addition, I would like to acknowledge all continuous supports from my Ph.D. committee members: Dr. Donald Paul, Dr. Isaac Sanchez, Dr. Christopher Ellison, and Dr. Todd Emrick.

I have always been grateful for continuous supports, academically and mentally, from all members in Freeman's research group. I would particularly like to acknowledge unlimited supports and a great teamwork from fouling research team in our group, which includes Dr. Daniel Miller, Albert Lee, Zhengwang (Lisa) He, Lu Wang, and Alon Kirschner. Collaborations and discussions in our fouling team has led to several great ideas and enabled discoveries of new knowledge. I specifically thank Dr. Daniel Miller for his immeasurable kindness and consideration to teach and guide me since I first started my research in this research group until the end of this journey. He has been my mentor and also my role model for his sincerity and devotion to his research work as well as his extreme effort and patience throughout his Ph.D. He has also been a great example of a very patient teacher to me. I will always owe him for his continuous advice and support for both my research and personal development. Several aspects of my research work has been influenced by Zhengwang (Lisa) He. She is one of the smartest and sharpest people I have known, and I learned so much from her, both academic and personal issues. Many good advices for results interpretation, tremendous support on experiments, and continuous encouragement have come from her. Also, Lu's and Alon's great supports will always be memorable. I am also in debt to other colleagues: Dr. Hee Jeung Oh and Dr. Joe Cook for their tremendous encouragement and unconditional

supports throughout my Ph.D. as well as a strong friendship. Others have set great examples for me to become a better researcher and have always kindly given advices, including Dr. Geoff Geise, Dr. Zach Smith, Dr. David Sanders, Dr. Kris Gleason, Dr. Michele Galizia, Dr. Ho Bum Park, and many more. I have always valued supports and friendship from our current group members: Ni Yan, Qiang Liu, Kevin Stevens, as well as former members: Dr. Grant Offord, Dr. Katrina Czenkusch, Dr. Kevin Tung, Dr. Elizabeth Wagner, Dr. Bryan McCloskey, Dr. Victor Kusuma, and all others that I cannot addressed here.

I am grateful for opportunities to attend conferences where I met and discussed with world-class professors and researchers to broaden my perspective on membrane research. They include Dr. Andrew Zydney, Dr. Robert Field, Dr. Anthony Fane, Dr. Pierre Aimar, Dr. Georges Belfort, Dr. William Krantz, Dr. Dibakar Bhattacharyya, Dr. Jeffrey McCutcheon, and many more. I would like to specifically acknowledge Dr. Andrew Zydney and Dr. Robert Field for their insight advices on my UF membrane pore size distribution modelling research work.

I hereby acknowledge financial supports from Gas Technology Institute, Pall Corporation, National Science Foundation, and Center for Layered Polymeric Systems. I would also like to thank Dow Water & Process Solutions for providing RO membranes used in this study. In addition, I highly grateful for the Fulbright scholarship awarded to me as it opened the first door to pursue my graduate studies in Chemical Engineering at UT Austin. With warm friendship and positive thinking from my friends in Chemical Engineering department, including Lynn Li, Nathan Crook, Jie Sun, Sun mi, Kim Jong Suk, and Erwan Chabert, I would like to thank them for their continuous supports and great friendship throughout my Ph.D. time.

I would also like to address my gratitude for a support from my company, Evonik Corporation, which understands challenges in the last phase of Ph.D. and allowed me to start my career while finishing up my Ph.D. work. An understanding and support from my supervisors and colleagues at Evonik has greatly impressed me and motivated me to drive myself for a greater contribution.

Finally, the biggest support and the most important drive for achieving my Ph.D., regardless of any obstacles, are my family and their love. I would like to thank my father and my mother for being such great role models to me for their perseverance, dedication, and honesty to their careers. I am greatly thankful for my father's passion in his work that has set an example for me to stay continuously passionate and motivated about what I chose to work on that is my Ph.D. and good research work. An unconditional encouragement from my sister during difficult times is always recognized, and my brother's perseverance to start again and become better always reminds me to keep learning, improving, sharing, and teaching.

Last but not least, I would like to express my gratitude to my meditation teacher, Suresh Venkumahanti, who continuously teaches me to live a life happily, peacefully, and positively regardless of the situation, as well as setting an example for me to see a reason for living a life that is to make contributions.

Thank you very much for all the people, opportunities, and difficulties I have come across during my Ph.D.

Surface Modification of Water Purification Membranes to Improve Fouling Resistance in Oily Water Filtration

Sirirat Kasemset, Ph.D.

The University of Texas at Austin, 2015

Supervisor: Benny D. Freeman

Co-Supervisor: Mukul M. Sharma

One of the biggest challenges in using water purification membranes is fouling. Surface modification using hydrophilic materials can reduce hydrophobic interactions between membrane surface and hydrophobic foulants, thereby alleviating fouling. In this Ph.D. research, polydopamine (PDA), a highly hydrophilic and universal coating agent, was used to surface-modified reverse osmosis (RO) and ultrafiltration (UF) membranes. PDA modification conditions (e.g., dopamine coating solution concentration, coating time, and pH of coating solution) control PDA deposition and can directly influence the modified membrane properties. Thus, the influence of PDA modification conditions on membrane physical, permeation, selective, and fouling properties were investigated systematically. A fundamental understanding relating the physical and permeation properties and the fouling characteristics of PDA-modified membranes was established.

The RO membranes were modified with PDA at various modification conditions. Permeate fluxes during pure water and oil/water emulsion filtrations were studied. The PDA modification increased the permeate fluxes during oil/water emulsion filtration (thus, improved membrane fouling resistance) relative to unmodified membranes regardless of the initial dopamine concentration or deposition time used. However, these

changes were only observed for the membranes coated under alkaline conditions, suggesting that the PDA did not deposit well under acidic condition.

For UF membranes, molecular weight cutoff (MWCO) and pure water permeance decreased with increasing initial dopamine concentration or deposition time. A permeability and selectivity tradeoff was also observed. Membrane mean pore size and pore size distribution (modeled using log-normal pore size distribution) were investigated via modelling using a hindered solute transport model, Hagen-Poiseuille equation, and a stagnant film model.

The PDA modification increased UF membrane surface hydrophilicity regardless of the coating conditions used, but it did not clearly change surface roughness or zeta potential (i.e., surface charge). Membrane fouling propensity was characterized using threshold flux. Compared to unmodified membranes, the threshold flux increased at minimal PDA coatings, but decreased at excessive PDA coatings. These threshold flux changes were likely governed by a tradeoff between surface hydrophilicity increase and pure water permeance decrease. Excessive PDA coatings resulted in decreased pure water permeance and possibly, pore blockage and pore size reduction, leading to higher local permeate flux causing severe fouling and decreased threshold flux.

Table of Contents

List of Tables

List of Figures

Chapter 1: Introduction

1.1 World Water Resources

Covering over 70% of the Earth's surface, water is an abundant resource. However, with the oceans accounting for 97% of this water, only about 2.5% is fresh water [1, 2]. Since most fresh water is located far below ground or frozen in icecaps and glaciers, less than 1% of the world's water is readily accessible as fresh water for human consumption [2, 3]. In the past century, three major driver contributions to a significant increase in freshwater withdrawals have been: (1) population growth; (2) changing standards of living; and (3) expansion of irrigated agriculture [4]. Freshwater scarcity is a severe problem in many regions of the world, and the number of people living in highly water-stressed areas is predicted to increase throughout the 21st century [1, 5]. According to the World Health Organization (WHO), the world's population is growing by about 80 million people per year and this growth rate will cause freshwater demand increase of about 64 billion cubic meters per year [5]. In addition, 90% of the population growth will occur in developing countries which mostly lack access to clean water [5]. To meet the additional demand for clean water, economical treatment of impaired water sources, such as seawater, brackish water, and produced/flowback water should be considered.

1.2 Water Reuse in Hydraulic Fracturing

With the growth of the oil and gas industry, produced water has emerged as a potential alternative water source in many areas. Produced water is a byproduct of crude oil and natural gas production and typically contains dispersed oils, soluble organics, salts, metals, and treatment chemicals [6, 7]. In 2007, nearly 21 billion barrels of produced water were generated in the U.S. To put this enormous volume of produced water in perspective, it is almost eight times the volume of crude oil produced by onshore

production in the same year [8]. Moreover, hydraulic fracturing, a necessary step in crude oil and natural gas production from unconventional shale formations, requires large amounts of water, typically between 1 and 4 million gallons of water for each well completion [9]. In addition, after hydraulic fracturing, about 10-40% of the injected water returns from the wells to the surface as wastewater, which is called flowback water [10]. From 2005 to 2010, shale gas production grew more than 45% per year in the U.S. [11]. The U.S. natural gas production from unconventional shale formations is forecast to double by 2035, and U.S. unconventional crude oil production will increase by 15% over the next several decades [10]. This rapid growth of oil and gas production from unconventional resources has led to several challenges in water management. The tremendous volumes of water requirement for hydraulic fracturing in arid regions can cause localized water shortage issues [10, 11]. This wastewater is usually considered unfit for municipal use and is reinjected into the ground. However, insufficient disposal wells and significant costs involved are becoming critical issues in some areas [12-14]. Rehabilitation of produced and flowback water for reuse in hydraulic fracturing could potentially contribute to addressing issues regarding water availability and disposal in hydraulic fracturing application [10, 14]. In addition, treated produced water could potentially be beneficially used for municipal, agricultural, and industrial purposes [6, 15].

1.3 Potential Use of Membrane Technology in Produced and Flowback Water Treatment

Primary chemicals that are typically added in hydraulic fracturing fluid include proppants (e.g., sand), friction reducers, biocides, and acids [10, 12]. Thus, flowback water, which is a mixture of injected fluid and brine from natural subsurface formation, contains both organic and inorganic chemicals as well as high concentration of salts [10].

Typical salinity of flowback and produced water ranges from 25,000 to 245,000 (7 times higher than seawater) mg/L, and the total dissolved organic carbon in produced water can be up to 5,500 mg/L [10]. Since some residual chemicals in flowback water can lead to poor productivity of the wells, and certain chemical additives (e.g., friction reducer) needed in the fracturing fluid cannot tolerate high salinity, flowback and produced water needs to be treated to remove some chemical components (especially salts) before reuse in hydraulic fracturing process [10]. Currently, an upper salinity limit that can be compatible with most friction reducers is 25,000 mg/L, although novel salt-tolerant friction reducers have been studied and recently developed [10].

Several pretreatment steps to remove iron, suspended solids, hardness, and bacteria are generally used prior to final salt (e.g., chloride and bromide salts) removal. These pretreatment techniques include filtration (such as filter press) and treatment with chemicals (such as soda/lime softening or sodium sulfate addition) [10, 12]. A common technology used in the final step is thermal distillation/evaporation such as mechanical vapor recompression to remove residual salts [10, 12, 13]. An advantage of this thermal distillation/evaporation is ability to crystallize salts from flowback water at even very high total dissolved solids (TDS) concentration [12, 13]. However, the widely-used thermal distillation/evaporation techniques are energy-intensive, require large footprints, and have large capital costs [13].

Polymer membranes are increasingly used to purify water [16, 17]. For example, membrane-based desalination has become the dominant desalination technology in terms of capacity [18] and is often the most economical choice for brackish and seawater desalination [16, 17, 19]. These membranes can reject very small contaminants, such as hydrated ions, while allowing a high flux of water through them. Their separation ability and relatively low use of energy (around ten percent of that of some thermal methods)

typically makes reverse osmosis (RO) membranes an economical choice over thermal desalination [19]. Typically, ultrafiltration (UF) membranes are used as pretreatment for RO membranes in produced water treatment to remove oil and grease as well as other chemical residuals that potentially severely foul RO membranes. Thus, UF/RO membranes are commonly employed as integrated unit for this application. Although RO membranes are limited to treat water with less than 40,000 mg/L TDS (because much higher hydrostatic pressure is needed for higher TDS levels, and RO becomes economically infeasible), RO membranes are still very promising alternatives for low to medium TDS flowback water treatment [12, 13]. Preliminary costs of flowback/produced water treatment with membrane systems are $2-3.50 per barrel while the costs from vapor compression evaporation are almost twice that of the membrane treatment [20]. Due to separation ability, energy efficiency, and small footprint, which could potentially lead to savings in overall costs of flowback/produced water treatment, membrane technology is well worth studying for hydraulic fracturing water reuse application.

1.4 Membrane Fouling and Polydopamine as a Fouling-Resistant Coating Material

A major barrier to widespread implementation of membrane-based produced water filtration despite feed water pretreatment is fouling [21-24]. Fouling, as shown in Figure 1.1, is the build-up of particulate and colloidal matter, including organics such as oil, on the surfaces and in the pores of the membrane [24, 25]. Produced water contains many particulates and dispersed contaminants not typically found in seawater or brackish water such as emulsified oil. The membrane surfaces in contact with such a mixture can become severely fouled. This fouling hinders the flow of water through the membranes that, in turn, increases operational costs [25].

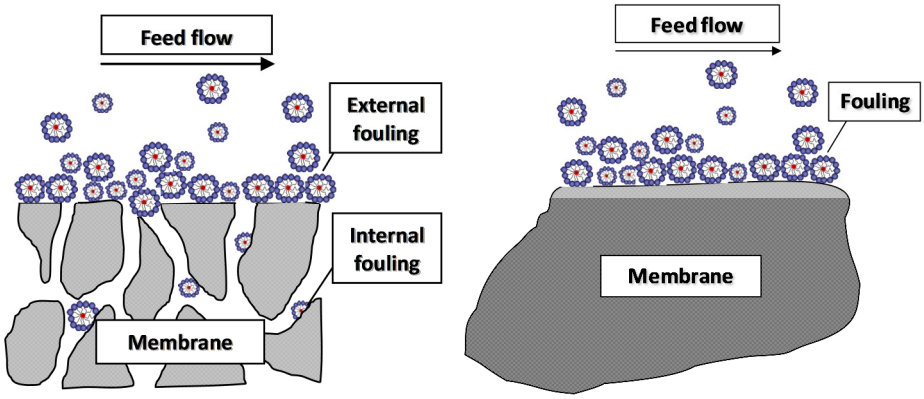

Figure 1.1: Fouling in porous (left) and non-porous (right) water purification membranes.

Surface modification is one approach to improve membrane fouling resistance. Surface characteristics such as hydrophilicity, roughness, and charge have been reported to influence fouling [26]. For hydrophobic foulants (e.g., oil), increased membrane hydrophilicity has been reported to help reduce membrane fouling by limiting surface-foulant hydrophobic interactions [27, 28]. Additionally, smooth membranes are reported to be less susceptible to fouling than rough membranes [29, 30]. Charge-charge interactions with foulants can be minimized on membranes with opposite surface charge to that of the foulants, leading to enhanced electrostatic repulsion and improved fouling behavior [26, 31].

A relatively new approach to improve membrane fouling resistance is surface coating with polydopamine [32-34]. Lee et al. reported that in aerobic, alkaline aqueous solutions, dopamine forms very thin layers of a material known in the literature as polydopamine [35]. The structure of dopamine is shown in Figure 1.2. However, there have been several proposed reaction mechanisms of polydopamine formation and proposed polydopamine structures reported in the literature, and the subject is still currently under active investigation in the field [33, 36-40]. Thin polydopamine coatings

deposit non-selectively from the coating solution onto virtually any surfaces, including polymers used for water purification membranes [35]. The polydopamine layer is hydrophilic [32, 41, 42], and its application decreases surface charge on some polymers [43]. Additionally, a slight reduction in surface roughness on membranes coated with polydopamine has been reported [42, 43]. Therefore, polydopamine is of interest as a fouling resistant membrane surface modification material [32-34].

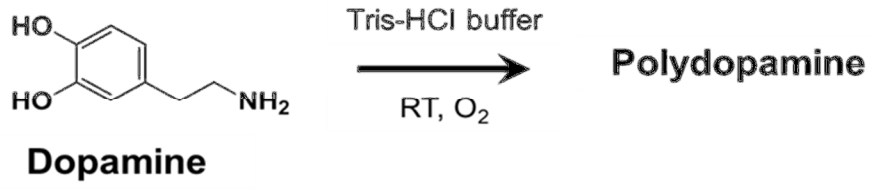

Figure 1.2: Chemical structure of dopamine and its conversion to polydopamine. RT represents room temperature.

1.5 GOALS AND ORGANIZATION OF THE DISSERTATION

Fouling is a critical issue in membrane filtration since foulants, which adsorb either externally (on membrane surfaces) or internally (in membrane pores), reduce membrane permeability and lead to lower membrane filtration productivity and higher operating costs. Currently, membrane processes are an emerging technology for flowback/produced water treatment for water reuse in hydraulic fracturing. However, one of the biggest challenges is membrane fouling. Membrane surface modification by using polydopamine can improve membrane fouling resistance to oil/water emulsions due to its hydrophilicity, which reduces hydrophobic-hydrophobic interactions between oil emulsion and native membrane surfaces, which are mostly hydrophobic. Other advantages of polydopamine include excellent adhesion to a variety of surfaces, ability to form very thin coating layers, and facile modification protocols. Although polydopamine

coating on membranes has been widely studied and characterized to show changes in membrane properties (e.g., surface hydrophilicity, surface roughness, surface charge, permeability, fouling behavior), there is still a lack of fundamental understanding and detailed evidence of the relationship between polydopamine coating properties and membrane performance. In addition, there is a limited number of studies systematically reporting the influence of polydopamine deposition and different modification conditions on fouling resistance properties of membranes used for oily water filtration, especially at constant permeate flux operation mode. A literature review of these topics is presented in Chapter 2. Thus, research described in this dissertation aims to fundamentally explore the influence of changes in membrane properties (e.g., coating thickness, surface hydrophilicity, surface roughness, surface charge, membrane pore size) due to polydopamine modification on changes in performance (i.e., membrane permeability, selectivity, and fouling properties) of ultrafiltration (UF) and reverse osmosis (RO) membranes.

The goals of this dissertation are described as below:

1. To determine the effect of polydopamine modification conditions (i.e., initial dopamine concentration, deposition time, and pH of buffered polydopamine coating solution) on physical, permeation, and oil/water emulsion fouling properties of RO membranes.
2. To compare polydopamine deposition on the surface and inside the pores of UF membranes, and to understand the influence of various polydopamine deposition conditions on pore properties (e.g., mean pore size, pore size distribution, porosity) of UF membranes.
3. To determine the effect of polydopamine deposition conditions on fouling-related UF membrane properties (e.g., surface hydrophilicity, charge, and roughness), and to

understand the influence of polydopamine coatings on membrane threshold flux during oil/water emulsion filtration.

1.6 REFERENCES

[1] T. Oki, S. Kanae, Global hydrological cycles and world water resources, Science 313 (2006) 1068–1072.

[2] S.L. Postel, G.C. Daily, P.R. Ehrlich, Human appropriation of renewable fresh water, Science 271 (1996) 785–788.

[3] P.H. Gleick, The World's Water 2000-2001: The Biennial Report on Freshwater Resources, Island Press, Washington D.C., 2000.

[4] P.H. Gleick, The changing water paradigm: A look at twenty-first century water resources development, Water International 25 127–138.

[5] The United Nations World Water Development Report 3: Water in a Changing World, The United Nations Educational, Scientific, and Cultural Organization (UNESCO), Paris, France, 2009.

[6] J.A. Veil, M.G. Puder, D. Elcock, R.J. Redweik, A White Paper Describing Produced Water from Production of Crude Oil, Natural Gas, and Coal Bed Methane, U.S. Department of Energy: National Energy Technology Laboratory, 2004.

[7] V. Rawn-Schatzinger, D. Arthur, B. Langhus, Coalbed natural gas produced water: Water rights and treatment technologies, GasTIPS 9 (2003) 13–18.

[8] C.E. Clark, J.A. Veil, Produced Water Volumes and Management Practices in the United States, U.S. Department of Energy: Office of Fossil Energy, National Energy Technology Laboratory, 2009.

[9] L.P. Galusky, Fort Worth Basin/Barnett Shale Natural Gas Play: An Assessment of Present and Projected Fresh Water Use, Gas Technology Institute, 2007.

[10] A. Vengosh, R.B. Jackson, N. Warner, T.H. Darrah, A. Kondash, A critical review of the risks to water resources from unconventional shale gas development and hydraulic fracturing in the United States, Environmental Science and Technology 48 (2014) 8334–8348.

[11] The United Nations World Water Development Report Volume 1: Water and Energy, The United Nations Educational, Scientific, and Cultural Organization (UNESCO), Paris, France, 2014.

[12] J.M. Silva, R.M. Gettings, W.L. Kostedt, V.H. Watkins, Produced water from hydrofracturing: Challenges and opportunities for reuse and recovery, in: R.M.

Latanision, C.H. Fletcher (Eds.) The Bridge, Vol. 44, No. 2, National Academy of Engineering, Washington D.C., 2014, pp. 34–40.

[13] K.B. Gregory, R.D. Vidic, D.A. Dzombak, Water management challenges associated with the production of shale gas by hydraulic fracturing, Elements 7 (2011) 181–186.

[14] M.S. Mauter, P.J.J. Alvarez, A. Burton, D.C. Cafaro, W. Chen, K.B. Gregory, G. Jiang, Q. Li, J. Pittock, D. Reible, J.L. Schnoor, Regional variation in water-related impacts of shale gas development and implications for emerging international plays, Environmental Science and Technology 48 (2014) 8298–8306.

[15] K. Guerra, K. Dahm, S. Dundorf, Science and Technology Program Report No. 157: Oil and Gas Produced Water Management and Beneficial Use in the Western United States, U.S. Department of the Interior, Bureau of Reclamation, Denver, CO, 2011.

[16] G.M. Geise, H. Lee, D.J. Miller, B.D. Freeman, J.E. McGrath, D.R. Paul, Water purification by membranes: The role of polymer science, Journal of Polymer Science: Part B: Polymer Physics 48 (2010) 1685–1718.

[17] L.F. Greenlee, D.F. Lawler, B.D. Freeman, B. Marrot, P. Moulin, Reverse osmosis desalination: Water sources, technology, and today's challenges, Water Research 43 (2009) 2317–2348.

[18] Review of the Desalination and Water Purification Technology Roadmap, The National Academies Press, Washington, D.C., 2004.

[19] R.F. Service, Desalination freshens up, Science 313 (2006) 1088–1090.

[20] T.D. Hayes, Barnett and Appalachian Shale Water Management and Reuse Technologies, Gas Technology Institute (GTI) Proposal Number 70100 (Technical Volume), Des Plaines, IL, 2009.

[21] M. Cakmakci, N. Kayaalp, I. Koyuncu, Desalination of produced water from oil production fields by membrane processes, Desalination 222 (2008) 176–186.

[22] C.V. Vedavyasan, Pretreatment trends — an overview, Desalination 203 (2007) 296–299.

[23] F.T. Tao, S. Curtice, R.D. Hobbs, J.L. Sides, J.D. Wieser, C.A. Dyke, D. Tuohey, P.F. Pilger, Reverse osmosis process successfully converts oil field brine into freshwater, Oil and Gas Journal 91 (1993) 88–91.

[24] R.L. Riley, Reverse Osmosis, Membrane Separation Systems — A Research & Development Needs Assessment, Publication Number DOE/ER/30133-H1-Vol. 2, in, Department of Energy, Springfield, VA, 1990, pp. 5(1)–5(53).

[25] R.W. Baker, Membrane Technology and Applications, 2nd ed., John Wiley & Sons Ltd., West Sussex, England, 2004.

[26] J.S. Louie, I. Pinnau, I. Ciobanu, K.P. Ishida, A. Ng, M. Reinhard, Effects of polyether-polyamide block copolymer coating on performance and fouling of reverse osmosis membranes, Journal of Membrane Science 280 (2006) 762–770.

[27] P. Le-Clech, V. Chen, T.A.G. Fane, Fouling in membrane bioreactors used in wastewater treatment, Journal of Membrane Science 284 (2006) 17–53.

[28] J. Gilron, S. Belfer, P. Vaisanen, M. Nystrom, Effects of surface modification on antifouling and performance properties of reverse osmosis membranes, Desalination 140 (2001) 167–179.

[29] E.M. Vrijenhoek, S. Hong, M. Elimelech, Influence of membrane surface properties on initial rate of colloidal fouling of reverse osmosis and nanofiltration membranes, Journal of Membrane Science 188 (2001) 115–128.

[30] M. Elimelech, X. Zhu, A.E. Childress, S. Hong, Role of membrane surface morphology in colloidal fouling of cellulose acetate and composite aromatic polyamide reverse osmosis membranes, Journal of Membrane Science 127 (1997) 101–109.

[31] A.C. Sagle, E.M. Van Wagner, H. Ju, B.D. McCloskey, B.D. Freeman, M.M. Sharma, PEG-coated reverse osmosis membranes: Desalination properties and fouling resistance, Journal of Membrane Science 340 (2009) 92–108.

[32] B.D. McCloskey, H.B. Park, H. Ju, B.W. Rowe, D.J. Miller, B.J. Chun, K. Kin, B.D. Freeman, Influence of polydopamine deposition conditions on pure water flux and foulant adhesion resistance of reverse osmosis, ultrafiltration, and microfiltration membranes, Polymer 51 (2010) 3472–3485.

[33] D.R. Dreyer, D.J. Miller, B.D. Freeman, D.R. Paul, C.W. Bielawski, Elucidating the structure of poly(dopamine), Langmuir 28 (2012) 6428–6435.

[34] B.D. McCloskey, H.B. Park, H. Ju, B.W. Rowe, D.J. Miller, B.D. Freeman, A bioinspired fouling-resistant surface modification for water purification membranes, Journal of Membrane Science 413–414 (2012) 82–90.

[35] H. Lee, S.M. Dellatore, W.M. Miller, P.B. Messersmith, Mussel-inspired surface chemistry for multifunctional coatings, Science 318 (2007) 426–430.

[36] Y. Liu, K. Ai, L. Lu, Polydopamine and its derivative materials: Synthesis and promising applications in energy, environmental, and biomedical fields, Chemical Reviews 114 (2014) 5057–5115.

[37] R.A. Zangmeister, T.A. Morris, M.J. Tarlov, Characterization of polydopamine thin films deposited at short times by autoxidation of dopamine, Langmuir 29 (2013) 8619–8628.

[38] N.F. Della Vecchia, R. Avolio, M. Alfè, M.E. Errico, A. Napolitano, M. d'Ischia, Building-block diversity in polydopamine underpins a multifunctional eumelanin-type platform tunable through a quinone control point, Advanced Functional Materials 23 (2013) 1331–1340.

[39] D.R. Dreyer, D.J. Miller, B.D. Freeman, D.R. Paul, C.W. Bielawski, Perspectives on poly(dopamine), Chemical Science 4 (2013) 3796–3802.

[40] H.W. Kim, B.D. McCloskey, T.H. Choi, C. Lee, M.J. Kim, B.D. Freeman, H.B. Park, Oxygen concentration control of dopamine-induced high uniformity surface coating chemistry, Applied Materials and Interfaces 5 (2013) 233–238.

[41] J. Jiang, L. Zhu, L. Zhu, B. Zhu, Y. Xu, Surface characteristics of a self-polymerized dopamine coating deposited on hydrophobic polymer films, Langmuir 27 (2011) 14180–14187.

[42] Z. Xi, Y. Xu, L. Zhu, Y. Wang, B. Zhu, A facile method of surface modification for hydrophobic polymer membranes based on the adhesive behavior of poly(DOPA) and poly(dopamine), Journal of Membrane Science 327 (2009) 244–253.

[43] B.D. McCloskey, Novel surface modifications and materials for fouling resistant water purification membranes, PhD thesis, University of Texas at Austin, 2009.

Chapter 2: Background and Theory

2.1 Polydopamine for Membrane Surface Modification

2.1.1 Polydopamine Modification to Improve Membrane Fouling Resistance

Recently, polydopamine (PDA) has been widely studied as a membrane surface modification agent to improve membrane properties, such as fouling resistance and wettability. Azari and Zou reported that deposition of a compound structurally related to dopamine, L-dopa, onto reverse osmosis desalination membranes reduced the static adhesion of bovine serum albumin (BSA) to the membrane surface and improved membrane fouling resistance when filtering aqueous solutions containing compounds such as BSA, alginic acid sodium salt, and dodecyltrimethyl ammonium bromide (DTAB) surfactant [1]. Additionally, Arena et al. reported that when polysulfone support membranes of desalination membranes were treated with PDA, the membrane performance in pressure retarded osmosis experiments was improved, possibly due to an increase in wetted porosity of the membranes [2]. Moreover, many studies showed that PDA surface modification could be used to improve fouling resistance to oil/water emulsion for various types of polymeric membranes [3-6].

2.1.2 Influence of Polydopamine Deposition Conditions on Membrane Properties

Many publications reported changes in surface characteristics (e.g., coating thickness, contact angle, charge, roughness, etc.) of different polymers modified with PDA using various dopamine concentrations, deposition times, and coating solution pH values [7-14]. Generally, the PDA film thickness increases with increasing initial dopamine concentration [8, 13-15] or coating time [7, 8, 12-14, 16-19]. Moreover, dopamine polymerization proceeds appreciably under alkaline conditions [15, 16, 20]. Pure water flux, permeance, or hydrodynamic permeability of PDA-modified membranes

is usually lower than that of unmodified membranes [5-7, 19]. It decreases with increasing initial dopamine concentration [6, 19], longer deposition time [5-7, 19], or higher pH value of the buffered coating solution [6, 19]. The decreased pure water flux or permeance (or permeability) is usually attributed to increased PDA coating thickness [7, 19], and membrane pore narrowing or blockage [19].

PDA surface treatment with higher initial dopamine concentration [9, 19] or longer coating time [9, 11, 13, 17, 19] decreases contact angle mainly due to surface hydrophilicity increase. In some studies, the contact angle of PDA-coated surfaces was also reported to be influenced by surface roughness [8, 13]. The surface roughness of PDA-coated films on substrates with flat surfaces has been reported to increase with increasing initial dopamine concentration [15] or PDA deposition time [11, 13, 15, 18]. However, PDA modification may either increase or decrease surface roughness of polymeric porous membranes [9, 10, 19]. The surface roughness change could be influenced by a variation in membrane pore size and porosity [9]. Studies with different membrane types showed that surface charge of PDA-modified membranes could be increased [21] or decreased [10] relative to that of unmodified membranes. Possibly, any changes in surface charge due to PDA modification were also influenced by the surface charge of the underlying membranes.

2.2 Fouling in Porous Membranes

Membrane filtration is a pressure-driven process. Transport of fluid through porous membranes can be modelled by Darcy's law as shown below [22, 23]:

$$J_o = \frac{TMP}{\mu R_m} \tag{2.1}$$

where J_o is the permeate flux (i.e., permeate flow rate/effective filtration area), *TMP* is the transmembrane pressure difference, μ is the permeate viscosity, and R_m is the intrinsic membrane resistance.

Once membranes are exposed to foulants, fouling can occur both externally (on membrane surfaces) or internally (in membrane pores). Fouling mechanisms that are usually considered in fouling model development for porous membranes are: (i) complete pore blocking, (ii) intermediate pore blocking, (iii) standard pore blocking (or so-called pore constriction), and (iv) cake formation [24-26]. As shown in Figure 2.1, these mechanisms are based on the physical phenomena of foulant attachment during fouling [27].

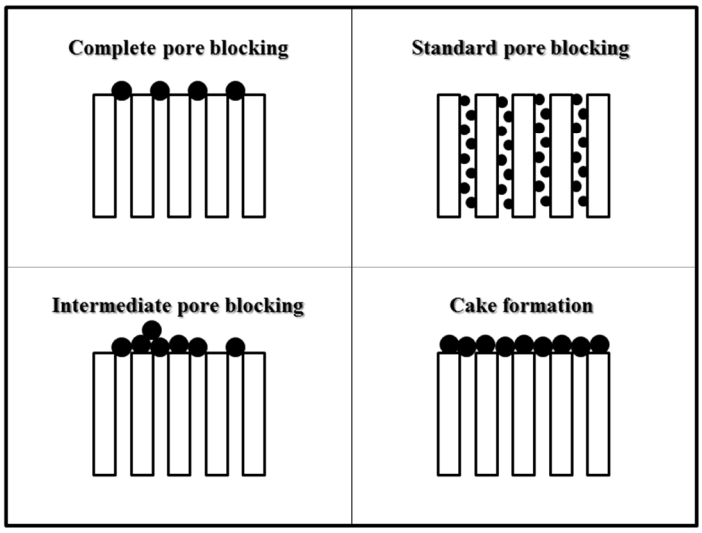

Figure 2.1: Fouling mechanisms on porous membranes [27].

Fouling due to pore blocking is often irreversible due to permanent adsorption inside or on top of membrane pores [22, 28, 29]. On the other hand, fouling due to cake deposition can be either reversible or irreversible process. The reversibility of cake formation depends on the nature of foulant solutions and operating conditions [30]. The resistance-in-series concept can be used with Darcy's law to develop a model describing

the relation between permeate flux and TMP [23]. The flux vs. TMP relationship with resistances based on the fouling mechanisms is shown in Equation (2.2):

$$J = \frac{TMP}{\mu(R_m + R_f)} = \frac{TMP}{\mu(R_m + R_{if} + R_c)} \tag{2.2}$$

where J is the permeate flux during fouling, R_m is the intrinsic membrane resistance (clean membrane resistance), R_f is the resistance due to overall fouling ($R_f = R_{if} + R_c$), R_{if} is the resistance due to internal fouling (pore blocking), and R_c is the resistance due to cake deposition. The flux vs. TMP relationship with resistances based on the reversibility of fouling is shown in Equation (2.3):

$$J = \frac{TMP}{\mu(R_m + R_f)} = \frac{TMP}{\mu(R_m + R_{rev} + R_{irrev})} \tag{2.3}$$

where R_f is the resistance due to overall fouling ($R_f = R_{rev} + R_{irrev}$), R_{rev} is the resistance due to reversible fouling, and R_{irrev} is the resistance due to irreversible fouling. The different fouling criteria used to defined the resistances in Equation (2.2) and (2.3) are typically used to identify fouling stability under constant permeate flux filtration. This fouling reversibility is also related to critical and threshold fluxes, which will be discussed in section 2.4.2.

2.3 Operational Modes of Membrane Filtration

Crossflow membrane filtration experiments are typically operated in one of two modes: (i) constant transmembrane pressure (TMP) or (ii) constant permeate flux [31-33]. While the membranes foul during filtration, total membrane resistance (clean membrane resistance combined with the resistance due to overall fouling), as presented in Equation (2.2) and Equation (2.3), increases. A decrease in permeate flux during constant TMP operation or an increase in TMP during constant permeate flux operation is usually associated with fouling. Advantages of constant TMP operation are a straightforward

experimental setup and its common usage in the literature [31]. In addition, the constant TMP operation allows a determination of steady state flux, which can directly be used for a comparison of fouling behavior among different membranes [34]. However, because permeate flux decreases during fouling, hydrodynamic conditions governing the rate of fouling are usually varied during the constant TMP filtration [33, 35].

Most industrial membrane filtration operates at constant permeate flux, so laboratory fouling tests using constant permeate flux mode are becoming of more interest [30]. Additionally, other advantages of the constant permeate flux filtration include a controllability of hydrodynamic conditions at the membrane. The permeate flux can directly affects the rate of fouling [34]. Thus, the fouling rate can be controlled and does not change during the constant permeate flux filtration tests [33, 35]. Nevertheless, some disadvantages of the constant permeate flux filtration include a complicated experimental setup. A comparison of membrane fouling behavior under constant TMP and constant permeate flux filtration has been discussed elsewhere [31]. For fouling studies reported in this dissertation, a constant TMP operational mode was used for RO membranes due to its straightforward filtration setup. For UF membranes, a constant permeate flux operational mode was used to ensure constant hydrodynamic conditions for a controllable fouling rate during the tests.

2.4 Threshold Flux Concept and Threshold Flux Determination

2.4.1 Influence of Transport Phenomena and Surface Interactions on Fouling

During crossflow filtration, net accumulation of foulant on membranes or the rate of fouling depends on different factors and can be described by Equation (2.4) [34]:

$$N = JC - D\frac{dC}{dy} + p(\zeta) + q(\tau) \tag{2.4}$$

where N is the net flux of foulant towards the membranes, J is the permeate flux, C is the concentration of foulant in feed solution, D is the Brownian diffusion coefficient of foulant in feed solution, y is the vertical axis from membrane surface in membrane boundary layer, $p(\zeta)$ is the flux of foulant due to membrane-foulant surface interactions (ζ represents zeta potential of the membrane), $q(\tau)$ is the flux of foulant due to local hydrodynamics (τ represents shear stress at the membrane surface). Equation (2.4) represents a balance between adding materials to and removing materials away from the membranes. In this equation, the possible settlement of particles due to gravity (for non-buoyant particles) is neglected. Major factors influencing fouling generally include permeate flux, feed concentration, foulant diffusion coefficient, interactions between foulant-foulant and membrane-foulant, and hydrodynamic conditions at the membrane surface (e.g., shear force, fluid turbulence). Some examples of membrane-foulant surface interactions, which are included in the term $p(\zeta)$, are electrostatic attraction/repulsion and hydrophilic/hydrophobic interactions. These interactions are not formally influenced by permeate flux (J). However, if the permeate flux increases foulant concentration at the membrane surface (i.e., higher permeate flux increases degree of concentration polarization), the surface interactions could be indirectly changed by the permeate flux [34]. The membrane-foulant repulsion, which results in a migration of foulant away from the membrane surface, is only efficient when the effect of these surface interactions is in the same order of magnitude as that of the convective flux [34]. An important operating parameter that can directly influence local hydrodynamics, $q(\tau)$, is crossflow velocity, which can be varied by controlling the feed flow rate. Higher crossflow velocity results in higher shear rate and turbulence at the membrane surface and, hence, higher removal rate of foulant from the membranes [23, 36].

In membrane filtration, each of the above factors (i.e., Brownian diffusion, surface interactions, and local hydrodynamics) can have different magnitudes and different levels of influence on fouling. A contribution of each factor to fouling mainly depends on feed solution properties (e.g, foulant type, foulant particle size, and foulant concentration) and membrane types. The membrane types can influence membrane pore size, foulant-membrane surface interactions, foulant transport, fouling mechanisms, etc. The influence of dispersive transport phenomena forces (i.e., $-D\frac{dC}{dy}$, $p(\zeta)$, and $q(\tau)$ terms) presented in Equation (2.4) on fouling can be categorized according to types of foulant and relevant membranes as described below [34]:

1. For large particles (ca. >1 μm) used with microfiltration (MF) membranes, shear-induced diffusion and inertial lift effects ($q(\tau)$) dominate [37, 38], while there is small influence from surface interactions ($p(\zeta)$) and almost no effect of Brownian diffusion ($-D\frac{dC}{dy}$).
2. For small particles (10-100 nm) used with ultrafiltration (UF) membranes, short range inter-particle forces (e.g, electrostatic, Van der Waals forces) dominate [38, 39]. Thus, the influence of surface interactions ($p(\zeta)$) is large, while Brownian diffusion ($-D\frac{dC}{dy}$) and local hydrodynamic conditions ($q(\tau)$) have only small effects.
3. For even smaller macromolecules used with ultrafiltration (UF) membranes and ions/molecules used with nanofiltration (NF) and reverse osmosis (RO) membranes, Brownian diffusion ($-D\frac{dC}{dy}$) has the largest effect, while there is only small influence of surface interactions ($p(\zeta)$) and almost no direct influence of local hydrodynamics ($q(\tau)$) on the removal of molecules. However, local

hydrodynamics such as high crossflow velocity could reduce concentration boundary layer thickness, increase mass transfer coefficient, and improve solvent transport to such membranes overall [28].

2.4.2 Critical Flux, Threshold Flux, and Sustainable Flux Concept

A concept of critical flux was first defined in 1995 by Field et al. [35] and Bacchin et al. [37]. Field et al. defined critical flux as a start-up flux below which a decline of flux (during constant TMP filtration) or a rise in TMP (during constant permeate flux filtration) with time does not occur. Bacchin et al. showed a mass-transfer equation balancing solute transport due to convection, diffusion, and surface interactions, and defined critical flux as a flux below which no fouling occurs. Below the critical flux, the fouling rate is zero [31, 40, 41], and TMP increases linearly with flux (i.e., the membrane resistance is constant and independent of flux) [31, 34, 41-44]. The rate of fouling may be determined from the rate of TMP change with time (i.e., d(TMP)/dt) [34]. The critical flux concept has been developed over years by many researchers since it was first introduced. In 2006, the critical flux definitions were summarized in a review by Bacchin et al. [34]. The critical flux can be divided into two categories [34, 42]:

1. **Critical flux based on net accumulation of foulants on membranes** [34, 42]

   For this criterion, the critical flux is a flux below which there is no accumulation of foulants on membranes (N in Equation (2.4) is equal to zero). This type of critical flux can be divided into two sub-classes:

   1.1 Strong form of critical flux (J_{cs}), which is defined as a flux below which no deposition of foulants due to adsorption or any other type of fouling occurs. The membrane resistance below J_{cs} is equal to that of pure water filtration.

1.2 Weak form of critical flux (J_{cw}), which is defined as a flux below which only deposition of foulants due to adsorption occurs without any other type of fouling. The membrane resistance below J_{cw} is equal to the resistance of membrane exposed to only adsorption of foulants.

2. Critical flux based on reversibility of fouling

This definition of critical flux is termed as critical flux for irreversibility (J_{ci}). Below J_{ci}, foulants deposited on membranes are dispersed, and the fouling can be reversible. Above J_{ci}, foulants become aggregates, and the fouling is irreversible. Thus, J_{ci} is a borderline between phase transition of foulants at a critical concentration in membrane concentration boundary layer, and this concentration can be influenced by filtration flux.

Membrane operation at zero rate of fouling (i.e., below the critical flux) is rarely a realistic possibility [43, 45, 46]. However, a permeate flux below which the rate of fouling is low, but not zero, and stable is often observed. In 2011, the definition of critical flux was revised slightly, and a new concept of threshold flux was introduced [42]. The threshold flux is the flux that separates the low-fouling, stable operating regime from the high-fouling, unstable operating regime [42]. The threshold flux has been referred to as the critical flux in some earlier studies [40, 43, 45, 47, 48]. Below the threshold flux, low and near constant rate of fouling occurs, and stable membrane operation can be achieved. Above the threshold flux, the rate of fouling increases markedly, and rapid fouling occurs during membrane operation. Another definition of threshold flux is based on a dependency of fouling on permeate flux [42, 44]. Below this flux, fouling occurs irrespective of the permeate flux, while above this flux, the fouling is influenced by the permeate flux. Many membranes foul as soon as they are exposed to foulants even at very low permeate flux [42, 43, 49]. Also, industrial membrane filtration is often operated

near, but below, the highest permeate flux that results in low and acceptable fouling rates so that the operation is most economical [42]. Thus, the threshold flux may be a more useful benchmark for practical membrane operation than critical flux. Similarities and differences between critical and threshold fluxes have been discussed in several publications [31, 42, 44]. A higher threshold flux allows a membrane to operate at a higher capacity (i.e., higher permeate throughput) at a low fouling rate and may prolong the operational time between cleaning steps [42], potentially resulting in long-term capital and operating cost savings.

The threshold flux can be useful for industrial membrane operation because industry generally seeks operating conditions where permeate flux can be sustainable (i.e., filtration without severe fouling) [34, 42]. However, actual membrane design usually takes economic factors into account, and the operation is run at an economically acceptable rate of fouling. The flux at which an actual membrane operation can be run economically and sustainably is defined as the sustainable flux [34, 42]. Since industry typically applies membrane cleaning periodically (when the fouling rate reaches acceptable upper limit), low fouling rate helps reduce operating cost due to longer filtration time during the required cleaning and less frequency of cleaning overall [42].

2.4.3 Threshold Flux Determination

Threshold flux can be determined using the flux stepping method under constant permeate flux filtration [4, 40, 43, 45]. As shown in Figure 2.2, during the flux stepping test, the TMP across the membrane is measured at each constant flux, and the flux is increased incrementally after being held constant for a certain period of time [4]. Three parameters used to estimate threshold flux are: (i) average TMP (TMP_{avg}), (ii) rate of TMP increase (dTMP/dt), and (iii) initial TMP increase (ΔTMP) [43, 45]. Figure 2.3

presents these three parameters used for threshold flux determination from the flux stepping method [43].

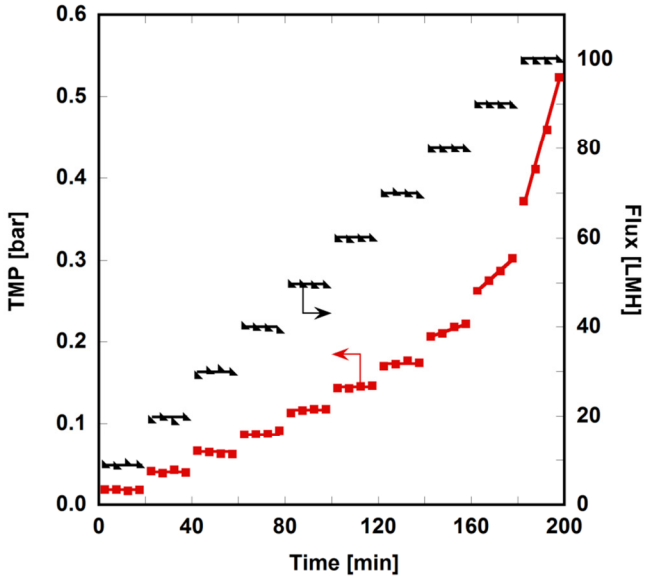

Figure 2.2: TMP vs. permeate flux profile during flux stepping test for threshold flux determination [4].

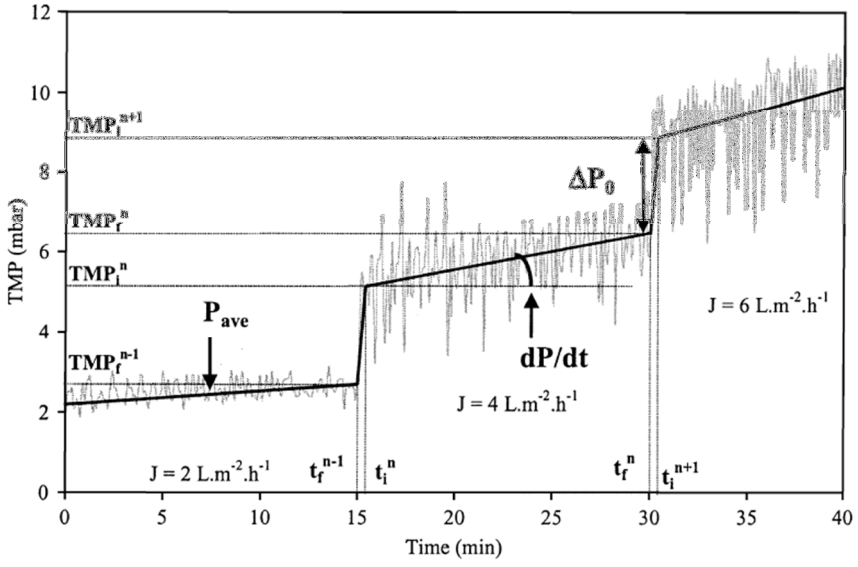

Figure 2.3: Three parameters used for threshold flux determination from the flux stepping method: P_{ave} (i.e., TMP_{avg}), dP/dt (i.e., dTMP/dt), and ΔP_o (i.e., ΔTMP) [43].

By using the TMP_{avg} parameter, the average TMP from each flux step is plotted against permeate flux as shown in Figure 2.4. The threshold flux is identified as the flux where the linearity of the TMP_{avg} vs. flux curve breaks [31, 34, 40, 42, 44]. Below the threshold flux, the TMP increases linearly with flux, and total membrane resistance (R_{total} = TMP/flux) is constant. Above the threshold flux, the TMP no longer increases linearly with flux, and R_{total} increases as flux increases (i.e., R_{total} becomes flux-dependent) [42, 44]. Although the threshold flux determination using TMP_{avg} parameter is often used, very small number of studies actually reported the criteria (e.g., coefficient of determination, R^2) used to generate the linear regression line below the threshold flux. In a few studies, values of the R^2 coefficient of linear regression higher than 0.99 [44] or 0.998 [50] were used to establish the best fit straight line through flux points below the threshold flux. However, in most cases, the linear trend of the TMP_{avg} vs. flux was established from visual observation, which could result in variations in the estimated threshold flux value.

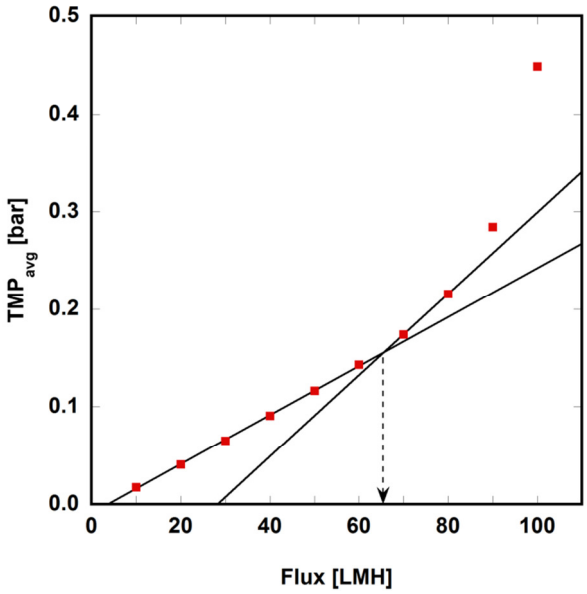

Figure 2.4: Threshold flux determination using TMP_{avg} parameter from the flux stepping method [4].

When the dTMP/dt parameter is used, the dTMP/dt determined from the slope of the linear regression line of the TMP data during each flux step is plotted versus permeate flux as shown in Figure 2.5. The threshold flux can be identified as the flux where d(TMP)/dt increases markedly relative to d(TMP)/dt values at lower fluxes [34, 40, 42, 43, 45]. This method directly monitors an increase in fouling rate at the threshold flux. Some researchers arbitrarily identified the sudden dTMP/dt increase by observing the trend in dTMP/dt vs. permeate flux plot [45]. Other studies chose an arbitrary d(TMP)/dt threshold, where the rate of fouling changed from a low and stable region to a region of markedly increased fouling rate, to determine the threshold flux [40, 43, 45]. The appropriate d(TMP)/dt limit used for the threshold flux determination usually varies according to types of membranes, model foulants, and operating conditions such as crossflow velocity. For example, Le Clech et al. used a d(TMP)/dt threshold of 0.1 mbar/min to determine threshold fluxes during synthetic and real sewage filtration [43].

In their study, threshold fluxes determined using this d(TMP/dt) threshold were almost identical to the threshold fluxes visually identified from the fouling rate increase in the d(TMP)/dt vs. flux curves. Beier and Jonsson defined a threshold for acceptable fouling rate as 1.1 Pa/s (40 mbar/h or 0.67 mbar/min) in their studies of membrane fouling by suspensions of baker yeast cells. This d(TMP)/dt threshold corresponded to a shift from slow to rapid fouling, so it was used to determine the threshold flux [45]. Choi and Dempsey used statistical analyses (i.e., F-test and T-test) to identify the d(TMP)/dt threshold above which the rate of fouling was non-zero or d(TMP)/dt significantly deviated from values at lower fluxes [40]. They identified the d(TMP)/dt threshold as 0.024 psi/min (1.66 mbar/min) for the threshold flux determination during synthetic natural water (i.e., river, spring, or reservoir water) filtration. Although the d(TMP)/dt threshold is commonly used and provides a straightforward approach to identify the threshold flux, this criterion is somewhat subjective and can vary from one filtration setup (i.e., a particular membrane type, model foulant, or operating condition) to another [40].

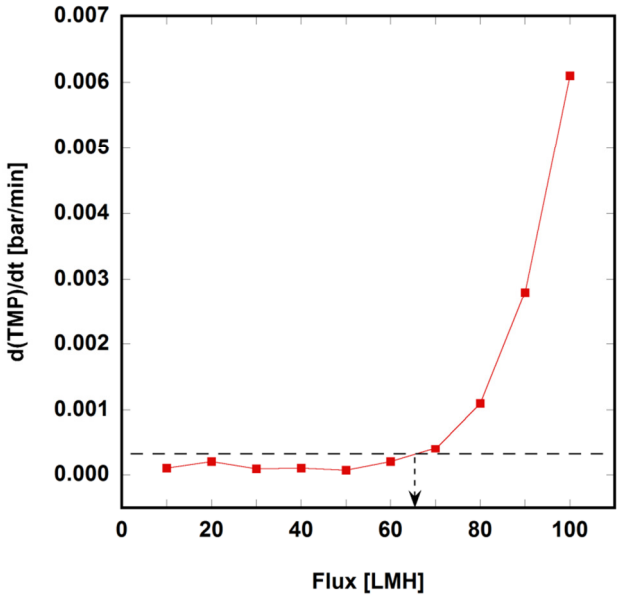

Figure 2.5: Threshold flux determination using dTMP/dt parameter from the flux stepping method [4].

The threshold flux may also be determined by plotting the TMP increase during each flux step (ΔTMP) against the flux [4, 43, 45]. This ΔTMP is calculated from the difference between the final TMP of one flux step and the initial TMP of the following flux step. The threshold flux is identified as the flux where a substantial increase in ΔTMP value (or its standard deviation) is observed. However, Beier and Jonsson reported large uncertainties in the ΔTMP values as permeate flux was increased in their study, so an exact threshold flux could not be identified by this method [45]. From flux stepping tests, the TMP_{avg} and d(TMP)/dt parameters are more commonly used in the literature and appear to produce more robust threshold flux values than ΔTMP. For this reason, the TMP_{avg} and d(TMP)/dt parameters were mainly used to estimate the membrane threshold flux in all studies presented in this dissertation.

2.4.4 Factors Influencing Threshold Flux

There are several factors that can influence threshold flux. These factors can be categorized into: (i) feed solution characteristics, (ii) membrane properties, and (iii) hydrodynamic conditions at the membrane surface [34, 40, 47, 48].

(i) Feed solution characteristics

The threshold flux has been observed to increase with increasing feed particle size [30, 34, 35, 38] and decreasing feed concentration [34, 38, 40].

(ii) Membrane properties

The threshold flux tends to be higher when the membrane surface hydrophilicity [38, 44, 51] or surface charge [30, 38, 48] leads to weaker or more repulsive membrane-foulant interactions. In addition, the threshold flux was reported to increase with increasing membrane porosity [34, 38]. The threshold flux can also be influenced by membrane pore size. Conflicting trends in the effect of membrane pore size on threshold flux have been reported [30, 41, 47, 52, 53]. A decrease in membrane pore size can lead to higher local permeate flux [54] and a threshold flux decrease [48]. In contrast, Wu et al. observed that the threshold flux decreased with increasing membrane molecular weight cut off (or pore size) [52]. However, in this latter study, they claimed that charge effects or changes in local porosity might also influence the threshold flux, so their observed effect of pore size on the threshold flux may not be conclusive. Such variations in the effect of membrane pore size on threshold flux may also be due to different foulant sizes relative to membrane pore sizes used in each study.

(iii) Hydrodynamic conditions at the membrane surface

The threshold flux has been observed to increase with higher shear forces on the membrane surface [34, 38] or higher crossflow velocity during membrane filtration [30, 34, 38, 40].

2.4.5 Local Permeate Flux and Its Influence on Threshold Flux

In constant permeate flux filtration, several studies report an abrupt TMP increase during long-term filtration experiments below the threshold flux of a clean membrane [43, 46, 54-56]. Foulants accumulated during filtration below the threshold flux gradually reduce the permeable porous area of the membrane by pore blocking. Consequently, local permeate velocity or flux through the remaining open pores increases because overall, global permeate flux is held constant [46, 54]. This increase in local flux through the membrane pores results in more severe fouling and a threshold flux decrease, which could result in a sudden TMP increase observed during these long-term filtrations. Ognier et al. reported that smaller pore size can result in higher local permeate flux which would locally modify the balance between accumulation and back transport of materials to and from the membrane surface, thereby decreasing the threshold flux [54]. Similarly, any pore size reduction or pore blockage (or membrane hydraulic resistance increase) due to membrane surface modification may lead to higher local permeate flux and, in turn, increase fouling propensity [4].

2.5 HYDRODYNAMIC MODELS OF SOLUTE AND SOLVENT TRANSPORT THROUGH POROUS MEMBRANES

2.5.1 Membrane Hydraulic Permeability

Hydraulic permeability of porous membranes is often based on idealized models assuming fluid flow through cylindrical pores using the Hagen-Poiseuille equation. The

average hydraulic permeability, based on a distribution of cylindrical pores with varying pore sizes, is [57, 58]:

$$\overline{L}_p = \frac{\varepsilon}{8\mu\delta_m} \frac{\int_0^\infty n(r) r^4 dr}{\int_0^\infty n(r) r^2 dr} \tag{2.5}$$

where $\overline{L}_p$ is the average membrane hydraulic permeability, ε is the membrane porosity, μ is the solvent viscosity (water in this study, so $\mu \approx 9\times10^{-4}$ kg/(m·s) at 25°C [59]), δ_m is the membrane selective layer thickness, r is the membrane pore radius, and $n(r)$ describes the pore size distribution. The factor ε/δ_m should also be viewed as accounting for any deviation of pores from straight cylinders (i.e., tortuosity effects).

In our study, the average membrane hydraulic permeability, $\overline{L}_p$, is the pure water permeance and can be calculated from experimental data as follows:

$$\overline{L}_p = \frac{\overline{J}_{pw}}{TMP_n} \tag{2.6}$$

where $\overline{J}_{pw}$ is the average steady state pure water flux (i.e., pure water volumetric flow rate per unit area), and TMP_n is the nominal measured transmembrane pressure during pure water filtration, which represents the average transmembrane pressure seen by the membrane filtration area.

A log-normal pore size distribution is often used for UF membranes [57, 60]:

$$n(r) = \frac{n_o}{r} \times \frac{1}{\sqrt{2\pi\, ln(1+(\sigma/\overline{r})^2)}} \times exp\left\{ -\left[ln(r/\overline{r}) \right]^2 \times \left[\frac{1+(\sigma/\overline{r})^2}{2ln[1+(\sigma/\overline{r})^2]} \right] \right\} \tag{2.7}$$

where $n(r)$ is the number of pores of radius r per unit area, n_o is the total number of pores per unit area, $\overline{r}$ is the mean pore size, and σ is the standard deviation of the log-normal distribution. In subsequent calculations involving Equation (2.5), n_o always appears in both the numerator and denominator, so it cancels. Based on this model, $\overline{L}_p$ depends on three parameters: $\overline{r}$, $\sigma/\overline{r}$, and ε/δ_m. However, these parameters cannot be determined

directly from Equation (2.5) using only pure water permeance data. Using the log-normal pore size distribution and the measured hydraulic permeability (i.e., pure water permeance), the ratio of porosity to selective layer thickness, ε/δ_m, may be calculated from the following rearranged form of Equation (2.5) if $\bar{r}$ and σ are known:

$$\frac{\varepsilon}{\delta_m} = 8\mu\bar{L}_p \frac{\int_0^\infty n(r)r^2 dr}{\int_0^\infty n(r)r^4 dr} = 8\mu\bar{L}_p \left(\frac{\left(1+(\sigma/\bar{r})^2\right)^{-\frac{6}{1+(\sigma/\bar{r})^2}}}{\bar{r}^2} \right) \tag{2.8}$$

Other models, including a model for hindered solute transport through membrane pores and a concentration polarization model, are used with Equation (2.8) and experimental water and solute transport data to estimate values of $\bar{r}$, $\sigma/\bar{r}$, and ε/δ_m.

2.5.2 Solute Mass Transport Near and Through Porous Membranes

As shown in Figure 2.6(a), during ultrafiltration in a stirred cell, solutes in the feed solution either partially or completely rejected by the membrane accumulate at the membrane surface forming a concentration boundary layer where the solute concentration is higher than that in the bulk feed solution [61]. The concentration boundary layer thickness, $\delta_c(r_c)$, depends on radial position in the stirred cell and develops from the outer edge towards the central axis of the stirred cell [62]. From a mass balance based on convective and diffusive solute transport in the concentration boundary layer, the mass transfer coefficient, k, relates permeate flux, J_v, and solute concentration driving force as follows [61]:

$$J_v = k \ln\left(\frac{C_m - C_f}{C_b - C_f} \right) \tag{2.9}$$

Generally, the permeate flux is proportional to the transmembrane pressure, TMP, across the membrane. In a stirred cell, the feed pressure at the membrane surface, $P_{feed}(r_c)$, can vary radially in the stirred cell, as shown in Figure 2.6(b), due to fluid

rotation. In a laboratory MWCO measurement, an overhead stirrer, operating at a rotation rate of ω, causes the fluid to rotate. Thus, the permeate flux, $J_v(r_c)$, may vary radially. As solutes transport from the bulk feed solution to the permeate, they pass through the concentration boundary layer and then the membrane pores. The solute transport mechanism through each of these resistances (i.e., concentration boundary layer and membrane pores) can be described using different models containing $\bar{r}$, $\sigma/\bar{r}$, and ε/δ_m. In this study, these models are used together with the Hagen-Poiseuille equation (i.e., Equation (2.8)) and experimental pure water permeance and solute sieving data to estimate values of $\bar{r}$, $\sigma/\bar{r}$, and ε/δ_m as a function of membrane modification conditions.

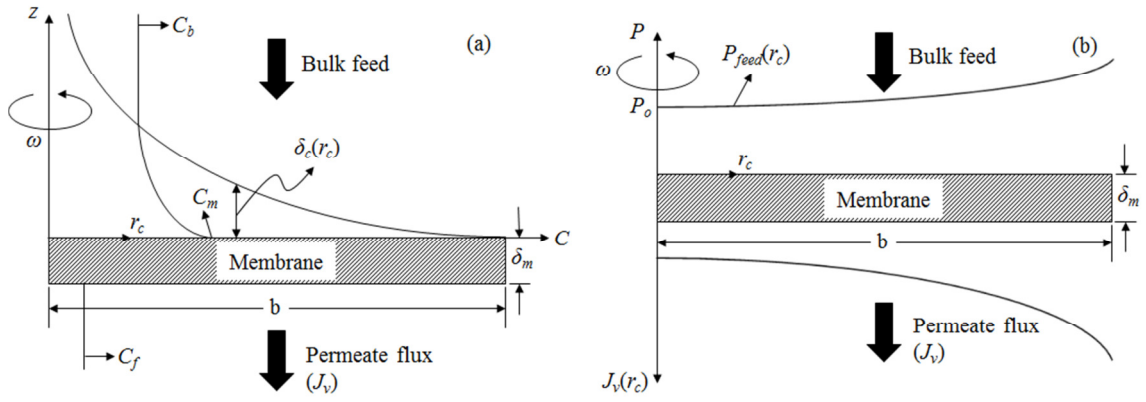

Figure 2.6: (a) Concentration and concentration boundary layer thickness profiles of partially or completely rejected solutes during ultrafiltration in a stirred cell. z represents the vertical distance from the membrane surface, r_c represents the radial distance from the center of the stirred cell, $\delta_c(r_c)$ is the concentration boundary layer thickness, δ_m is the membrane selective layer thickness, b is the membrane radius, C_f is the filtrate solute concentration, C_b is the bulk feed solute concentration, and C_m is the solute concentration on the feed side of the membrane surface. ω is the stirring speed in the stirred cell. (b) Radial dependence of feed pressure ($P_{feed}(r_c)$) and permeate flux ($J_v(r_c)$) in the stirred cell. P_o is the feed pressure at the central axis of the stirred cell at the membrane surface. The filtrate feed pressure is P_f, which is assumed to be independent of r_c. The local transmembrane pressure, $TMP_{local}(r_c)$, is defined as $P_{feed}(r_c)$-P_f.

2.5.2.1 Concentration Polarization

Solute transport through porous membranes is often described in terms of an actual sieving coefficient, S_a, or an actual retention coefficient, R_a. S_a is the ratio of C_f to C_m, and S_a is related to R_a as follows [61, 63]:

$$S_a = 1 - R_a = \left(\frac{C_f}{C_m} \right) \tag{2.10}$$

Since solute concentration in the boundary layer is higher than in the bulk feed, concentration polarization causes the actual sieving coefficient to be lower than the observed sieving coefficient [61, 63]. The observed sieving coefficient, S_o, and observed retention coefficient, R_o, are defined based on measurable, bulk solute concentrations in the bulk feed and filtrate, C_b and C_f, as follows [61, 64]:

$$S_o = 1 - R_o = \left(\frac{C_f}{C_b} \right) \tag{2.11}$$

The observed sieving coefficient is measured in solute filtration experiments. However, the actual sieving coefficient cannot be measured directly because the solute concentration at the membrane surface (i.e., C_m) is not known. A mass transfer model, developed based on Equations (2.9) – (2.11), is typically employed to relate S_a to S_o. The stagnant film model for this purpose is [61, 63]:

$$S_o = \frac{S_a}{(1 - S_a) \exp\left(-\frac{\overline{J}_v}{\overline{k}} \right) + S_a} \tag{2.12}$$

where $\overline{J}_V$ is the measured average permeate flux, and $\overline{k}$ is the average mass transfer coefficient in the concentration boundary layer. A mass transfer coefficient model, presented later, is used to calculate $\overline{k}$. Alternatively, S_a in Equation (2.12) can be estimated using a hindered solute transport model as discussed in the next section. This model can be used to calculate S_a and, in turn, S_o, which can then be compared with experimental values of S_o.

2.5.2.2 Solute Transport through Porous Membranes

Solute transport through a membrane occurs due to both convection and diffusion. A hydrodynamic model describing solute transport through porous membranes based on hindered convection and diffusion was reported by Opong and Zydney [63]. This model calculates S_a as a function of the ratio of solute size to membrane pore size and the hydrodynamic conditions of solute transport, which are characterized by the Peclet number inside the membrane pores, Pe_m. The actual sieving coefficient of a membrane of pore radius r and a solute of radius a at radial position r_c in the stirred cell, $S_a(r, a, r_c)$, is given by the following expression [61-63]:

$$S_a(r, a, r_c) = \frac{S_\infty(r, a)\exp[Pe_m(r, a, r_c)]}{S_\infty(r, a) + \exp[Pe_m(r, a, r_c)] - 1} \tag{2.13}$$

where $S_\infty(r, a)$ is the so-called asymptotic sieving coefficient, and $Pe_m(r, a, r_c)$ is the Peclet number in a pore of radius r. Pe_m depends sensitively on permeate flux, solute diffusivity, and membrane properties (i.e., ε/δ_m). Pe_m is given by [62, 63]:

$$Pe_m(r, a, r_c) = \left(\frac{S_\infty(r, a)}{\phi(r, a)K_d(r, a)}\right)\left(\frac{J_v(r_c)\delta_m}{D_\infty\varepsilon}\right) = \left(\frac{K_c(r, a)}{K_d(r, a)}\right)\left(\frac{J_v(r_c)\delta_m}{D_\infty\varepsilon}\right) \tag{2.14}$$

where $\phi(r, a)$ is the equilibrium partition coefficient of the solute between the fluid in the membrane pore and the fluid adjacent to the membrane. D_∞ is the solute diffusion coefficient at infinite dilute solution. For poly(ethylene glycol) (PEG) in water at 25°C, D_∞ is calculated as follows [65, 66]:

$$D_\infty = 1.465\times10^{-8}\left(M^{-0.557}\right) \tag{2.15}$$

where D_∞ has units of m^2/s, and M is the PEG molecular weight (as specified by the manufacturer) in g/mol.

$K_c(r, a)$ and $K_d(r, a)$ are hindrance factors for solute convection and diffusion, respectively, and they depend on the ratio of solute radius to membrane pore radius [63]. Algebraic expressions for them are given below [61, 63]:

$$K_c(r,\ a) = \frac{(2-\phi(r,\ a))K_s(r,\ a)}{2K_t(r,\ a)} \tag{2.16}$$

$$K_d(r,\ a) = \frac{6\pi}{K_t(r,\ a)} \tag{2.17}$$

$$K_s(r,\ a) = \frac{9}{4}\pi^2\sqrt{2}\left(1-\left(\frac{a}{r}\right)\right)^{-5/2}\left[1+\frac{7}{60}\left(1-\left(\frac{a}{r}\right)\right)-\frac{2227}{50400}\left(1-\left(\frac{a}{r}\right)\right)^2\right]+ \\ 4.0180-3.9788\left(\frac{a}{r}\right)-1.9215\left(\frac{a}{r}\right)^2+4.392\left(\frac{a}{r}\right)^3+5.006\left(\frac{a}{r}\right)^4 \tag{2.18}$$

$$K_t(r,\ a) = \frac{9}{4}\pi^2\sqrt{2}\left(1-\left(\frac{a}{r}\right)\right)^{-5/2}\left[1-\frac{73}{60}\left(1-\left(\frac{a}{r}\right)\right)+\frac{77293}{50400}\left(1-\left(\frac{a}{r}\right)\right)^2\right]- \\ 22.5083-5.6117\left(\frac{a}{r}\right)-0.3363\left(\frac{a}{r}\right)^2-1.216\left(\frac{a}{r}\right)^3+1.647\left(\frac{a}{r}\right)^4 \tag{2.19}$$

The asymptotic sieving coefficient, $S_\infty(r, a)$, is S_a at very large permeate flux values [62] and can be calculated from Equation (2.20):

$$S_\infty(r,\ a) = \phi(r,\ a)K_c(r,\ a) \tag{2.20}$$

For a spherical solute in a cylindrical pore, $\phi(r, a)$ is given by [62, 63]:

$$\phi(r,\ a) = \left[1-\left(\frac{a}{r}\right)\right]^2 \tag{2.21}$$

where r is the membrane pore radius. a is the solute radius, which can be estimated from Stokes radius of the solute. The Stokes radius of PEG can be estimated as follows [33]:

$$a = 16.73\times10^{-12}M^{0.557} \tag{2.22}$$

where a is the Stokes radius of PEG (m), and M is the PEG molecular weight (as specified by the manufacturer) (g/mol).

In Equation (2.14), the membrane porosity to thickness ratio, ε/δ_m, can be set as a constant [57] or estimated from the rearranged form of the Hagen-Poiseuille equation, Equation (2.8). Equation (2.8) can be combined with Equation (2.14) to yield:

$$Pe_m(r, a, r_c) = \left(\frac{K_c(r, a)}{K_d(r, a)}\right)\left(\frac{J_v(r_c)}{D_\infty}\right)\left[\frac{1}{8\mu\bar{L}_p}\left(\frac{\bar{r}^2}{\left(1+(\sigma/\bar{r})^2\right)^{-\frac{6}{1+(\sigma/\bar{r})^2}}}\right)\right] \tag{2.23}$$

In some cases (e.g., large diameter membrane test cells), permeate flux could vary with radial position in the stirred cell due to the radial pressure gradient which naturally develops due to the fluid rotation as depicted in Figure 2.6(b). In this case, the local permeate flux would be given by [67]:

$$J_v(r_c) = \bar{L}_p \times TMP_{local}(r_c) = \bar{L}_p \times [P_{feed}(r_c) - P_f] = \bar{L}_p \times [P_o + \frac{1}{2}\rho\omega^2 r_c^2 - P_f] \tag{2.24}$$

where $TMP_{local}(r_c)$ is the local transmembrane pressure at a particular radial position r_c in the stirred cell. $P_{feed}(r_c)$ is the applied feed pressure at radial position r_c at the membrane surface, P_o is the applied feed pressure at the central axis (i.e., $r_c = 0$) at the membrane surface, and P_f is the filtrate pressure. ω is the stirring speed (radians/s). P_o-P_f is constant during the filtration. In the MWCO experiments, the average permeate flux, $\bar{J}_v$, is fixed in the experiments. Since P_o is not measured directly from the experiments, the value of P_o-P_f is determined from average permeate flux, $\bar{J}_v$, measured during a solute filtration experiment:

$$\bar{J}_v = \frac{\int J_v(r_c)dA}{\int dA} = \bar{L}_p \times \left[(P_o - P_f) + \frac{1}{4}\rho\omega^2 b^2\right] \tag{2.25}$$

where A is the effective membrane filtration area. Combining Equations (2.24) and (2.25) and eliminating P_o-P_f yields:

$$J_v(r_c) = \bar{J}_v + \left[\frac{1}{4}\bar{L}_p\rho\omega^2 \times \left(2r_c^2 - b^2\right)\right] \tag{2.26}$$

In this study, membrane pure water permeance, determined experimentally, was used for $\overline{L}_p$. In many cases, the variation of permeate flux with radial position is very minor even in rather large diameter laboratory test cells. When the dependence of J_v on r_c is not important, $\overline{J}_v$ can be used instead of $J_v(r_c)$ in Equation (2.14) to calculate Pe_m once the remaining parameters in Equation (2.14) (r, a, D_∞, and ε/δ_m) are established. Then, $S_a(r, a)$ can be calculated using Equation (2.13).

The average actual sieving coefficient for a solute of radius a at radial position r_c in the stirred cell, $\overline{S}_a(a, r_c)$, is calculated by summing the contributions to S_a from all pores in the membrane that are capable of permeating the solute of interest (i.e., all pores whose radius, r, is greater than the solute particle radius, a) [57, 62]:

$$\overline{S}_a(a, r_c) = \frac{\int_a^\infty S_a(r, a, r_c) n(r) r^4 dr}{\int_0^\infty n(r) r^4 dr} \tag{2.27}$$

If permeate flux does not vary significantly with radial position, $\overline{S}_a$ only depends on a (i.e., $\overline{S}_a(a, r_c)$ becomes $\overline{S}_a(a)$). In this case, S_o can be estimated by substituting this $\overline{S}_a(a)$ for S_a in Equation (2.12).

2.5.2.3 Mass Transfer Coefficient Determination

For laminar flow (Re < 32,000) in a stirred cell, the average mass transfer coefficient, $\overline{k}$, is [61, 63]:

$$\overline{k} = \alpha_{stir} Re^{0.567} Sc^{1/3} \left(\frac{D_\infty}{b} \right) \tag{2.28}$$

where Re is the Reynolds number (= $\omega b^2/\nu$), Sc is the Schmidt number (= ν/D_∞), b is the membrane radius determined from the effective membrane filtration area, ω is the stirring speed (radians/s), and ν is the kinematic viscosity of the solution. In this work, ν is that of pure water ($\nu \approx \mu_{water}/\rho_{water} \approx 9\times10^{-7}$ m^2/s, $\mu_{water} \approx 9\times10^{-4}$ kg/(m·s), and $\rho_{water} \approx 997$ kg/m^3 at 25°C [59]) due to the dilute concentration of the solute solutions. α_{stir} is a constant

based on the filtration device geometry. An α_{stir} value of 0.23 was reported by Opong and Zydney for a stirred cell [61, 63], and this value was used in Equation (2.28) in this study. This α_{stir} value is very close to the value (α_{stir} = 0.25) calculated from the correlation proposed by Smith et al. [68].

In practice, the concentration boundary layer thickness, δ_c varies with radial position in the stirred cell, r_c. Therefore, the mass transfer coefficient ($k = \frac{D_\infty}{\delta_c(r_c)}$ [64]) also varies with radial position. Zydney and Xenopoulos proposed the following model for the local mass transfer coefficient in the stirred cell [62]:

$$k(r_c) = \alpha_{stir} Re^{0.567} Sc^{1/3} \left(\frac{D_\infty}{b}\right) \frac{r_c}{\left(b^3 - r_c^3\right)^{1/3}} \tag{2.29}$$

As the distance from the cell center, r_c, increases, the mass transfer coefficient goes from zero at the center of the stirred cell (i.e., the boundary layer is infinitely thick when r_c is equal to zero) to infinity when r_c is equal to the membrane radius, b (i.e., the boundary layer thickness goes to zero at the edge of the membrane, cf., Figure 2.6(a)). An α_{stir} value of 0.23 was again used in Equation (2.29) in our study.

If the local mass transfer coefficient, $k(r_c)$, and the local permeate flux, $J_v(r_c)$, are used in the analysis (rather than $\overline{k}$ and $\overline{J}_v$), the expression for the observed sieving coefficient (i.e., Equation (2.12)) is replaced by the following analog, which accounts for the radial dependence of the mass transfer coefficient and filtration flux [62]:

$$S_o = \frac{C_f}{C_b} = \frac{1}{\int J_v(r_c) dA} \int \left[J_v(r_c) \frac{S_a}{(1 - S_a) \exp\left[-\frac{J_v(r_c)}{k(r_c)}\right] + S_a} \right] dA \tag{2.30}$$

where C_f is the mixing cup average filtrate composition (i.e., the filtration composition that would be collected during an experiment). In this case, $\overline{S}_a(a, r_c)$ estimated from

Equation (2.27) is used for S_a in Equation (2.30). In brief, model calculations can be performed to estimate S_o using two approaches: (i) average k and J_v values ($\overline{k}$ and $\overline{J}_v$) with Equation (2.12), and (ii) radially-dependent k and J_v values ($k(r_c)$ and $J_v(r_c)$) with Equation (2.30). For mean pore size and pore size distribution analysis in our study, model calculations were performed using both approaches. The model fitting results, including best fit $\bar{r}$ and σ parameters, determined from these two model calculation approaches are then compared.

2.6 REFERENCES

[1] S. Azari, L. Zou, Using zwitterionic amino acid L-DOPA to modify the surface of thin film composite polyamide reverse osmosis membranes to increase their fouling resistance, Journal of Membrane Science 401–402 (2012) 68–75.

[2] J.T. Arena, B.D. McCloskey, B.D. Freeman, J.R. McCutcheon, Surface modification of thin film composite membrane support layers with polydopamine: Enabling use of reverse osmosis membranes in pressure retarded osmosis, Journal of Membrane Science 375 (2011) 55–62.

[3] B.D. McCloskey, H.B. Park, H. Ju, B.W. Rowe, D.J. Miller, B.D. Freeman, A bioinspired fouling-resistant surface modification for water purification membranes, Journal of Membrane Science 413–414 (2012) 82–90.

[4] D.J. Miller, S. Kasemset, L. Wang, D.R. Paul, B.D. Freeman, Constant flux crossflow filtration evaluation of surface-modified fouling-resistant membranes, Journal of Membrane Science 452 (2014) 171–183.

[5] D.J. Miller, D.R. Paul, B.D. Freeman, An improved method for surface modification of porous water purification membranes, Polymer 55 (2014) 1375–1383.

[6] S. Kasemset, A. Lee, D.J. Miller, B.D. Freeman, M.M. Sharma, Effect of polydopamine deposition conditions on fouling resistance, physical properties, and permeation properties of reverse osmosis membranes in oil/water separation, Journal of Membrane Science 425–426 (2013) 208–216.

[7] B.D. McCloskey, H.B. Park, H. Ju, B.W. Rowe, D.J. Miller, B.J. Chun, K. Kin, B.D. Freeman, Influence of polydopamine deposition conditions on pure water flux and foulant adhesion resistance of reverse osmosis, ultrafiltration, and microfiltration membranes, Polymer 51 (2010) 3472–3485.

[8] J. Jiang, L. Zhu, L. Zhu, B. Zhu, Y. Xu, Surface characteristics of a self-polymerized dopamine coating deposited on hydrophobic polymer films, Langmuir 27 (2011) 14180–14187.

[9] Z. Xi, Y. Xu, L. Zhu, Y. Wang, B. Zhu, A facile method of surface modification for hydrophobic polymer membranes based on the adhesive behavior of poly(DOPA) and poly(dopamine), Journal of Membrane Science 327 (2009) 244–253.

[10] B.D. McCloskey, Novel surface modifications and materials for fouling resistant water purification membranes, PhD thesis, University of Texas at Austin, 2009.

[11] Y.M. Shin, Y.B. Lee, H. Shin, Time-dependent mussel-inspired functionalization of poly(L-lactide-co-ε-caprolactone) substrates for tunable cell behaviors, Colloids and Surfaces B: Biointerfaces 87 (2011) 79–87.

[12] B. Li, W. Liu, Z. Jiang, X. Dong, B. Wang, Y. Zhong, Ultrathin and stable active layer of dense composite membrane enabled by poly(dopamine), Langmuir 25 (2009) 7368–7374.

[13] J. Ou, J. Wang, S. Liu, J. Zhou, S. Ren, S. Yang, Microtribological and electrochemical corrosion behaviors of polydopamine coating on APTS-SAM modified Si substrate, Applied Surface Science 256 (2009) 894–899.

[14] F. Pan, H. Jia, S. Qiao, Z. Jiang, J. Wang, B. Wang, Y. Zhong, Bioinspired fabrication of high performance composite membranes with ultrathin defect-free skin layer, Journal of Membrane Science 341 (2009) 279–285.

[15] V. Ball, D.D. Frari, V. Toniazzo, D. Ruch, Kinetics of polydopamine film deposition as a function of pH and dopamine concentration: Insights in the polydopamine deposition mechanism, Journal of Colloid and Interface Science 386 (2012) 366–372.

[16] H. Lee, S.M. Dellatore, W.M. Miller, P.B. Messersmith, Mussel-inspired surface chemistry for multifunctional coatings, Science 318 (2007) 426–430.

[17] K. Kang, I.S. Choi, Y. Nam, A biofunctionalization scheme for neural interfaces using polydopamine polymer, Biomaterials 32 (2011) 6374–6380.

[18] R.A. Zangmeister, T.A. Morris, M.J. Tarlov, Characterization of polydopamine thin films deposited at short times by autoxidation of dopamine, Langmuir 29 (2013) 8619–8628.

[19] C. Cheng, S. Li, W. Zhao, Q. Wei, S. Nie, S. Sun, C. Zhao, The hydrodynamic permeability and surface property of polyethersulfone ultrafiltration membranes with mussel-inspired polydopamine coatings, Journal of Membrane Science 417–418 (2012) 228–236.

[20] Q. Wei, F. Zhang, J. Li, B. Li, C. Zhao, Oxidant-induced dopamine polymerization for multifunctional coatings, Polymer Chemistry 1 (2010) 1430–1433.

[21] M. Vaselbehagh, H. Karkhanechi, S. Mulyati, R. Takagi, H. Matsuyama, Improved antifouling of anion-exchange membrane by polydopamine coating in electrodialysis process, Desalination 332 (2014) 126–133.

[22] D. Hughes, T. Taha, Z. Cui, Chapter 5 Mass Transfer: Membrane Processes, in: S.S. Sablani, A.K. Datta, M.S. Rahman, A.S. Mujumdar (Eds.) Handbook of Food and Bioprocess Modeling Techniques, CRC Press, Taylor & Francis Group, Boca Raton, FL, 2007.

[23] M. Cheryan, Ultrafiltration Handbook, Technomic Publishing Co., Inc., Lancaster, PA, 1986.

[24] M.C. Vincent Vela, S.Á. Blanco, J.L. García, E.B. Rodríguez, Analysis of membrane pore blocking models adapted to crossflow ultrafiltration in the ultrafiltration of PEG, Chemical Engineering Journal 149 (2009) 232–241.

[25] M.C. Vincent Vela, S.Á. Blanco, J.L. García, E.B. Rodríguez, Analysis of membrane pore blocking models applied to the ultrafiltration of PEG, Separation and Purification Technology 62 (2008) 489–498.

[26] J. Hermia, Constant pressure blocking filtration laws – Application to power-law non-Newtonian fluids, Trans. Inst. Chem. E. 60 (1982) 183–187.

[27] S. Giglia, G. Straeffer, Combined mechanism fouling model and method for optimization of series microfiltration performance, Journal of Membrane Science 417-418 (2012) 144–153.

[28] J.E. Flinn, Membrane Science and Technology: Industrial, Biological, and Waste Treatment Processes, Plenum Press, New York, NY, 1970.

[29] P. Le-Clech, V. Chen, T.A.G. Fane, Fouling in membrane bioreactors used in wastewater treatment, Journal of Membrane Science 284 (2006) 17–53.

[30] M. Mänttäri, M. Nyström, Critical flux in NF of high molar mass polysaccharides and effluents from the paper industry, Journal of Membrane Science 170 (2000) 257–273.

[31] D.J. Miller, S. Kasemset, D.R. Paul, B.D. Freeman, Comparison of membrane fouling at constant flux and constant transmembrane pressure conditions, Journal of Membrane Science 454 (2014) 505–515.

[32] V.V. Tarabara, R.M. Hovinga, M.R. Wiesner, Constant transmembrane pressure vs. constant permeate flux: Effect of particle size on crossflow membrane filtration, Environmental Engineering Science 19 (2002) 343–355.

[33] H.K. Vyas, R.J. Bennett, A.D. Marshall, Performance of crossflow microfiltration during constant transmembrane pressure and constant flux operations, International Dairy Journal 12 (2002) 473–479.

[34] P. Bacchin, P. Aimar, R.W. Field, Critical and sustainable fluxes: Theory, experiments and applications, Journal of Membrane Science 281 (2006) 42–69.

[35] R.W. Field, D. Wu, J.A. Howell, B.B. Gupta, Critical flux concept for microfiltration fouling, Journal of Membrane Science 100 (1995) 259–272.

[36] G. Belfort, R.H. Davis, A.L. Zydney, The behavior of suspensions and macromolecular solutions in crossflow microfiltration, Journal of Membrane Science 96 (1994) 1–58.

[37] P. Bacchin, P. Aimar, V. Sanchez, Model for colloidal fouling of membranes, AIChE J. 41 (1995) 368–376.

[38] S. Metsämuuronen, J. Howell, M. Nyström, Critical flux in ultrafiltration of myoglobin and baker's yeast, Journal of Membrane Science 196 (2002) 13–25.

[39] P. Harmant, P. Aimar, Coagulation of colloids in a boundary layer during cross-flow filtration, Colloids Surf. A 138 (1998) 217–230.

[40] K.Y. Choi, B.A. Dempsey, Bench-scale evaluation of critical flux and TMP in low-pressure membrane filtration, Journal of American Water Works Association 97 (2005) 134–143.

[41] D.Y. Kwon, S. Vigneswaran, A.G. Fane, R.B. Aim, Experimental determination of critical flux in cross-flow microfiltration, Separation and Purification Technology 19 (2000) 169–181.

[42] R.W. Field, G.K. Pearce, Critical, sustainable and threshold fluxes for membrane filtration with water industry applications, Advances in Colloid and Interface Science 164 (2011) 38–44.

[43] P. Le-Clech, B. Jefferson, I.S. Chang, S.J. Judd, Critical flux determination by the flux-step method in a submerged membrane bioreactor, Journal of Membrane Science 227 (2003) 81–93.

[44] J. Luo, S.T. Morthensen, A.S. Meyer, M. Pinelo, Filtration behavior of casein glycomacropeptide (CGMP) in an enzymatic membrane reactor: fouling control by membrane selection and threshold flux operation, Journal of membrane Science 469 (2014) 127–139.

[45] S.P. Beier, G. Jonsson, Critical flux determination by flux-stepping, AIChE Journal 56 (2010) 1739–1747.

[46] B.D. Cho, A.G. Fane, Fouling transients in nominally sub-critical flux operation of a membrane bioreactor, Journal of Membrane Science 209 (2002) 391–403.

[47] S.S. Madaeni, A.G. Fane, D.E. Wiley, Factors influencing critical flux in membrane filtration of activated sludge, Journal of Chemical Technology and Biotechnology 74 (1999) 539–543.

[48] V. Chen, Performance of partially permeable microfiltration membranes under low fouling conditions, Journal of Membrane Science 147 (1998) 265–278.

[49] P. van der Marel, A. Zwijnenburg, A. Kemperman, M. Wessling, H. Temmink, W. van der Meer, An improved flux-step method to determine the critical flux and the critical flux for irreversibility in a membrane bioreactor, Journal of Membrane Science 332 (2009) 24–29.

[50] J. Luo, L. Ding, Y. Wan, M.Y. Jaffrin, Threshold flux for shear-enhanced nanofiltration: Experimental observation in dairy wastewater treatment, Journal of Membrane Science 409–410 (2012) 276–284.

[51] L. Defrance, M.Y. Jaffrin, Comparison between filtrations at fixed transmembrane pressure and fixed permeate flux: application to a membrane bioreactor used for wastewater treatment, Journal of Membrane Science 152 (1999) 203–210.

[52] D. Wu, J.A. Howell, R.W. Field, Critical flux measurement for model colloids, Journal of Membrane Science 152 (1999) 89–98.

[53] Z. Wu, Z. Wang, S. Huang, S. Mai, C. Yang, X. Wang, Z. Zhou, Effects of various factors on critical flux in submerged membrane bioreactors for municipal wastewater treatment, Separation and Purification Technology 62 (2008) 56–63.

[54] S. Ognier, C. Wisniewski, A. Grasmick, Membrane bioreactor fouling in sub-critical filtration conditions: A local critical flux concept, Journal of Membrane Science 229 (2004) 171–177.

[55] R. Chan, V. Chen, The effects of electrolyte concentration and pH on protein aggregation and deposition: critical flux and constant flux membrane filtration, Journal of Membrane Science 185 (2001) 177–192.

[56] J. Zhang, H.C. Chua, J. Zhou, A.G. Fane, Factors affecting the membrane performance in submerged membrane bioreactors, Journal of Membrane Science 284 (2006) 54–66.

[57] A. Mehta, A.L. Zydney, Permeability and selectivity analysis for ultrafiltration membranes, Journal of Membrane Science 249 (2005) 245–249.

[58] S. Mochizuki, A.L. Zydney, Theoretical analysis of pore size distribution effects on membrane transport, Journal of Membrane Science 82 (1993) 211–227.

[59] B.E. Poling, G.H. Thomson, D.G. Friend, R.L. Rowley, W.V. Wilding, Section 2 Physical and Chemical Data, in: D.W. Green, R.H. Perry (Eds.) Perry's Chemical Engineer's Handbook, 8th ed., McGraw-Hill, New York, 2008.

[60] A.L. Zydney, P. Aimar, M. Meirele, J.M. Pimbley, G. Belfort, Use of the log-normal probability density function to analyze membrane pore size distributions: Functional forms and discrepancies, Journal of Membrane Science 91 (1994) 293–298.

[61] L.J. Zeman, A.L. Zydney, Microfiltration and Ultrafiltration: Principles and Applications, Marcel Dekker, Inc., New York, NY, 1996.

[62] A.L. Zydney, A. Xenopoulos, Improving dextran tests for ultrafiltration membranes: Effect of device format, Journal of membrane Science 291 (2007) 180–190.

[63] W.S. Opong, A.L. Zydney, Diffusive and convective protein transport through asymmetric membranes, AIChE Journal 37 (1991) 1497–1510.

[64] C. Causserand, S. Rouaix, A. Akbari, P. Aimar, Improvement of a method for the characterization of ultrafiltration membranes by measurements of tracers retention, Journal of Membrane Science 238 (2004) 177–190.

[65] J. Shao, R.E. Baltus, Hindered diffusion of dextran and polyethylene glycol in porous membranes, AIChE Journal 46 (2000) 1149–1156.

[66] C.Y. Chang, W.T. Tsai, C.H. Ing, C.F. Chang, Adsorption of polyethylene glycol (PEG) from aqueous solution onto hydrophobic zeolite, Journal of Colloid and Interface Science 260 (2003) 273–279.

[67] S.T. Johnston, K.A. Smith, W.M. Deen, Concentration polarization in stirred ultrafiltration cells, AIChE Journal 47 (2001) 1115–1125.

[68] K.A. Smith, C.K. Colton, E.W. Merrill, L.B. Evans, Convective transport in a batch dialyzer: Determination of true membrane permeability from a single measurement, AIChE Symposium Series 64 (1968) 45–58.

Chapter 3: Materials and Experimental Methods

3.1 MATERIALS

Flat-sheet polyamide reverse osmosis (XLE RO) membranes were kindly provided by DOW Water & Process Solutions (Edina, MN). Flat-sheet polysulfone ultrafiltration membranes (PS-20, 20 kDa MWCO as specified by the manufacturer) were purchased in rolls from Ultura (formerly Sepro Membranes, Inc.) (Oceanside, CA). Polysulfone (UDEL P-3500 LCD MB) was obtained from Solvay Specialty Polymers (Alpharetta, GA). Dopamine hydrochloride (3-hydroxytyramine hydrochloride), Trizma hydrochloride (Tris-HCl), sodium bicarbonate ($NaHCO_3$), potassium chloride (KCl), cyclopentanone, *n*-decane, and poly(ethylene glycol) (PEG) (i.e., poly(ethylene oxide) (PEO) for PEGs $\geq$ 100 kDa) were purchased from Sigma Aldrich (St. Louis, MO). Sodium hydroxide (NaOH), hydrochloric acid (HCl), sodium chloride (NaCl), and ethanol were purchased from Fisher Scientific (Pittsburgh, PA). Isopropyl alcohol (IPA, BDH Chemicals) was purchased from VWR International (Radnor, PA). Wesson vegetable (100% soybean) oil was purchased from a local supermarket. Xiameter OFX-0193 (formerly DC193C), which is a silicone-based, non-ionic surfactant, was obtained from Dow Corning (Midland, MI). All chemicals were used as received. Ultrapure water was obtained from a Millipore Milli-Q Advantage A10 water purification system (18.2 MΩ-cm at 25^{o}C, 1.2 ppb TOC) (Billerica, MA).

Acrylic plates/frames and rubber gaskets of 8 in. × 11 in. (20 cm × 28 cm) size were obtained from Interstate Plastics (Austin, TX) and Advanced Gasket & Supply, Inc. (Fort Worth, TX), respectively. 25 mm Puradisc PTFE syringe filters (Whatman) of 0.1, 0.2, 0.45, and 1.0 μm pore sizes were purchased from GE Healthcare Life Sciences (Piscataway, NJ). Silicon wafers (6 in. diameter) were purchased from Nova Electronic Materials, LLC (Flower Mound, TX).

3.2 MEMBRANE STORAGE, HANDLING, AND PRETREATMENT

The XLE RO and PS20 UF membranes were received as rolls of dry, flat-sheet membranes. The membrane rolls were stored vertically in a dark, cool container to limit possible oxidation of the membrane surfaces [1]. According to the manufacturer's pretreatment procedures, the XLE RO membrane samples were soaked in 25% (v/v) aqueous IPA solution for 20 minutes to wet the membrane pores and to remove glycerin, which had been applied by the manufacturer to maintain the porous structure of the polysulfone support [1]. The membrane coupons were then soaked in ultrapure water to remove the alcohol and residual glycerin. The soaking water was changed three times, and the membranes were stored for approximately 16 – 24 hours in ultrapure water prior to surface modification or further experiments.

The PS-20 UF membranes were pretreated by soaking in ethanol overnight. The membrane was carefully immersed into the ethanol with the selective surface facing down to avoid air bubbles being trapped inside the pores as described previously [2-4]. The membranes were then rinsed thoroughly with fresh ultrapure water at least four times to displace the ethanol. All pretreated membrane samples were stored in ultrapure water until use.

3.3 MEMBRANE MODIFICATION WITH POLYDOPAMINE (PDA)

3.3.1 PDA Modification on RO Membranes

Each XLE RO membrane sample was coated with PDA by exposing its selective top layer to aqueous dopamine solution at room temperature, as shown in Figure 3.1. The RO membrane sample, with its selective side up, was anchored to a glass plate, and a glass ring (5 in. diameter) was secured atop the membrane with vacuum grease. Aqueous dopamine coating solutions were prepared by dissolving dopamine hydrochloride in 15

mM Tris-HCl buffer solution. The 15 mM Tris-HCl buffer solution was prepared by dissolving 2.634 g of Tris-HCl in 1 L of ultrapure water.

The dopamine coating solution was prepared at several initial concentrations which were 0.1, 0.5, 2, 4, and 8 mg/mL and used at a coating time of 60 minutes. The pH of Tris-HCl buffer solution was adjusted to three different values (i.e., 5, 8.8, and 11) by adding HCl or NaOH prior to use. The PDA deposition time was varied to 30, 60, and 120 minutes at an initial dopamine concentration of 2 mg/mL.

The dopamine coating solution (50 mL) was poured into the secured glass ring. Then the glass plate with secured membrane exposing to dopamine solution was rocked on a rocking platform shaker (VWR International, Radnor, PA) for a desired coating time. A rocking speed of 30 tilts per minute and a tilt level of 4 were used for the modification. After the PDA deposition step was complete, the membrane was rinsed with ultrapure water once and soaked in 25% (v/v) IPA solution for 10 minutes to remove unattached or weakly-bound PDA from the membrane surface. Finally, the membrane was rinsed thoroughly under running ultrapure water to remove the alcohol and stored in ultrapure water before testing. The membrane sheet was cut into circular samples having a diameter of 1.7 in. (4.31 cm), using a cutting die, for use in pure water flux tests or square samples of 3 in. × 1 in. (7.62 cm × 2.54 cm) size for use in crossflow filtration tests.

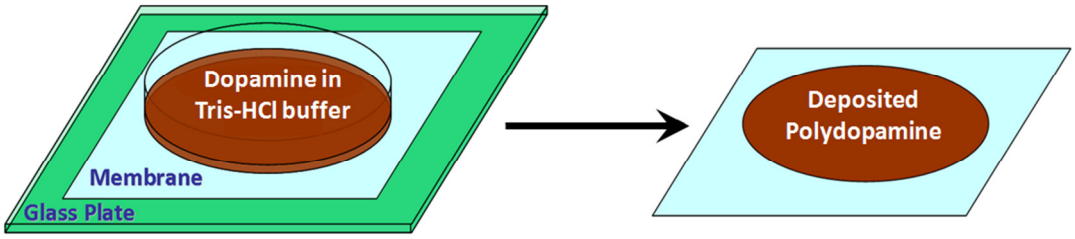

Figure 3.1: Polydopamine membrane modification technique.

3.3.2 PDA Modification on UF Membranes

A square acrylic frame and a rubber gasket (8 in. × 11 in. size with 6 in. × 9 in. internal open surface for coating) were used and secured onto the membrane and an acrylic plate by large paper clips. The UF membranes were cut into the same size (i.e., 8 in. × 11 in.) as the plate/frame and gasket used for PDA surface modification. The dopamine coating solution was prepared as described in the earlier section. Generally, the dopamine concentration in the coating solution decreases over time as the dopamine reacts to form PDA [5]. Thus, in this study, the dopamine concentration refers to the initial dopamine concentration in the modification solution.

Several initial concentrations of dopamine in Tris-HCl buffer solution and different coating times were used for UF membrane modification. The pH of Tris-HCl buffer solution was adjusted to 8.8 using NaOH prior to mixing with the dopamine hydrochloride. The initial dopamine concentrations of 0.1, 0.5, 1, 2, 4, and 8 mg/mL were used at a deposition time of 60 minutes. The PDA deposition times of 15, 30, 60, 120, and 240 minutes were also used at an initial dopamine concentration of 2 mg/mL.

Each membrane sheet was coated with PDA by exposing its selective face to the aqueous dopamine solution. The dopamine coating solution (100 mL) was poured onto the membrane secured on the acrylic plate/frame and rubber gasket setup. During the modification, the membrane sheet was set on a rocking platform shaker (VWR International, Radnor, PA) at a rocking speed of 30 tilts per minute and a tilt level of 4 for the prescribed deposition time. After the desired deposition time was reached, the membrane sheet was rinsed with running ultrapure water and soaked in ethanol for 10 minutes to remove any weakly-bound PDA from the membrane surface. Then the membrane sheet was rinsed thoroughly with several batches of ultrapure water to remove the ethanol and stored in ultrapure water until used. Using a cutting die, the membrane

sheet was cut into circular samples with a diameter of 1.5 in. (3.83 cm) for use in pure water permeance tests or 2.38 in. (6.04 cm) for use in the MWCO tests. For crossflow filtration test, the membrane was cut into square samples with 3 in. × 1 in. (7.62 cm × 2.54 cm) size.

3.4 SURFACE ROUGHNESS MEASUREMENT

Surface roughness of unmodified and PDA-modified UF membranes was characterized using an atomic force microscope (AFM) (Digital Instruments Dimension 3000 with NanoScope software 6.13, Veeco, Plainview, NY) operated in tapping mode. The membranes were vacuum-dried overnight to ensure complete evaporation of liquid from the membrane surfaces and pores. The membrane samples were taped onto Si wafers. The analysis was performed using a 5×5 μm image size, a 0.5 Hz scan rate, and a 512 samples/line setting. The root-mean-square roughness (R_{rms}) of each membrane was reported as an average of at least 5 measurements on membranes at each set of modification conditions considered. The uncertainties represent one standard deviation.

3.5 CONTACT ANGLE MEASUREMENT

Contact angles of membrane surfaces were measured to assess membrane surface hydrophilicity. The contact angle measurements were performed using a contact angle goniometer (Ramé-Hart Model 200) with DROPimage Standard software version 2.4 (Ramé-Hart Instrument Co., Netcong, NJ). Figure 3.2 illustrates the experimental apparatus. The measurements were performed using a captive bubble method where a static contact angle between a captive *n*-decane bubble in water and the membrane surface was measured [6, 7]. This captive bubble technique was used instead of the sessile drop technique to allow the membranes to be immersed in water during the contact angle measurement, similar to their environment during water filtration [8].

Membranes were cut into long strips approximately 3 – 4 mm wide. Each membrane sample was mounted in a sample holder with its selective surface facing down, and the mounted sample was placed into a transparent chamber filled with ultrapure water. A droplet of *n*-decane was dispensed underneath the membrane surface using a Gilmont Instruments microliter syringe (Cole-Parmer, Vernon Hills, IL) equipped with a J-hook needle. The tip of the needle was placed under the membrane such that the dispensed droplet would rise through the water and contact the feed-side face of the membrane. The static contact angles (θ) were measured as shown in Figure 3.2. Each reported contact angle value is an average of at least five measurements on membranes at each set of modification conditions considered. An average value of the left and right side contact angles was used for each measurement. The uncertainties, denoted by error bars, represent one standard deviation. A smaller contact angle represents a more hydrophilic membrane surface.

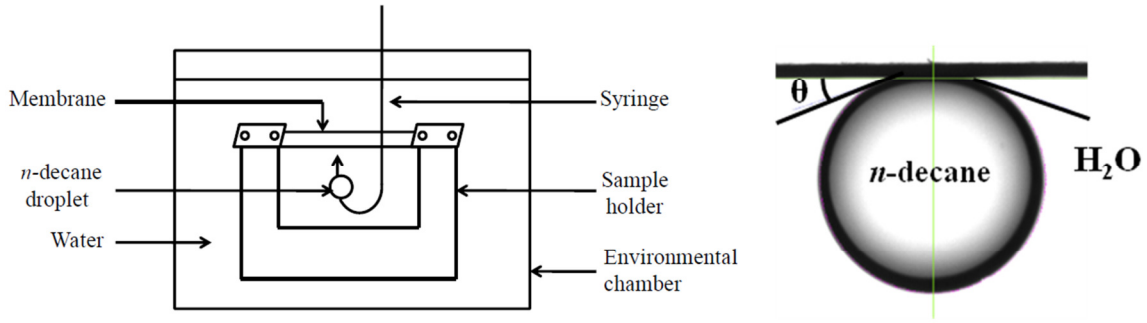

Figure 3.2: Experimental set up of (*n*-decane)-in-water contact angle measurement (left) [6], and contact angle (θ) from captive-bubble method (right) [9].

3.6 ZETA POTENTIAL MEASUREMENT

Zeta potentials of unmodified and PDA-modified UF membranes were measured to characterize changes in membrane surface charge due to PDA modification. Membranes coated with PDA at 0.5 and 2 mg/mL initial dopamine concentrations for 60

minutes were used in this analysis to represent low and moderate PDA coatings, respectively. The zeta potential was determined based on streaming potential measurement using a SurPASS electrokinetic analyzer (Anton Paar, Ashland, VA) with the associated SurPASS software. Each membrane (25×55 mm) was clamped in a flat-sheet tangential flow module equipped with two spacers to create an electrolyte flow channel between the membrane and the reference material. The measurement was performed using 0.001 M KCl as the background electrolyte solution over a pH range of 4 – 10. The pH was initially adjusted to 10 by dosing the electrolyte solution with 0.1 M NaOH, and then the pH was decreased in a stepwise fashion by adding 0.1 M HCl until the pH was reduced to 4. The pH adjustment was automatically controlled by the instrument. The zeta potential values were evaluated by the SurPASS software using a Helmholtz-Smoluchowski (H-S) model. For each membrane type, the reported zeta potential profile as a function of pH is representative of at least three replicates. In addition, the zeta potential of the soybean oil emulsion used in this study was measured using a Zetasizer Nano (Malvern Instruments, United Kingdom) at 25°C with DTS-1070 cells.

3.7 ELLIPSOMETRY

PDA coating thicknesses on dense, nonporous polysulfone (PSf) films were measured using spectroscopic ellipsometry (model M-2000V with CompleteEASE software, J.A. Woollam Co., Inc., Lincoln, NE). 3 wt% PSf in cyclopentanone solution was prepared and pre-filtered with 1, 0.45, 0.2, and 0.1 μm syringe filters, in this order, to remove any particulates or contaminants. PSf flat dense films were obtained by spin casting the polymer solution on silicon (Si) wafers at 1000 rpm for 60 seconds. The method of PSf film preparation is described in detail elsewhere [10]. PDA was coated

onto PSf-coated Si wafers using a protocol similar to that used for membrane modification described in section 3.3. Initial dopamine concentrations of 0.1, 0.5, 1, 2, 4, and 8 mg/mL at a coating time of 60 minutes and deposition times of 15, 30, 60, 120, and 240 minutes at an initial dopamine concentration of 2 mg/mL were used. After each modification, the coated samples were rinsed thoroughly with ultrapure water and air-dried overnight prior to thickness measurement. Samples were rinsed carefully to prevent leaching of PSf from the Si wafer.

Thickness measurements were conducted at variable incidence angles (65, 70, and 75 degrees) and variable wavelengths (370-1000 nm) on at least 3 different locations for each sample. The PSf layer thickness of each individual sample was measured prior to PDA modification by using a Cauchy two-layer model [11]. The first layer was presumed to be silicon dioxide (SiO_2), whose thickness was measured before spin coating with PSf, and the second layer was the PSf film. For PDA thickness analysis, a third layer was added on top of the PSf and SiO_2 layers. The thicknesses of the PSf and SiO_2 layers were fixed using values measured on that particular sample prior to PDA modification. The PDA coating thickness was estimated using a General Oscillator (Gen-Osc) layer (provided in CompleteEASE software) with a Tauc-Lorentz oscillatory model. (The B-Spline layer was initially used, and the Tauc-Lorentz oscillatory model was then used to parameterize the optical constants of the B-Spline layer. After parameterization, the B-Spline layer was replaced by the Gen-Osc layer.) This method of analysis accounts for light absorption of PDA at all wavelengths. More details of the ellipsometry data analysis from light-absorbing thin films can be found elsewhere [11]. We measured a refractive index (n) of 1.73 and a k amplitude of 0.12 at a wavelength (λ) of 632.8 nm for the thickest PDA film, which was coated using an 8 mg/mL initial dopamine concentration solution and a 240-minute deposition time. Analysis of very thin films can introduce

uncertainty in the fitted n and k parameters. Thus, for samples with PDA film thickness less than 10 nm, an n value of 1.73 and a k value of 0.12, obtained from samples with thick PDA coatings, were used instead of allowing the n and k parameters to be fit. Each reported thickness is an average of measurements on at least three locations on each sample, and the uncertainty is reported as one standard deviation.

3.8 PURE WATER FLUX OR PERMEANCE MEASUREMENT

The pure water flux of unmodified and PDA-modified membranes was measured using dead-end filtration cells. For RO membranes, the filtration cell was HP4750 from Sterlitech Corp. (Kent, WA) with an effective filtration area of 14.6 cm^2. The applied transmembrane pressure difference (TMP) of 150 psi (10.3 bar) was used for RO membranes. For UF membranes, the filtration cell was UHP43 from Advantec MFS, Inc. (Dublin, CA) with an effective filtration area of 11.5 cm^2. The applied TMP of 30 psi (2 bar) was used for UF membranes. During the filtration experiments, permeate was collected, and permeate volume or mass data were recorded as a function of filtration time. If the permeate volume data was collected, the pure water flux of each membrane was calculated from the effective filtration area (A) and the slope of permeate volume (V) vs. filtration time (t) [12]. If the permeate mass data was collected, the slope of permeate mass (m) vs. filtration time (t), the density of water (ρ_{water}), and the effective filtration area (A) were used to determine the pure water permeate flux as follows [4, 7, 12]:

$$\overline{J}_{pw} = \frac{1}{A}\left(\frac{\Delta V}{\Delta t}\right) = \frac{1}{\rho_{water} A}\left(\frac{\Delta m}{\Delta t}\right) \tag{3.1}$$

where $\overline{J}_{pw}$ is the average steady state pure water flux (i.e., pure water volumetric flow rate per unit area). The membrane hydraulic permeability or pure water permeance, $\overline{L}_p$, was calculated from pure water flux divided by TMP as shown in Equation (2.6). The average pure water flux or permeance values from measurements on at least three

separate membrane samples are reported. The uncertainties, denoted by error bars, represent one standard deviation.

3.9 Molecular Weight Cut Off (MWCO) Determination

MWCO measurements were conducted in continuous dead-end filtration of aqueous poly(ethylene glycol) (PEG) solutions. PEG samples with 4, 8, 10, 12, 20, 35, 100, and 200 kDa molecular weights were used. Aqueous solutions containing 0.1 wt% (1,000 ppm) PEG were prepared with one PEG molecular weight for each solution. The filtration was conducted with PEG solutions of one molecular weight at a time in order of ascending (i.e., low to high) molecular weight. The filtration system was cleaned thoroughly with ultrapure water between filtrations of PEG solutions of different molecular weights.

Except for the choice of solute, the filtration setup was constructed and operated according to ASTM standard E1343 – 90 [13]. The diagram and photograph of the system are shown in Figure 3.3 and Figure 3.4, respectively. The ASTM standard uses dextran as a solute marker [13], and dextran is generally regarded as more suitable for determination of MWCO over a high molecular weight range, such as above 10 kDa [14]. In contrast, PEG is generally used for the determination of MWCO in a wide molecular weight range, even below 10 kDa [14-17]. Dextran is commercially available with molecular weights higher than 1 kDa, while PEG is commercially available with molecular weight values as low as 0.2 kDa. Since the PDA-modified membranes were expected to have MWCO values in a low range, PEG was chosen for our MWCO tests. Other literature studies also report the use of PEG to determine MWCO [14-17].

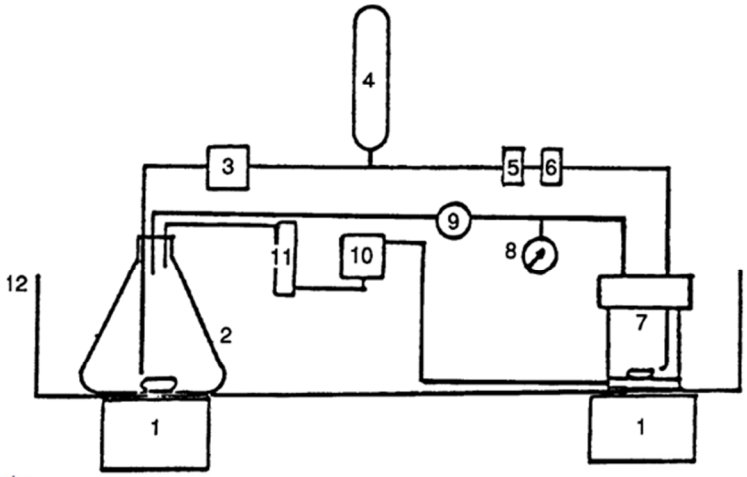

Identification of components:

(1) Magnetic stirrers,
(2) Erlenmeyer flask used for test solution reservoir,
(3) Diaphragm pump,
(4) Five-hundred c^3 sample cylinder used as a pulse dampener,
(5) Fifteen-µm in-line filter,
(6) Two-µm in-line filter,
(7) Ultrafiltration cell modified for flow through of test solution,
(8) Zero to 15 psig (or other suitable range) pressure gage,
(9) Two to 30 psig (or other suitable range) back pressure regulator,
(10) Highly reproducible peristaltic pump,
(11) Flowmeter, and
(12) Constant temperature bath.

Figure 3.3: A diagram showing filtration system for molecular weight cut off determination from ASTM standard [13].

Figure 3.4: A photograph of continuous dead-end filtration system for molecular weight cut off determination.

Dead-end filtration cells (model 8200, Millipore, Corp., Billerica, MA), with an effective filtration area of 28.7 cm^2, were used. The PEG solution in the dead-end filtration cells was stirred at 250 rpm ($\omega \approx 26.2$ radian/s) at all times during the experiments. The feed flow rate was 100±10 mL/min, and feed pressure was 6±0.5 psig. The permeate flow rate was 0.17±0.01 mL/min and was controlled by a peristaltic pump (catalog number for drive: 7522-30, for head: 7519-20, for cartridge: 7519-85, for tubing: 6447-12, Cole-Parmer, Vernon Hills, IL) with feedback control from a permeate flow meter (model number: M12P-ABD-11-0-S, Bronkhorst, Bethlehem, PA). This permeate flow rate corresponds to an average permeate flux of 0.0001 cm/s or 3.6 $L/m^2/h$ (LMH). A very low permeate flow rate was used to minimize concentration polarization. Each filtration test with each PEG molecular weight was run for at least 30 minutes prior to collecting feed and permeate samples to ensure that the system had reached steady state. The feed and permeate sample concentrations were analyzed using a total organic carbon analyzer (TOC-Vcsh, Shimadzu Corp., Japan). The observed sieving coefficient, S_o, was calculated using Equation (2.11). The MWCO values were determined from the actual PEG rejections, calculated from the S_o data, as discussed in more detail in Chapter 5, section 5.2.3 Molecular Weight Cutoff and Nominal Pore Size.

3.10 OIL/WATER EMULSION PREPARATION

To be consistent with earlier studies from our laboratories on the topic of oil/water fouling [18, 19], the model foulant used in this study was a 1,500 ppm emulsion of soybean oil/Xiameter OFX-0193 surfactant in water (9:1 ratio of oil to surfactant). For fouling study with RO membranes, the emulsion was prepared by blending 40.5 g of soybean oil with 4.5 g of Xiameter OFX-0193 surfactant in 3 L of 2,000 ppm NaCl solution. To prepare a stable emulsion, the mixture was blended in a high-speed blender

(Waring Laboratory, Torrington, CT) at ~20,000 rpm (highest rotational speed) for 3 minutes. The emulsion was then cooled to ~25^{o}C before dilution in the crossflow system feed tank containing 27 L of 2,000 ppm NaCl solution to achieve a 1,500 ppm soybean oil emulsion (with a total volume of 30 L).

For fouling study with UF membranes, the emulsion was prepared by blending 10.8 g of soybean oil with 1.2 g of Xiameter OFX-0193 surfactant in 1 L of ultrapure water. The mixture was blended in a high speed blender as described above. The mixture was then diluted with 7 L of ultrapure water, resulting in a 1,500 ppm (i.e., 1,350 ppm soybean oil and 150 ppm surfactant) soybean oil emulsion (with a total volume of 8 L). The oil/water emulsion droplet size, measured using a Coulter counter, was approximately in the range of 0.8 – 3.0 μm and had an average size of 1.4 μm [18, 20].

3.11 CONSTANT TRANSMEMBRANE PRESSURE DIFFERENCE (TMP) CROSSFLOW FILTRATION

For RO membranes, fouling studies were conducted using a constant TMP (i.e., variable permeate flux) crossflow filtration system (Separation Systems Technology, San Diego, CA). The diagram of this filtration system is shown in Figure 3.5. The details of the apparatus are presented elsewhere [1].

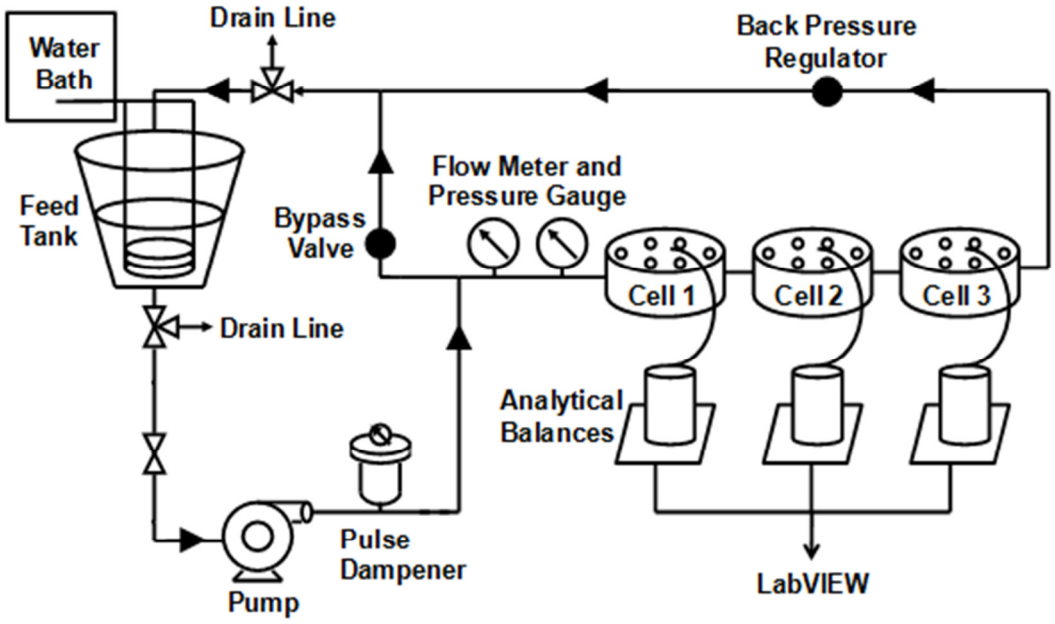

Figure 3.5: Constant TMP crossflow filtration system [1].

The system was cleaned prior to each filtration experiment by circulating 0.3% (v/v) of bleach (Clorox®) solution for 30 minutes to disinfect the system and 0.2% (v/v) aqueous solution of Nalgene L900 liquid detergent (Fisher Scientific, Pittsburgh, PA) for another 30 minutes to remove residual organics (e.g., oil and surfactant). The system was then rinsed for at least three cycles with tap water and one cycle with ultrapure water. For each rinse cycle, the feed tank was filled with 30 L of water, and the water was run through the system in a single pass (i.e., without recirculation). All filtration experiments were conducted at a feed pressure of 150 psig (10.3 barg), permeate pressure of atmospheric (i.e., the TMP was 150 psi (10.3 bar)) and feed flow rate of 1 gallon per minute (3.8 liters per minute), which corresponded to a Reynolds number of 4900 inside our crossflow cells. The Reynolds number was calculated based on a calculation for turbulent flow in noncircular tubes by employing a mean hydraulic radius (R_h) as shown in Equation (3.2) and Equation (3.3) [21]. The geometry of the flow channels was 3 in.

long × 1 in. wide × 0.125 in. deep (or approximately 76 mm long × 25 mm wide × 3 mm deep).

$$R_h = \frac{S}{Z} \tag{3.2}$$

In Equation (3.2), R_h is the mean hydraulic radius, S is the cross section of the flow channel (~25 mm × 3 mm), and Z is the wetted perimeter (~57 mm). The Reynolds number (Re_h) is defined as [21]:

$$\mathrm{Re}_h = \frac{4R_h \langle v_z \rangle \rho}{\mu} \tag{3.3}$$

where $\langle v_z \rangle$ is the average velocity in the flow channel (~0.78 m/s), ρ is the density of oil emulsion at 25°C (~997 kg/m^3), and μ is the viscosity of oil emulsion at 25°C (~9 × 10^{-4} kg/(m·s)) [22]. The properties of oil emulsion (i.e., ρ and μ) were approximated from the properties of water in this calculation.

Throughout the experiments, the feed temperature was maintained at ~25°C, and the pH of the feed solution was controlled at ~8 (which was the membrane manufacturer's suggested value) by adding $NaHCO_3$ to the feed tank at the beginning of the experiments [1]. The permeate flux, Jw, during the oil/water emulsion filtration was calculated as follows:

$$J_w = \frac{1}{\rho_{water} A}\left(\frac{\Delta m}{\Delta t}\right) \tag{3.4}$$

where J_w is the permeate water flux, Δm is the mass of permeate collected during a filtration time of Δt, ρ_w is the density of water, and A is the effective filtration area of the membrane sample (~19 cm^2). The mass of permeate was measured using an analytical balance connected to a computer. Labview software (National Instruments, Austin, TX) was used to record the permeate mass every 60 seconds during an experiment.

Each filtration experiment consisted of three steps as illustrated in Figure 3.6. For the first 30 minutes of the experiment, ultrapure water was the feed solution. After 30 minutes of pure water filtration, NaCl was added to the feed solution in an amount that brought the feed solution NaCl concentration to approximately 2,000 mg/L. Then, the permeate flux, as well as bulk feed and permeate salt concentrations, were measured. Salt concentrations were measured using a conductivity meter (Oakton CON 11, Oakton Instruments, Vernon Hills, IL) that had been previously calibrated using salt solutions of known composition. The reported apparent NaCl rejection values were calculated from bulk feed and permeate salt concentrations according to Equation (3.5) [1, 23, 24]. The reported true NaCl rejections were corrected for concentration polarization using the apparent NaCl rejections, pure water flux, and permeate flux from NaCl solution filtration as suggested in the literature [1, 24]. The reported average apparent and true NaCl rejection values were calculated from results on at least three membrane coupons; the reported uncertainty values (denoted by error bars) represent one standard deviation. After 30 minutes of NaCl solution filtration, the oil/water emulsion was introduced to the feed stream, and the fouling test was run for 24 hours. The reported permeate flux as a function of time during the fouling test was averaged from flux values measured using at least three membrane samples. At the beginning and the end of the experiments, feed and permeate samples of unmodified membranes and polydopamine-modified membranes (prepared by using 2 mg/mL initial dopamine concentration, 60 minutes deposition time, and Tris-HCl buffer at a pH of 8.8) were collected, and organic carbon concentrations were determined using Total Organic Carbon Analyzer (TOC-Vcsh, Shimadzu Corp., Japan). The organic rejection values were calculated according to Equation (3.5) [25], and the average values and uncertainty values (one standard deviation) of at least three membrane samples were reported.

$$R = \left(1 - \frac{C_f}{C_b}\right) \times 100\% \tag{3.5}$$

where R is the apparent NaCl rejection or organic rejection, C_f is NaCl concentration (for NaCl rejection) or organic concentration (for organic rejection) in the filtrate, and C_b is NaCl concentration (for NaCl rejection) or organic concentration (for organic rejection) in the bulk feed.

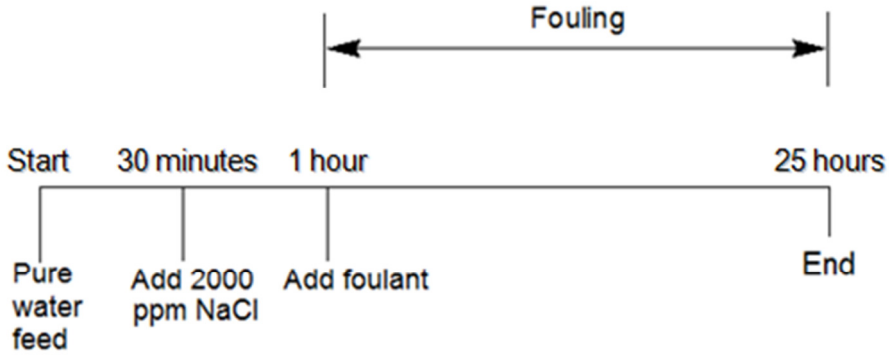

Figure 3.6: Timeline of the crossflow filtration experiment [1].

3.12 Constant Permeate Flux Crossflow Filtration and Threshold Flux Determination

For UF membranes, a constant permeate flux (i.e., variable TMP) crossflow filtration was used to determine threshold fluxes of unmodified and PDA-modified membranes. The UF membranes modified with PDA at initial dopamine concentrations of 0.1, 0.5, 2, and 8 mg/mL (using a 60-minute coating time) and deposition times of 15, 60, and 240 minutes (using a 2 mg/mL initial dopamine concentration) were used in this threshold flux analysis. A 1,500 ppm soybean oil emulsion was used as a model foulant feed solution.

At constant flux operation, the change in TMP at each permeate flux considered was recorded throughout the experiments. The diagram of constant permeate flux crossflow filtration system is shown in Figure 3.7. Details of the constant flux crossflow

filtration system and its operation are explained elsewhere [3, 26]. A flux stepping method was used for the threshold flux determination [27-29]. The flux stepping experiments were conducted with an initial flux of 10 LMH, a step length of 20 minutes, and a step height of 10 LMH. The feed flow rate was 0.8 L/min (corresponding to a crossflow velocity of 0.18 m/s and a Reynolds number of ~1000 [3, 4]). The feed pressure was 2.1 barg (30 psig). For every filtration test, ultrapure water was initially run at a permeate flux level of 10 LMH for at least 20 minutes to ensure that the system operation had reached steady state. Then, the feed was switched to the 1,500 ppm soybean oil emulsion, and flux stepping experiments were performed by increasing the permeate flux by 10 LMH every 20 minutes. Each flux stepping experiment was terminated when the TMP reached the gauge feed pressure to avoid vacuum in the permeate line as explained in more detail elsewhere [3, 4]. The temperature of the feed water and feed oil/water emulsion was controlled at ~25^{o}C throughout the experiments. The threshold fluxes of unmodified and PDA-modified UF membranes were determined from TMP_{avg} vs. flux and d(TMP)/dt vs. flux curves acquired from the flux stepping experiments as explained in Chapter 5. Each reported TMP_{avg} vs. flux profile is representative of at least three replicates. The reported threshold flux value determined using the TMP_{avg} parameter of each membrane is an average from three membrane samples, and the uncertainties (i.e., error bars) denote one standard deviation.

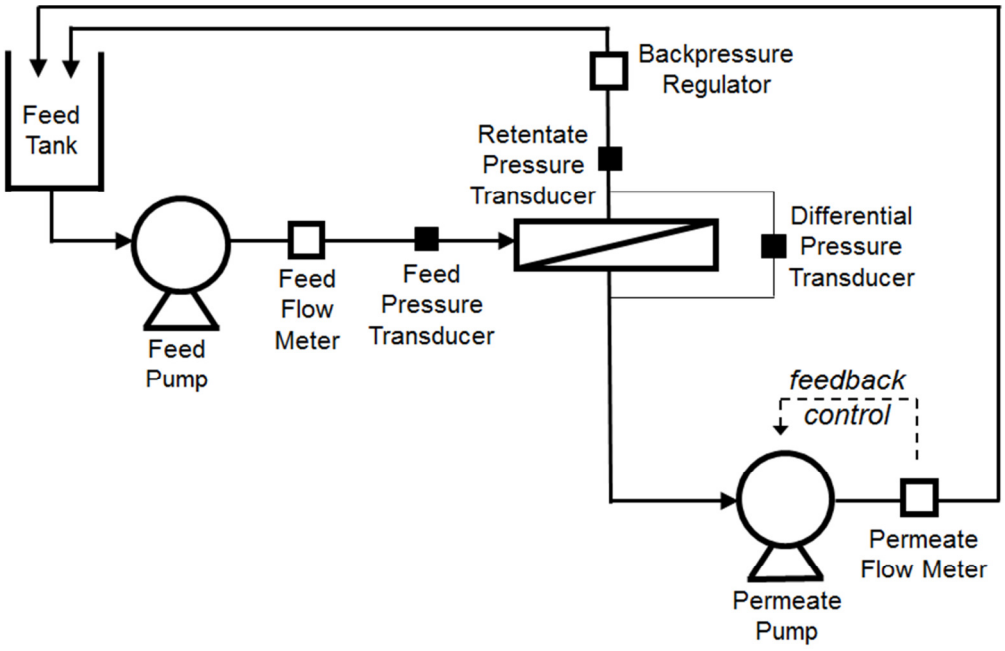

Figure 3.7: Constant permeate flux crossflow filtration system.

3.13 REFERENCES

[1] E.M. Van Wagner, A.C. Sagle, M.M. Sharma, B.D. Freeman, Effect of crossflow testing conditions, including feed pH and continuous feed filtration, on commercial reverse osmosis membrane performance, Journal of Membrane Science 345 (2009) 97–109.

[2] D.J. Miller, S. Kasemset, D.R. Paul, B.D. Freeman, Comparison of membrane fouling at constant flux and constant transmembrane pressure conditions, Journal of Membrane Science 454 (2014) 505–515.

[3] D.J. Miller, S. Kasemset, L. Wang, D.R. Paul, B.D. Freeman, Constant flux crossflow filtration evaluation of surface-modified fouling-resistant membranes, Journal of Membrane Science 452 (2014) 171–183.

[4] D.J. Miller, D.R. Paul, B.D. Freeman, An improved method for surface modification of porous water purification membranes, Polymer 55 (2014) 1375–1383.

[5] V. Ball, D.D. Frari, V. Toniazzo, D. Ruch, Kinetics of polydopamine film deposition as a function of pH and dopamine concentration: Insights in the polydopamine deposition mechanism, Journal of Colloid and Interface Science 386 (2012) 366–372.

[6] E.M. Van Wagner, A.C. Sagle, M.M. Sharma, Y.-H. La, B.D. Freeman, Surface modification of commercial polyamide desalination membranes using

poly(ethylene glycol) diglycidyl ether to enhance membrane fouling resistance, Journal of Membrane Science 367 (2011) 273–287.

[7] S. Kasemset, A. Lee, D.J. Miller, B.D. Freeman, M.M. Sharma, Effect of polydopamine deposition conditions on fouling resistance, physical properties, and permeation properties of reverse osmosis membranes in oil/water separation, Journal of Membrane Science 425–426 (2013) 208–216.

[8] A.W. Neumann, J.K. Spelt, Applied Surface Thermodynamics, Marcel Dekkar, Inc., New York, NY, 1996.

[9] E.M. Van Wagner, Polyamide desalination membrane characterization and surface modification to enhance fouling resistance, PhD thesis, University of Texas at Austin, 2010.

[10] Y. Huang, D.R. Paul, Experimental methods for tracking physical aging of thin glassy polymer films by gas permeation, Journal of Membrane Science 244 (2004) 167–178.

[11] CompleteEASE Data Analysis Manual, J.A. Woollam Co. Inc., Lincoln, NE, 2011.

[12] A.C. Sagle, E.M. Van Wagner, H. Ju, B.D. McCloskey, B.D. Freeman, M.M. Sharma, PEG-coated reverse osmosis membranes: Desalination properties and fouling resistance, Journal of Membrane Science 340 (2009) 92–108.

[13] ASTM Standard E1343 – 90, 1996 (2001), "Standard Test Method for Molecular Weight Cutoff Evaluation of Flat Sheet Ultrafiltration Membranes," ASTM International, West Conshohocken, PA, 2001, DOI: 10.1520/E1343-90R01, www.astm.org.

[14] R. Rohani, M. Hyland, D. Patterson, A refined one-filtration method for aqueous based nanofiltration and ultrafiltration membrane molecular weight cut-off determination using polyethylene glycols, Journal of Membrane Science 382 (2011) 278–290.

[15] C.M. Tam, A.Y. Tremblay, Membrane pore characterization – comparison between single and multicomponent solute probe techniques, Journal of Membrane Science 57 (1991) 271–287.

[16] S.P. Nunes, M.L. Sforça, K.-V. Peinemann, Dense hydrophilic composite membranes for ultrafiltration, Journal of Membrane Science 106 (1995) 49–56.

[17] Y.H. Wu, Y.L. Liu, Y. Chang, A. Higuchi, B.D. Freeman, Effect of UV intensity on structure, water sorption, and transport properties of crosslinked N-vinyl-2-pyrrolidone/N,N'-methylenebisacrylamide films, Journal of Membrane Science 348 (2010) 47–55.

[18] H. Ju, Water transport study in crosslinked poly(ethyleneoxide) hydrogels as fouling-resistant membrane coating materials, PhD thesis, University of Texas at Austin, 2010.

[19] B.D. McCloskey, H. Ju, B.D. Freeman, Composite membranes based on a selective chitosan–poly(ethylene glycol) hybrid layer: Synthesis, characterization, and performance in oil-water purification, Industrial and Engineering Chemistry Research 49 (2010) 366–373.

[20] H. Ju, B.D. Freeman, Desalination and water purification research and development program report no. 129: Novel fouling-resistant membranes for water purification, U.S. Department of the Interior, Bureau of Reclamation, Denver, CO, 2008.

[21] R.B. Bird, W.E. Stewart, E.N. Lightfoot, Transport Phenomena, 2nd ed., John Wiley & Sons, Inc., New Jersey, NY, 2002.

[22] B.E. Poling, G.H. Thomson, D.G. Friend, R.L. Rowley, W.V. Wilding, Section 2 Physical and Chemical Data, in: D.W. Green, R.H. Perry (Eds.) Perry's Chemical Engineer's Handbook, 8th ed., McGraw-Hill, New York, 2008.

[23] R.W. Baker, Membrane Technology and Applications, 2nd ed., John Wiley & Sons Ltd., West Sussex, England, 2004.

[24] I. Sutzkover, D. Hasson, R. Semiat, Simple technique for measuring the concentration polarization level in a reverse osmosis system, Desalination 131 (2000) 117–127.

[25] B.D. McCloskey, H.B. Park, H. Ju, B.W. Rowe, D.J. Miller, B.D. Freeman, A bioinspired fouling-resistant surface modification for water purification membranes, Journal of Membrane Science 413–414 (2012) 82–90.

[26] D.J. Miller, D.R. Paul, B.D. Freeman, A crossflow filtration system for constant permeate flux membrane fouling characterization, Review of Scientific Instruments 84 (2013) 035003.

[27] K.Y. Choi, B.A. Dempsey, Bench-scale evaluation of critical flux and TMP in low-pressure membrane filtration, Journal of American Water Works Association 97 (2005) 134–143.

[28] P. Le-Clech, B. Jefferson, I.S. Chang, S.J. Judd, Critical flux determination by the flux-step method in a submerged membrane bioreactor, Journal of Membrane Science 227 (2003) 81–93.

[29] S.P. Beier, G. Jonsson, Critical flux determination by flux-stepping, AIChE Journal 56 (2010) 1739–1747.

Chapter 4: Effect of Polydopamine Deposition Conditions on Fouling Resistance, Physical Properties, and Permeation Properties of Reverse Osmosis Membranes in Oil/Water Separation

4.1 SUMMARY

A commercial polyamide reverse osmosis (RO) membrane was surface-modified with polydopamine deposited from buffered, aqueous dopamine solution at ambient conditions. The influence of various modification conditions (i.e., dopamine solution concentration, polydopamine deposition time, and initial pH of Tris-HCl buffer) on pure water flux, flux during filtration of an oil/water emulsion, and NaCl rejection was investigated. Dead-end filtration results showed decreased pure water flux with increasing dopamine solution concentration and polydopamine deposition time. Membranes modified at a pH of 5 exhibited no change in pure water flux or flux during fouling experiments compared to the native membranes, suggesting that polydopamine was not deposited under such acidic coating conditions. All polydopamine-modified membranes, except those coated at a pH of 5, had higher flux when filtering an oil/water emulsion than that of unmodified membranes. NaCl rejection values in all membranes were within the manufacturer's specification. The increased flux when filtering an oil/water emulsion was not sensitive to dopamine concentration, coating time greater than 60 minutes, or alkaline buffer pH value. Short deposition times slightly reduced the fouling resistance of coated membranes, and membranes modified at acidic pH values showed no improvement in fouling.

4.2 RESULTS AND DISCUSSION

4.2.1 Effect of Dopamine Concentrations Used in Membrane Modification on Contact Angle

Table 4.1 presents static contact angles of XLE RO membranes modified using solutions of varying dopamine concentration. The contact angle of an unmodified membrane is included for comparison. The polydopamine deposition time was 60 minutes, and the initial pH of the Tris-HCl buffer was 8.8 in all cases. Because a hydrophobic oil droplet was brought into contact with the sample in an aqueous environment, small contact angles are indicative of a hydrophilic surface. All modified membranes and the unmodified membrane exhibited contact angle values of approximately 19°. For many hydrophobic materials, including polymers used for membrane preparation, polydopamine surface treatment increases hydrophilicity of the coated surfaces, which is typically seen as a decrease in contact angle in experiments such as ours [1-6]. The hydroxyl, carboxylic acid, and amine functional groups of polydopamine are thought to contribute to the hydrophilicity of coated surfaces [3, 6, 7]. However, on membranes that are already hydrophilic, such as XLE RO and hydrophilized PVDF microfiltration membranes, McCloskey et al. observed only minimal changes in contact angle upon polydopamine treatment [1]. The selective polyamide layer of the XLE RO membranes used in this study is synthesized via interfacial polymerization of *m*-phenylene diamine with trimesoyl chloride [8]. The polymerization leaves hydrophilic amine and carboxylic acid groups [8] that are likely responsible for the hydrophilic nature of the native membranes. Since the membranes were hydrophilic before polydopamine modification, surface modification with polydopamine did not appreciably change contact angle as measured in this experiment.

Table 4.1: Captive (*n*-decane)-in-water bubble contact angles of XLE RO membranes modified at different dopamine concentrations.

Dopamine concentration (mg/mL)	Contact angle (degree)
0 (unmodified)	20.1 ± 0.8
0.1	19 ± 2
0.5	20 ± 2
2	19 ± 1
4	19 ± 1
8	19 ± 2

Note: All samples were prepared using deposition solutions at an initial pH of 8.8 and a deposition time of 60 minutes.

4.2.2 Effect of Polydopamine Modification Conditions on Pure Water Flux

The pure water flux of membranes modified at varying conditions is presented in Figures 4.1 – 4.3. These measurements were performed in dead-end test cells as described in Chapter 3 (Experimental section). The average water permeance of unmodified membranes was 9.0 ± 0.3 LMH/bar at a transmembrane pressure difference of 150 psi (10.3 bar), which is within the manufacturer's specified water permeance of 6.5 – 9.6 LMH/bar reported by Van Wagner et al. [9].

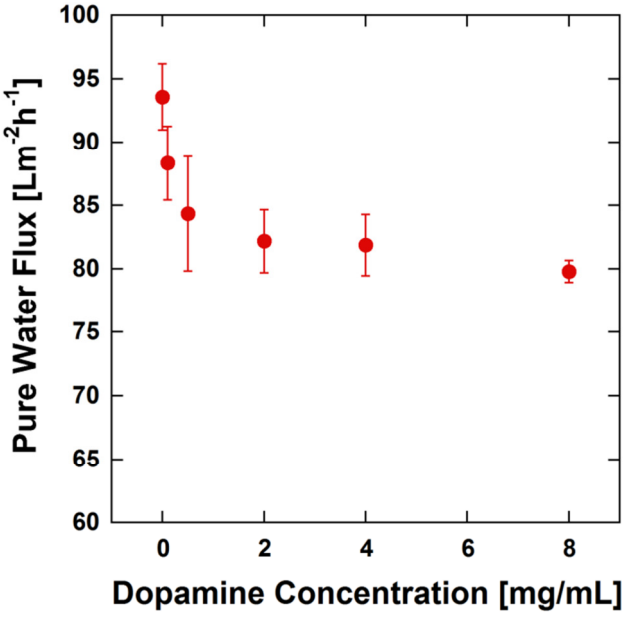

Figure 4.1: Pure water flux as a function of dopamine concentration. The dopamine deposition time was 60 minutes, and the Tris-HCl buffer was at an initial pH of 8.8.

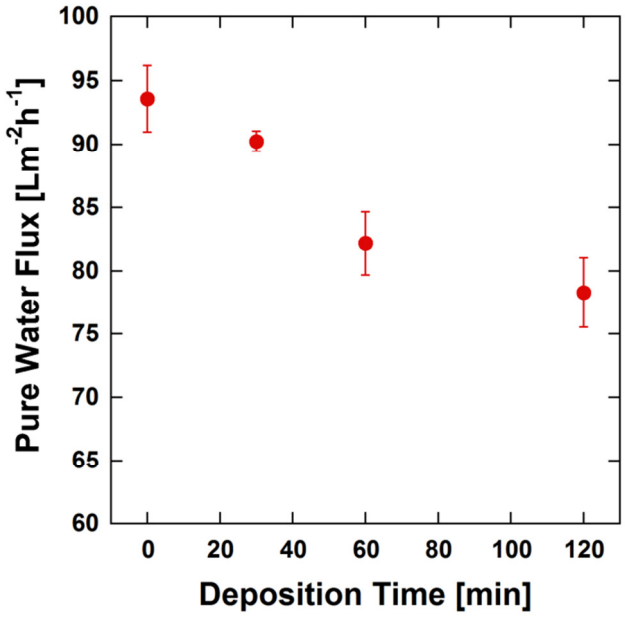

Figure 4.2: Pure water flux as a function of polydopamine deposition time. The dopamine deposition solution concentration was 2 mg/mL, and the Tris-HCl buffer was at an initial pH of 8.8.

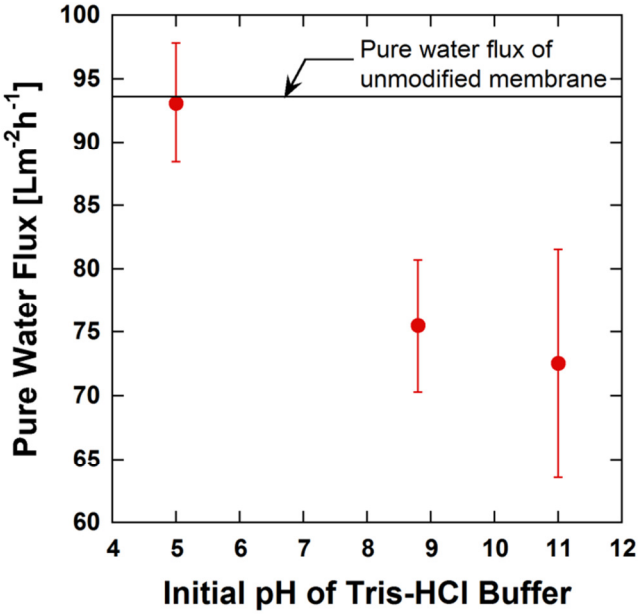

Figure 4.3: Pure water flux as a function of Tris-HCl buffer initial pH. The dopamine deposition solution concentration was 2 mg/mL, and the dopamine deposition time was 60 minutes.

Figure 4.1 presents pure water flux of unmodified membranes and membranes modified with dopamine concentrations of 0.1, 0.5, 2, 4, and 8 mg/mL (in Tris-HCl buffer at a pH of 8.8 for 60 minutes). As dopamine coating solution concentration increased, water flux decreased somewhat, with the largest decrease occurring at low dopamine concentrations. Figure 4.2 shows pure water flux of unmodified membranes and of membranes modified at polydopamine deposition times of 30, 60, and 120 minutes; these studies were conducted using 2 mg/mL dopamine in Tris-HCl buffer at a pH of 8.8. Water flux decreased with increasing polydopamine deposition time. Several previous studies demonstrated that the polydopamine film thickness increases at higher dopamine concentration in the deposition solution [10-12] or with longer deposition time [1, 2, 4, 10-12]. Also, the polydopamine coating growth rate [11] and dopamine reaction rate [13] increase with dopamine concentration. Our results corroborate McCloskey et

al.'s findings in that the pure water flux of polydopamine-modified XLE RO membranes decreased relative to that of unmodified XLE RO membranes as deposition time increased [1]. Thicker polydopamine coatings, which result from high dopamine concentrations or long deposition times, were likely responsible for the reduced pure water flux observed in these experiments.

Figure 4.3 presents pure water flux of membranes modified with Tris-HCl buffer at initial pH values of 5, 8.8, and 11. The concentration of dopamine was 2 mg/mL, and the deposition time was 60 minutes. The unmodified membrane pure water flux is represented by the horizontal line. The pure water flux of membranes modified at a pH of 5 was nearly identical to that of unmodified membranes. The membranes modified under alkaline conditions (i.e., at initial pH values of 8.8 and 11) exhibited lower flux values than those modified at a pH of 5 or not modified at all. Interestingly, the pH of the coating solution (dopamine in Tris-HCl buffer) remained constant throughout the 60-minute contact time of the solution with the membrane when the buffer initial pH was 5 or 8.8. When the initial pH of the buffer was 11, the pH of the coating solution decreased to 8.8 after the dopamine had been mixed in Tris-HCl buffer for about 15 seconds. The pure water flux of the membranes treated at a pH of 11 was, therefore, similar to the pure water flux of the membrane modified at a pH of 8.8. Previous studies suggest that dopamine polymerization begins with oxidation of the catechol moiety to a quinone [2, 3, 6, 12, 14-16]. A study on DOPA, the amino acid closely related to dopamine and largely responsible for the adhesive qualities of mussel byssus protein, suggested that oxidation of DOPA enhances its adhesion to organic surfaces (e.g., polymers) [17]. Alkaline pH enables rapid oxidation as the catechol/quinone equilibrium (pK_a = 9.2) favors the quinone [17]. Dopamine polymerization has been reported to proceed under acidic conditions only with the addition of oxidants (e.g., ammonium persulfate); under ambient

atmosphere with oxygen present as the sole oxidant, dopamine polymerization does not proceed appreciably at acidic pH, which is consistent with the results shown in Figure 4.3 [18].

4.2.3 Effect of Polydopamine Modification Conditions on NaCl Rejection

Apparent, R_{app}, and true, R_{true}, NaCl rejection values during filtration of 2,000 ppm NaCl feed are shown in Figure 4.4. Figure 4.4(a) and Figure 4.4(b), which show results from membranes modified at various dopamine concentrations and deposition times, respectively, demonstrate that rejection generally decreased slightly with increasing dopamine solution concentration and polydopamine deposition time. Figure 4.4(c) shows that true rejection was somewhat lower for membranes modified at alkaline conditions than for unmodified membranes and membranes modified at a pH of 5. Membranes modified at a pH of 5 exhibited essentially the same rejection as unmodified membranes.

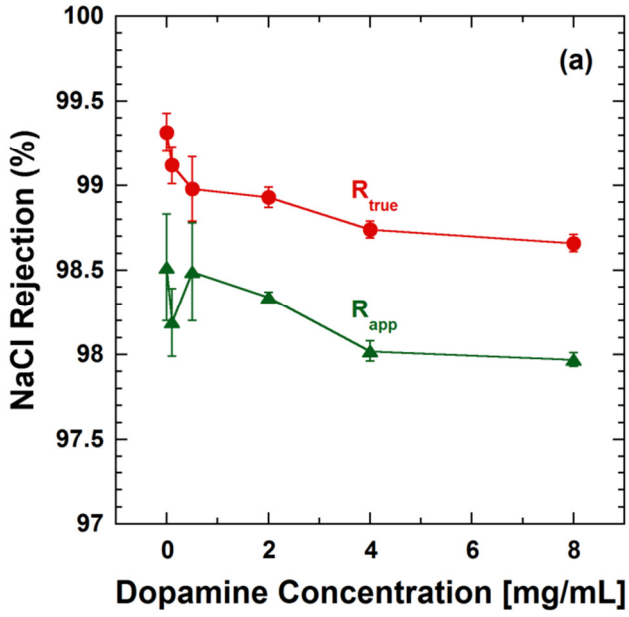

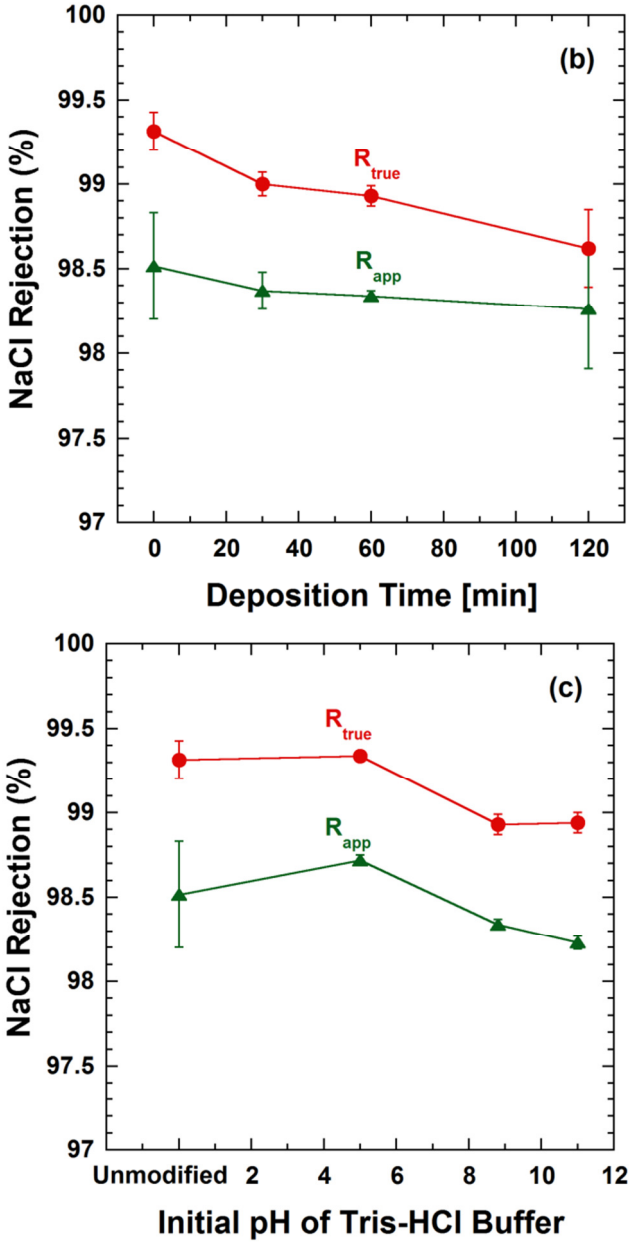

Figure 4.4: Apparent NaCl rejections and true NaCl rejections of XLE RO membranes from 2,000 ppm NaCl feed as a function of polydopamine modification conditions: (a) dopamine concentration, (b) polydopamine deposition time, and (c) initial pH of Tris-HCl buffer.

Several possibilities may explain the observed results. First, a slight reduction in surface charge from polydopamine coatings, as reported by McCloskey et al. [19], may

contribute to decreased salt rejection. Second, as described by Sagle et al. using a series-resistance model, coating a high salt rejection RO membrane with a lower rejection surface coating could reduce salt rejection [20]. Third, the polydopamine coating may penetrate the selective polyamide layer of the membranes, slightly altering the transport properties of the polyamide. Although a systematic decrease in true NaCl rejection with increasing dopamine concentration and deposition time was observed, the effect was small enough that all measured NaCl rejection values fall within the manufacturer's specified NaCl rejection range (>98%) [21]. Therefore, while the polydopamine modification may result in some reduction in true NaCl rejection, the effect is small, so polydopamine modification had little effect on NaCl rejection of these reverse osmosis membranes.

4.2.4 Effect of Polydopamine Modification Conditions on Permeate Flux during Oil/Water Emulsion Crossflow Filtration

Table 4.2 shows organic rejection values of unmodified XLE RO membranes and polydopamine-modified XLE RO membranes (prepared by using 2 mg/mL dopamine concentration, 60 minutes deposition time, and Tris-HCl buffer at a pH of 8.8). The rejection values were taken at the beginning and at the end (24 hours) of oil/water emulsion crossflow filtration. In all cases, the organic rejection values were more than 99.9% which indicates that these membranes are suitable for oil/water separation.

Table 4.2: Organic rejection values of unmodified and polydopamine-modified XLE RO membranes at the beginning and end (24 hours) of oil/water emulsion crossflow filtration.

Membrane modification	**Organic rejection (%)**	
	Beginning	**End**
Unmodified	99.91 ± 0.01	99.95 ± 0.02
Polydopamine-modified	99.91 ± 0.05	99.9 ± 0.1

Note: Polydopamine-modified membranes were prepared using deposition solutions at 2 mg/mL dopamine concentration, an initial pH of 8.8, and a deposition time of 60 minutes.

Figure 4.5 presents permeate flux during oil/water emulsion crossflow filtration with XLE RO membranes modified at various: (a) dopamine coating solution concentrations (0.1, 0.5, 2, 4, and 8 mg/mL in Tris-HCl buffer at a pH of 8.8 for 60 minutes), (b) deposition times (30, 60, and 120 minutes with 2 mg/mL of dopamine in Tris-HCl buffer at a pH of 8.8), and (c) initial pH values of Tris-HCl buffer (5, 8.8, and 11 with 2 mg/mL of dopamine solution for 60 minutes). These figures also include results on unmodified membranes for comparison.

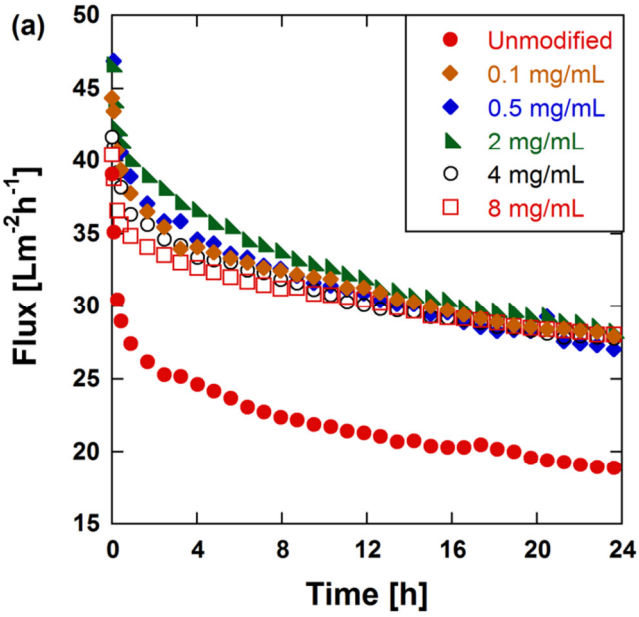
(a)
Unmodified
0.1 mg/mL
0.5 mg/mL
2 mg/mL
4 mg/mL
8 mg/mL
Flux [Lm-2h-1]
Time [h]
50
45
40
35
30
25
20
15
0
4
8
12
16
20
24

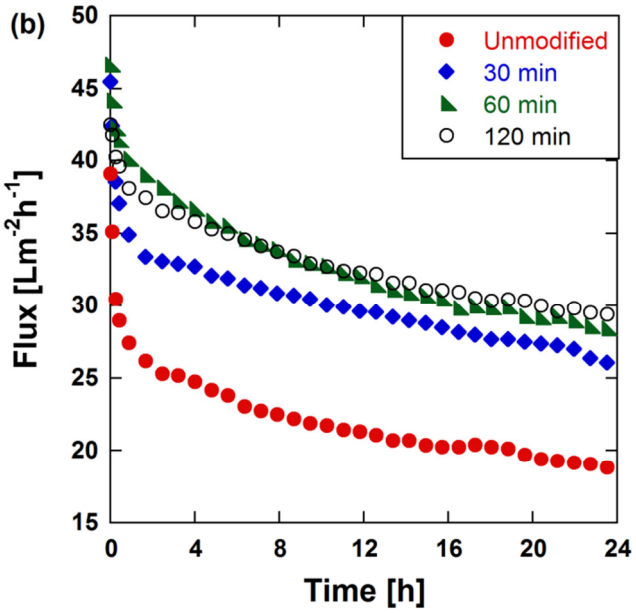
(b)
Unmodified
30 min
60 min
120 min
Flux [Lm-2h-1]
Time [h]
50
45
40
35
30
25
20
15
0
4
8
12
16
20
24

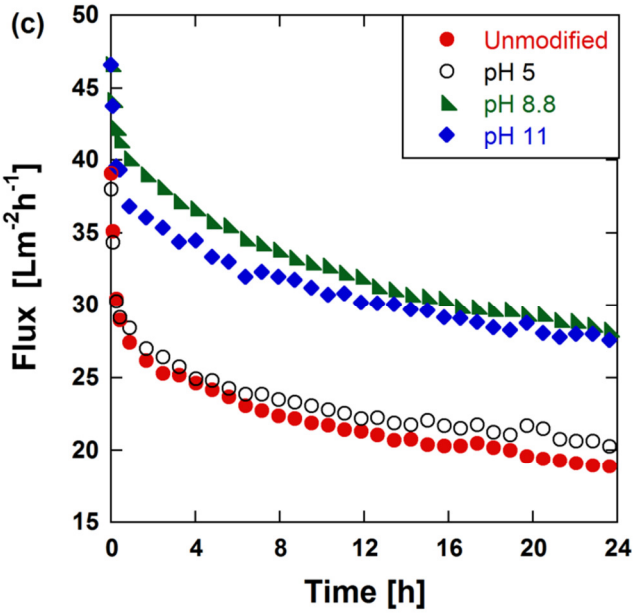

Figure 4.5: Permeate flux as a function of time during oil/water emulsion crossflow filtration of XLE RO membranes modified with varied (a) dopamine concentrations, (b) polydopamine deposition times, and (c) initial pH values of Tris-HCl buffer.

Figure 4.5(a) presents the fouling behavior of membranes modified with various dopamine solution concentrations. All modified membranes exhibited higher flux than unmodified membranes, but increasing the dopamine concentration did not further increase flux, particularly at longer filtration times. Although a decrease in pure water flux was observed with increasing dopamine concentration (as shown in Figure 4.1), this did not result in lower flux during filtration of oily water. Thus, a large contribution to mass transfer resistance during fouling was likely to be foulant accumulation on the membrane surface; the changes in mass transfer resistance observed in the pure water flux test due to the polydopamine coating are masked by the mass transfer resistance of adsorbed foulants. For this reason, variations in the dopamine concentration did not produce systematic changes in the permeate flux during fouling.

As shown in Figure 4.5(b), membranes modified for 30, 60, and 120 minutes all exhibited higher flux than unmodified membranes. The membranes modified for 30 minutes showed a slightly lower permeate flux throughout the fouling experiment than those prepared at deposition times of 60 and 120 minutes. Previous studies reported that polydopamine film thickness decreases with shorter deposition times [1, 2, 4, 10-12], and at short coating times, less polydopamine may present on the coated substrate surface relative to that obtained following longer coating times [22]. Therefore, the membranes modified for 30 minutes showed less fouling resistance than those prepared using deposition times of 60 and 120 minutes. Increasing the deposition time from 60 minutes to 120 minutes did not significantly improve the fouling resistance of the modified membranes, leading to the same permeate flux at extended filtration time.

From Figure 4.5(c), membranes modified at alkaline conditions (i.e., at initial pH values of 8.8 and 11) had higher flux than unmodified membranes. Membranes modified at a pH of 5 showed no enhancement in flux over that of unmodified membranes. As noted previously, dopamine oxidation, an initial step in dopamine polymerization, proceeds very slowly under acidic conditions at ambient conditions [18]. Membranes modified at a pH of 5, therefore, were likely not successfully coated with polydopamine, and they showed no improvement in flux during fouling tests relative to that of unmodified membranes. Polydopamine formation occurs readily at alkaline pH [4, 13, 17, 18]; membranes modified with dopamine coating solution by using Tris-HCl buffer at initial pH values of 8.8 and 11 exhibited improved flux values during oily water filtration. Modification at both alkaline coating conditions (i.e., initial pH values of 8.8 and 11) appeared to lead to similar polydopamine coatings on the membranes, as judged by their similar flux values in the fouling experiment. This result is consistent with pure water

flux data reported in Figure 4.3, since pure water flux values for membranes modified at initial pH values of 8.8 and 11 are essentially indistinguishable from each other.

Membrane surface modification to decrease roughness has been associated with reduced membrane fouling in many studies [23, 24]. McCloskey et al. reported a slight decrease in the surface roughness of polydopamine-modified XLE RO membranes relative to unmodified membranes [19]. The decrease in surface roughness from polydopamine coatings may contribute to improvement of modified membrane fouling resistance. Additionally, an increase in surface hydrophilicity has been suggested to reduce organic fouling, such as that from oil emulsions [25-27]. Although we did not see increased hydrophilicity of the modified membranes over that of unmodified membranes via our contact angle experiments, perhaps the technique we used was not sensitive to small or subtle changes in hydrophilicity which may also help alleviate membrane fouling. However, a complete understanding of the cause for the observed increase in fouling performance is not yet available, and further studies are needed to more completely understand this phenomenon.

4.3 CONCLUSIONS

XLE RO membranes were modified with polydopamine using various dopamine concentrations, polydopamine deposition times, and Tris-HCl buffer initial pH. The pure water flux of coated membranes decreased with increasing dopamine concentration and deposition time, presumably because the polydopamine coating layer thickness increased. Membranes modified at a pH of 5 exhibited no change in pure water flux or fouling resistance relative to unmodified membranes, suggesting that polydopamine was not successfully deposited onto the membranes under acidic conditions. Membranes modified with polydopamine at all dopamine concentrations, deposition times, and alkaline pH

values were significantly more resistant to fouling in oil/water emulsion fouling tests than uncoated membranes, as judged by higher permeate flux values when filtering oil/water emulsions. Additionally, they maintained salt rejection values within the manufacturer's specification. Variations in dopamine concentration, deposition times of at least 60 minutes, and alkaline pH values had little effect on the fouling resistance of coated membranes, suggesting that the mass transfer resistance of the polydopamine coating was insignificant relative to that of the foulant layer.

4.4 REFERENCES

[1] B.D. McCloskey, H.B. Park, H. Ju, B.W. Rowe, D.J. Miller, B.J. Chun, K. Kin, B.D. Freeman, Influence of polydopamine deposition conditions on pure water flux and foulant adhesion resistance of reverse osmosis, ultrafiltration, and microfiltration membranes, Polymer 51 (2010) 3472–3485.

[2] H. Lee, S.M. Dellatore, W.M. Miller, P.B. Messersmith, Mussel-inspired surface chemistry for multifunctional coatings, Science 318 (2007) 426–430.

[3] Z. Xi, Y. Xu, L. Zhu, Y. Wang, B. Zhu, A facile method of surface modification for hydrophobic polymer membranes based on the adhesive behavior of poly(DOPA) and poly(dopamine), Journal of Membrane Science 327 (2009) 244–253.

[4] B. Li, W. Liu, Z. Jiang, X. Dong, B. Wang, Y. Zhong, Ultrathin and stable active layer of dense composite membrane enabled by poly(dopamine), Langmuir 25 (2009) 7368–7374.

[5] S. Azari, L. Zou, Using zwitterionic amino acid L-DOPA to modify the surface of thin film composite polyamide reverse osmosis membranes to increase their fouling resistance, Journal of Membrane Science 401–402 (2012) 68–75.

[6] J. Jiang, L. Zhu, X. Li, Y. Xu, B. Zhu, Surface modification of PE porous membranes based on the strong adhesion of polydopamine and covalent immobilization of heparin, Journal of Membrane Science 364 (2010) 194–202.

[7] L. Zhu, J. Yu, Y. Xu, Z. Xi, B. Zhu, Surface modification of PVDF porous membranes via poly(DOPA) coating and heparin immobilization, Colloids and Surfaces B: Biointerfaces 69 (2009) 152–155.

[8] E.M. Van Wagner, A.C. Sagle, M.M. Sharma, Y.-H. La, B.D. Freeman, Surface modification of commercial polyamide desalination membranes using

poly(ethylene glycol) diglycidyl ether to enhance membrane fouling resistance, Journal of Membrane Science 367 (2011) 273–287.

[9] E.M. Van Wagner, A.C. Sagle, M.M. Sharma, B.D. Freeman, Effect of crossflow testing conditions, including feed pH and continuous feed filtration, on commercial reverse osmosis membrane performance, Journal of Membrane Science 345 (2009) 97–109.

[10] J. Jiang, L. Zhu, L. Zhu, B. Zhu, Y. Xu, Surface characteristics of a self-polymerized dopamine coating deposited on hydrophobic polymer films, Langmuir 27 (2011) 14180–14187.

[11] J. Ou, J. Wang, S. Liu, J. Zhou, S. Ren, S. Yang, Microtribological and electrochemical corrosion behaviors of polydopamine coating on APTS-SAM modified Si substrate, Applied Surface Science 256 (2009) 894–899.

[12] F. Pan, H. Jia, S. Qiao, Z. Jiang, J. Wang, B. Wang, Y. Zhong, Bioinspired fabrication of high performance composite membranes with ultrathin defect-free skin layer, Journal of Membrane Science 341 (2009) 279–285.

[13] C. Foppoli, R. Coccia, C. Cini, M.A. Rosei, Catecholamines oxidation by xanthine oxidase, Biochimica et Biophysica Acta 1334 (1997) 200–206.

[14] D.R. Dreyer, D.J. Miller, B.D. Freeman, D.R. Paul, C.W. Bielawski, Elucidating the structure of poly(dopamine), Langmuir 28 (2012) 6428–6435.

[15] H. Lee, J. Rho, P.B. Messersmith, Facile conjugation of biomolecules onto surfaces via mussel adhesive protein inspired coatings, Advanced Materials 21 (2009) 431–434.

[16] F. Yu, S. Chen, Y. Chen, H. Li, L. Yang, Y. Chen, Y. Yin, Experimental and theoretical analysis of polymerization reaction process on the polydopamine membranes and its corrosion protection properties for 304 stainless steel, Journal of Molecular Structure 982 (2010) 152–161.

[17] H. Lee, N.F. Scherer, P.B. Messersmith, Single-molecule mechanics of mussel adhesion, Proceedings of the National Academy of Sciences of the United States of America 103 (2006) 12999–13003.

[18] Q. Wei, F. Zhang, J. Li, B. Li, C. Zhao, Oxidant-induced dopamine polymerization for multifunctional coatings, Polymer Chemistry 1 (2010) 1430–1433.

[19] B.D. McCloskey, Novel surface modifications and materials for fouling resistant water purification membranes, PhD thesis, University of Texas at Austin, 2009.

[20] A.C. Sagle, E.M. Van Wagner, H. Ju, B.D. McCloskey, B.D. Freeman, M.M. Sharma, PEG-coated reverse osmosis membranes: Desalination properties and fouling resistance, Journal of Membrane Science 340 (2009) 92–108.

[21] DOW Water & Process Solutions XLE-440 Product Specification, http://www.dowwaterandprocess.com/products/membranes/xle_440.htm

[22] Y.M. Shin, Y.B. Lee, H. Shin, Time-dependent mussel-inspired functionalization of poly(L-lactide-co-ε-caprolactone) substrates for tunable cell behaviors, Colloids and Surfaces B: Biointerfaces 87 (2011) 79–87.

[23] E.M. Vrijenhoek, S. Hong, M. Elimelech, Influence of membrane surface properties on initial rate of colloidal fouling of reverse osmosis and nanofiltration membranes, Journal of Membrane Science 188 (2001) 115–128.

[24] M. Elimelech, X. Zhu, A.E. Childress, S. Hong, Role of membrane surface morphology in colloidal fouling of cellulose acetate and composite aromatic polyamide reverse osmosis membranes, Journal of Membrane Science 127 (1997) 101–109.

[25] J.S. Louie, I. Pinnau, I. Ciobanu, K.P. Ishida, A. Ng, M. Reinhard, Effects of polyether-polyamide block copolymer coating on performance and fouling of reverse osmosis membranes, Journal of Membrane Science 280 (2006) 762–770.

[26] P. Le-Clech, V. Chen, T.A.G. Fane, Fouling in membrane bioreactors used in wastewater treatment, Journal of Membrane Science 284 (2006) 17–53.

[27] J. Gilron, S. Belfer, P. Vaisanen, M. Nystrom, Effects of surface modification on antifouling and performance properties of reverse osmosis membranes, Desalination 140 (2001) 167–179.

Chapter 5: Influence of Polydopamine Deposition Conditions on Hydraulic Permeability and Sieving Coefficients for a Polysulfone Ultrafiltration Membrane

5.1 SUMMARY

Membrane surface modification with polydopamine (PDA) coatings can reduce fouling in oily water filtration due, at least in part, to enhanced surface hydrophilicity. In this study, polysulfone (PSf) UF membranes were coated with PDA. PDA coating conditions (solution concentration and deposition time) were varied, and the effect of coating conditions on membrane molecular weight cutoff (MWCO) and hydraulic permeability was measured. Membrane MWCO decreased and PDA film thickness increased as initial dopamine coating solution concentration or deposition time increased. The MWCO decrease confirmed that PDA restricted the membrane pores. While the PDA coating thickness on membrane surfaces grew progressively with increasing initial dopamine concentration or coating time, coating inside the membrane pores was limited by the finite membrane pore size. A tradeoff between selectivity and hydraulic permeability of unmodified and PDA-modified membranes was noted. This tradeoff is reminiscent of that observed in other separation membranes. Zydney's hindered solute transport model of flow through porous membranes was used to estimate changes in membrane mean pore size and pore size distribution. Based on the modelling results, membrane mean pore radius, $\bar{r}$, increased at low initial dopamine concentrations or short deposition times and decreased at high initial dopamine concentrations or long deposition times with increasing initial dopamine concentration or increasing PDA coating time. The pore size distribution narrowed as the membranes were modified with PDA. The porosity to thickness ratio of PDA-modified membranes remained unchanged or was only slightly higher than that of unmodified membranes.

5.2 Results and Discussion

5.2.1 Polydopamine (PDA) Surface Coating Thickness

PDA was coated on nonporous PSf dense films. PSf film thicknesses were in the range of 160 – 170 nm. The PDA coating thicknesses determined by spectroscopic ellipsometry are presented in Figure 5.1. The PDA surface coating thickness increased with increasing initial dopamine concentration and increasing deposition time. These trends correspond qualitatively to similar data reported by others [1-10]. The surface coating thickness was less than 10 nm at 0.1 mg/mL initial dopamine concentration for all deposition times studied. At the most aggressive modification condition (i.e., at 8 mg/mL initial dopamine concentration and 240 minutes coating time), the PDA surface coating thickness was nearly 50 nm.

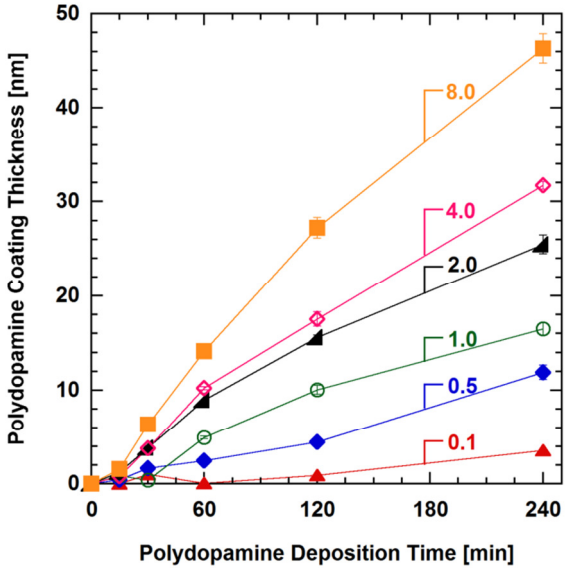

Figure 5.1: PDA coating thickness on dense PSf films (measured by ellipsometry) as a function of PDA deposition time and initial dopamine concentration. Numbers noted in the plot represent initial dopamine coating solution concentration in mg/mL.

The thickness of PDA coatings has been evaluated on many substrates, both inorganic and organic [1-10]. Regardless of the substrate material, PDA coating thickness reportedly increases as initial dopamine coating solution concentration increases [5, 6, 8, 9] or deposition time increases [1-4, 6-10]. Table 5.1 summarizes literature reports of PDA coating thickness on various substrates. All data shown are at an initial dopamine concentration of 2 mg/mL and a deposition time of 4 hours. Unless otherwise noted, these studies were performed at ambient conditions. The reported thicknesses varied from 2 to 45 nm even though the initial dopamine coating solution concentration and deposition time were the same. There was no obvious correlation of coating thickness with either buffer concentration or buffer solution pH. The reported thickness values were different even for studies using the same substrate, Tris buffer concentration, and thickness measurement technique (i.e., Ball et al., 2012 [5] and Bernsmann et al., 2009 [11]). Most of these studies did not report detailed stirring conditions of the coating solution during PDA deposition. However, because oxygen is required to convert dopamine to PDA [12-16], variations in dissolved oxygen content in the PDA coating solution due to different stirring conditions could influence deposition thickness. Although this hypothesis concerning the variability in literature reports cannot be definitively tested using the data in Table 5.1, it is one potential avenue for future studies.

Table 5.1: Summary of reported PDA deposition thicknesses on various substrates using 2 mg/mL initial dopamine coating solution concentration and 4 hours of deposition time.

Reference	Substrate	Tris buffer concentration (mM)	Tris buffer pH	Thickness measurement technique	PDA deposition thickness (nm)
This study	PSf-coated Si	15	8.8	Ellipsometry	25
Ball et al., 2012 [5]	Si	50	8.5	Ellipsometry	8
Jiang et al., 2011 [6]	Si	10	8.5	Ellipsometry	7*
Jiang et al., 2011 [6]	PVDF-coated Si	10	8.5	Ellipsometry	22*
McCloskey et al., 2010 [2]	PSf-coated Si	15	8.8	Ellipsometry	45
Pan et al., 2009 [9]	Si	100	9.4	Stylus profiler	38
Bernsmann et al., 2009 [11]	Si	50	8.5	Ellipsometry	2
Li et al., 2009 [10]	Si	N/A	8.5	Stylus profiler	26
Lee et al., 2007 [1]	Si	10	8.5	Atomic Force Microscopy	25

Note: All PDA deposition thickness values were extracted from plots reported in the literature using UN-SCAN-IT 6.0 software. * PDA modification at 30^{o}C.

5.2.2 Pure Water Permeance

The influence of initial dopamine coating solution concentration and deposition time on pure water permeance of PS-20 UF membranes is presented in Figure 5.2(a) and Figure 5.2(b), respectively. PDA coating thicknesses, determined using ellipsometry on dense PSf films coated with PDA under identical conditions, are also included in Figure 5.2. The pure water permeance of PDA-modified membranes decreased with increasing initial dopamine coating solution concentration or with increasing deposition time. This decrease in pure water permeance was presumably due to the growth of increasingly thick PDA coatings and, also, pore narrowing and pore blockage [2, 3]. However, the pure water permeance values of membranes modified with PDA at low initial dopamine

concentrations (i.e., 0.1 and 0.5 mg/mL) or short coating time (i.e., 15 minutes) remained near those of unmodified membranes, possibly because of relatively thin PDA coatings at these coating conditions. A significant pure water permeance decrease was observed at moderate initial dopamine concentrations or moderate deposition times, but the decrease was more gradual at high initial dopamine concentrations or long deposition times. The PDA coating thickness changed more gradually at more extensive PDA coating conditions and reached a plateau at long coating times [2]. Perhaps the gradual change in PDA coating thickness led to slower pure water permeance reduction at extensive PDA modification conditions. Similar trends in pure water flux or hydraulic permeability of unmodified and PDA-modified UF and RO membranes were observed by Miller et al. [17], McCloskey et al. [2], and Cheng et al. [3].

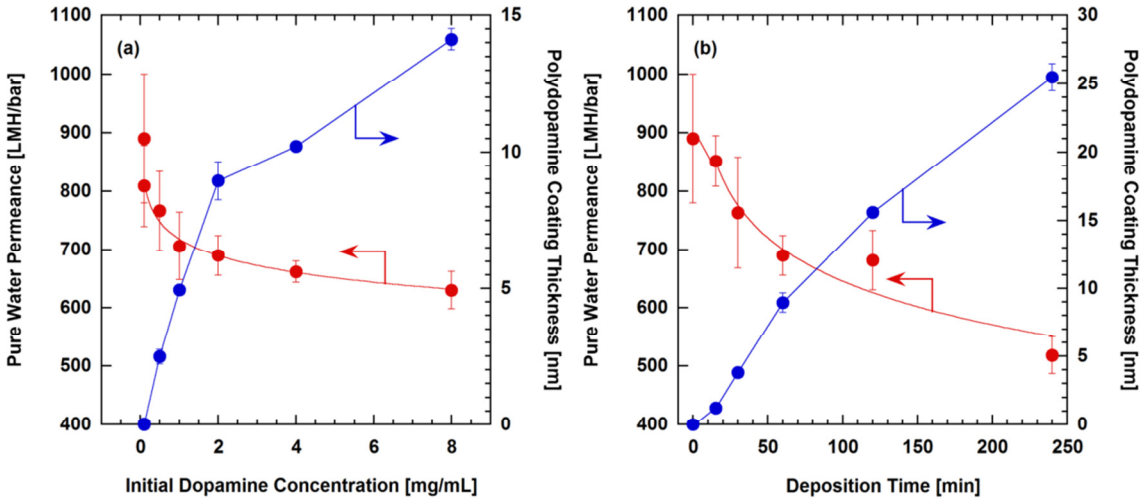

Figure 5.2: Influence of: (a) initial dopamine coating solution concentration and (b) PDA deposition time on pure water permeance of PDA-modified UF membranes (PS-20) and PDA coating thickness on dense PSf film measured by ellipsometry. A deposition time of 60 minutes was used in (a) and an initial dopamine concentration of 2 mg/mL was used in (b). The lines are to guide the eye.

5.2.3 Molecular Weight Cutoff and Nominal Pore Size

In this study, the molecular weight cutoff (MWCO) was defined as the molecular weight of PEG for which the actual membrane rejection was 90% in the ASTM MWCO test [18-22]. The ASTM standard assumes no polarization during the filtration tests, so the observed rejection is directly used to determine the MWCO. However, when concentration polarization is significant, the observed rejection, R_o, is lower than the actual rejection, R_a, and the MWCO value determined from the R_o curve can be significantly higher than the MWCO determined from the R_a curve [23]. Causserand et al. estimated the R_a values from the R_o values, using a stagnant film model (with average k and J_v), and compared the retention profiles and MWCO values from these two cases [23]. In their study, the MWCO was overestimated when the R_o was used directly, and thus, the R_a instead should be used to determine the true MWCO since the R_a values represent the true selective properties of the membranes [23]. Our MWCO analysis followed an approach proposed by Causserand et al., so the R_a values of PEG were calculated and used to determine the MWCO in our study.

Unless a filtration is conducted at very low Peclet number, where R_a is equal to R_o, the actual rejection may not be reflected in the observed MWCO values. Several studies proposed Peclet number ranges in the membrane boundary layer (i.e., $Pe_{BL} = \overline{J}_V / \overline{k}$) where concentration polarization could be neglected (and, therefore, $R_a \approx R_o$). These proposed ranges are: (i) $0.405 < \overline{J}_V / \overline{k} < 0.693$, (ii) $\overline{J}_V / \overline{k} < 1$, and (iii) $\overline{J}_V / \overline{k} < 0.18$ [24]. In general, $\overline{J}_V / \overline{k}$ increases with increasing PEG molecular weight due to decreased PEG diffusivity (which decreases $\overline{k}$) of larger PEG molecules [23]. In this study, although $\overline{J}_V / \overline{k}$ was small (less than 1) for most PEGs (4 – 35 kDa), $\overline{J}_V / \overline{k}$ was greater than 1 for 100 and 200 kDa PEGs. Thus, concentration polarization could not be neglected, at least for the highest molecular weight PEGs considered.

A stagnant film model, Equation (2.12), with $\overline{k}$ calculated using Equation (2.28) was used to estimate S_a values of PEG from the experimental S_o values acquired from the MWCO filtration tests. Percent actual PEG rejection ($\%R_a = R_a \times 100$) was calculated from S_a using Equation (2.10). The concentration polarization model (i.e., stagnant film model) was mainly used with $\overline{k}$ and $\overline{J}_v$ in this MWCO determination, following Causserand et al.'s study [23]. This model was also used with radially-dependent k and J_v ($k(r_c)$ and $J_v(r_c)$) in the mean pore size and pore size distribution analysis, and the results were compared with those obtained using $\overline{k}$ and $\overline{J}_v$ as discussed later in section 5.2.6.

Figure 5.3 and Figure 5.4 present percent actual PEG rejection values, $\%R_a$, as a function of PEG molecular weight for PS-20 UF membranes modified with PDA at various initial dopamine coating solution concentrations and deposition times, respectively. MWCO values were determined from the PEG molecular weights that gave 90% R_a values in Figure 5.3 and Figure 5.4. These values estimated by interpolating between the two PEG molecular weights closest to an R_a value of 90%, are recorded in Table 5.2 and Table 5.3. Moreover, the steepness of the PEG rejection curves qualitatively reflects the width of the membrane pore size distribution [25-28]. A steeper slope suggests a narrower pore size distribution [25-28]. For membranes modified at higher initial dopamine coating solution concentrations or longer times, the slopes of the rejection curves appear, qualitatively, to be steeper (cf., Figure 5.3 and Figure 5.4) than those of membranes modified at lower initial dopamine coating solution concentrations or shorter times. Thus, more extensive PDA deposition appears to narrow the pore size distribution.

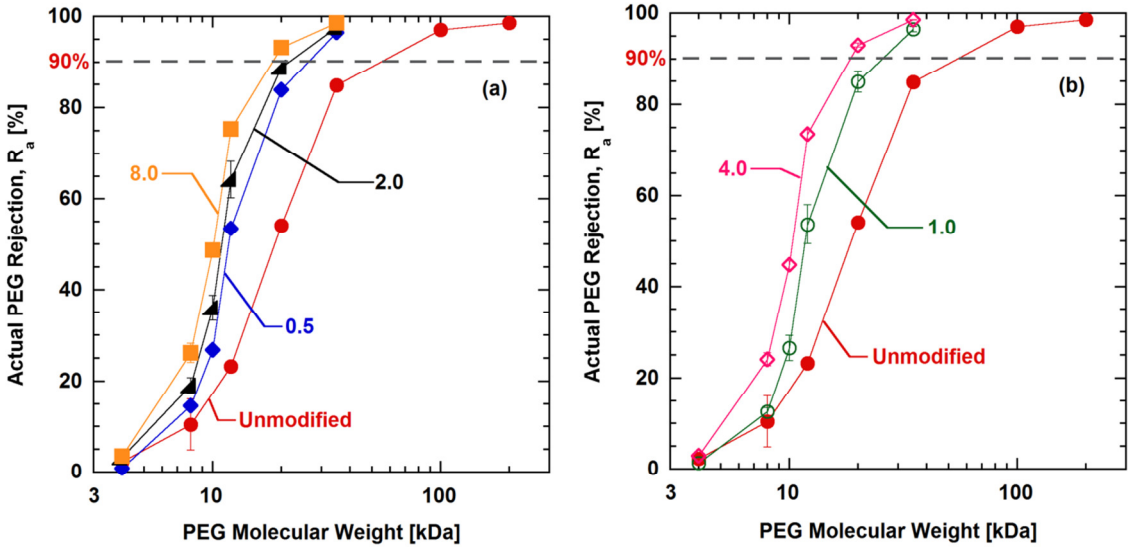

Figure 5.3: Actual rejection values of poly(ethylene glycol) (PEG) as a function of PEG molecular weight for PS-20 UF membranes modified with PDA at various initial dopamine coating solution concentrations. The numbers in (a) and (b) represent initial dopamine concentration in mg/mL. A deposition time of 60 minutes was used. Data are plotted separately in (a) and (b) to permit easier viewing of the rejection curves. The solid and dashed lines are provided to guide the eye.

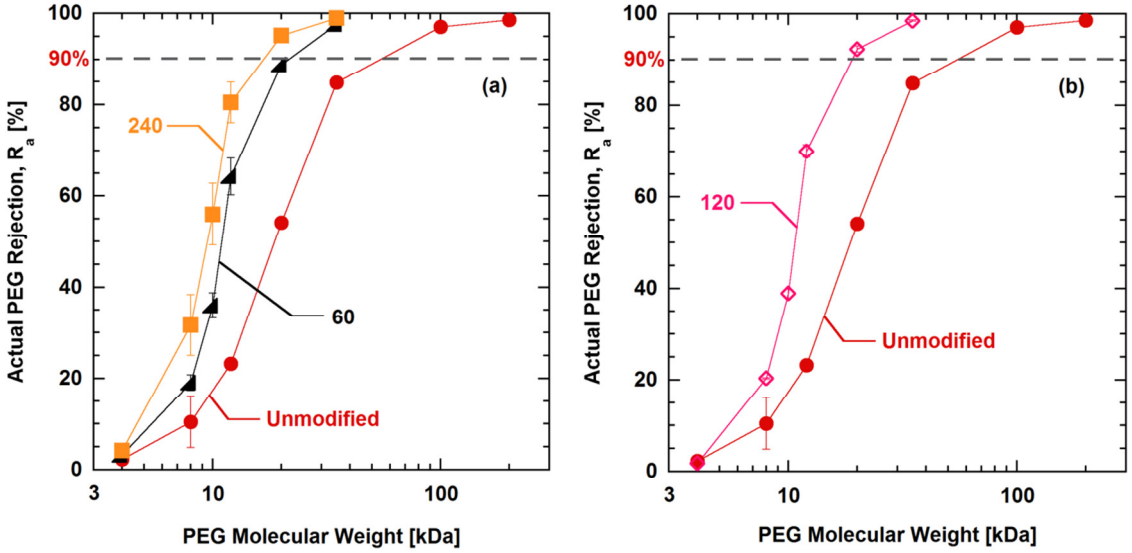

Figure 5.4: Actual rejection values of poly(ethylene glycol) (PEG) as a function of PEG molecular weight for PS-20 UF membranes modified with PDA at various PDA deposition times. The numbers in (a) and (b) represent PDA deposition time in minutes. An initial dopamine concentration of 2 mg/mL was used. Data are plotted separately in (a) and (b) to permit easier viewing of the rejection curves. The solid and dashed lines are provided to guide the eye.

The nominal (or effective) pore sizes of unmodified and PDA-modified membranes are also presented in Table 5.2 and Table 5.3. These values were PEG Stokes radii estimated from the MWCO data using Equation (2.22). One measure of the nominal pore radius of UF membranes is the Stokes radius of a solute molecule with a molecular weight equal to the MWCO value [29]. Others proposed estimation of the nominal membrane pore size from the molecular size of the solute marker [30] or more specifically, its radius of gyration (R_g) [31]. The radius of gyration of PEG is close to its Stokes radius (R_s) ($R_s \approx 0.875R_g$) [32]. In this study, the PEG Stokes radius was used as an approximation of the membrane nominal pore size. Other similar correlations between PEG Stokes radius and molecular weight are reported in the literature, but the values of front factors and exponents on M are somewhat different from those in Equation (2.22)

[32-34]. Using other PEG Stokes radius correlations gives somewhat different values of the nominal pore size, but the relative changes in nominal pore radius of unmodified and PDA-modified membranes remained similar to those reported here.

Table 5.2: Influence of initial dopamine concentration on MWCO, nominal pore radius, PDA coating thickness estimated from changes in MWCO, and PDA coating thickness from ellipsometry on flat dense PSf films.

Initial dopamine concentration (mg/mL)	**MWCO (kDa)**	**Nominal pore radius from MWCO (nm)**	**PDA coating thickness from changes in MWCO (nm)**	**PDA coating thickness from ellipsometry on dense films (nm)**
Unmodified	54±2	7.3±0.2		
0.5	26.2±0.4	4.84±0.04	2.4	2.5 ± 0.3
1	25±2	4.7±0.2	2.5	4.9 ± 0.2
2	21±2	4.3±0.2	2.9	9.0 ± 0.7
4	18.5±0.3	3.98±0.03	3.3	10.2 ± 0.2
8	18.2±0.2	3.95±0.03	3.3	14.1 ± 0.4

Note: All samples (except unmodified membranes) were modified using a PDA deposition time of 60 minutes. Each reported MWCO is an average of MWCO values of three membrane samples, and the uncertainties represent one standard deviation. The uncertainties of nominal pore radius are one standard deviation and were determined from propagation of errors [35].

Table 5.3: Influence of PDA deposition time on MWCO, nominal pore radius, PDA coating thickness estimated from changes in MWCO, and PDA coating thickness from ellipsometry on flat dense PSf films.

Deposition time (minutes)	MWCO (kDa)	Nominal pore radius from MWCO (nm)	PDA coating thickness from changes in MWCO (nm)	PDA coating thickness from ellipsometry on dense films (nm)
Unmodified	54±2	7.3±0.2		
60	21±2	4.3±0.2	2.9	9.0 ± 0.7
120	19.0±0.3	4.04±0.04	3.2	15.6 ± 0.2
240	17±2	3.7±0.2	3.5	25 ± 1

Note: All samples (except unmodified membranes) were modified using an initial dopamine coating solution concentration of 2 mg/mL. Each reported MWCO is an average of MWCO values of three membrane samples, and the uncertainties represent one standard deviation. The uncertainties of nominal pore radius are one standard deviation and were determined from propagation of errors [35].

The MWCO of unmodified PS-20 UF membranes determined in our experiments was 54 kDa, which was higher than that specified by the manufacturer (i.e., 20 kDa). The manufacturer determines the MWCO using constant TMP crossflow filtration of 0.1 wt% aqueous PEG solution at 1.2 gal/min feed flow rate and 30 psig feed pressure [36]. Because their operating conditions, including feed pressure, permeate flow rate, and crossflow filtration mode, were different from those specified by the ASTM standard used in this study, the manufacturer-reported MWCO value may be different from that determined in this study [37, 38]. Variations in TMP and permeate flow rate can lead to differences in observed rejection values and, therefore, different MWCO values [23, 39-41]. Several studies reported a deviation in experimentally determined MWCO values from manufacturers' specifications due to variations in MWCO test conditions [24, 30, 41]. In addition, the membrane manufacturer does not apply a concentration polarization correction to their PEG rejection data, so observed PEG rejections are used to specify the MWCO [36]. In our study, as explained above, a stagnant film model was used to

calculate actual PEG rejections for the MWCO determination. Variations in MWCO values due to concentration polarization corrections have been reported [23].

Based on the results in Table 5.2 and Table 5.3, the MWCO and nominal pore radius of PS-20 UF membranes decrease with increasing initial dopamine coating solution concentration or deposition time. Thus, PDA likely deposits not only on the surface of the membrane but also in its pores, thereby changing membrane pore size and possibly pore size distribution. Therefore, increasing the initial dopamine coating solution concentration or coating time leads to thicker PDA coatings on the membrane surface and to reductions in nominal pore size due to pore narrowing.

PDA coating thicknesses measured by ellipsometry are also presented in Table 5.2 and Table 5.3. The coating thickness estimated from changes in MWCO was calculated by subtracting the nominal pore radius of a PDA-modified membrane from that of an unmodified membrane. A schematic of PDA coating on a PSf surface (estimated via ellipsometry) and the reduction of nominal pore size (estimated from MWCO measurements) is presented in Figure 5.5. PDA thickness values determined from ellipsometry and estimated from MWCO values are plotted for comparison in Figure 5.6.

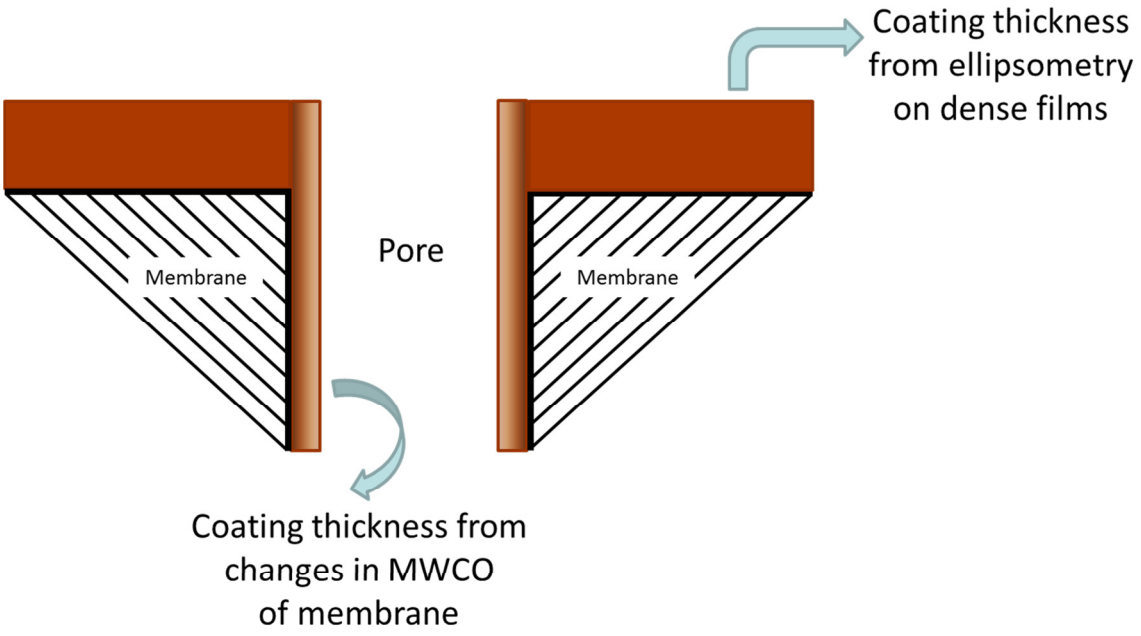

Figure 5.5: A diagram showing PDA coating thickness from ellipsometry on dense film and PDA coating thickness estimated from changes in molecular weight cutoff.

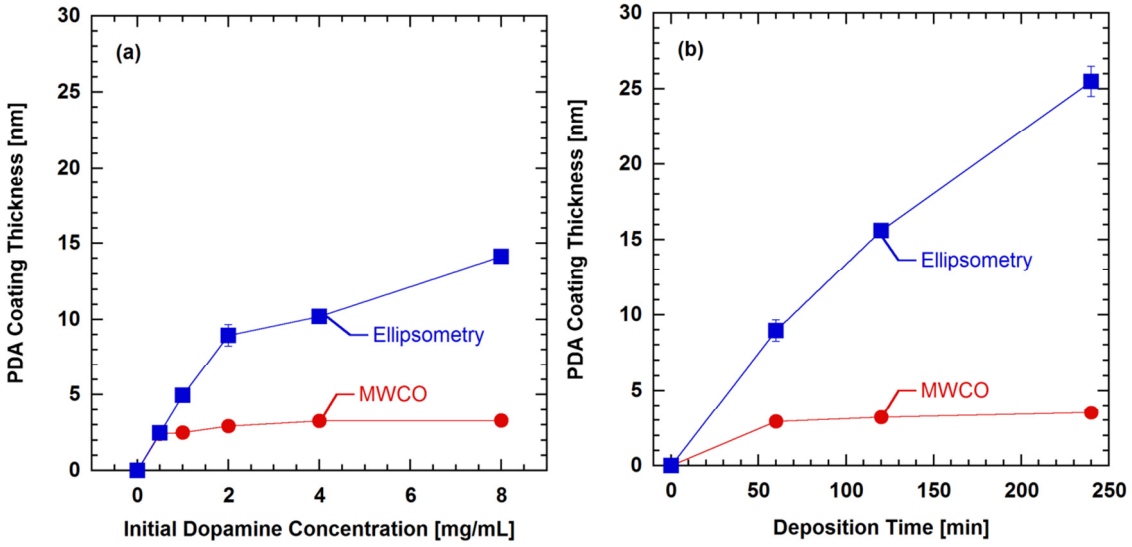

Figure 5.6: Comparison of PDA thickness from ellipsometry measurements on PSf films (■) and PDA thickness estimated from nominal pore size changes from MWCO data (●). A deposition time of 60 minutes was used in (a) and an initial dopamine concentration of 2 mg/mL was used in (b).

Based on Figure 5.6(a) and Figure 5.6(b), the PDA coating thickness on the surface (as characterized by ellipsometry) increased monotonically with increasing initial dopamine concentration or coating time. However, the PDA coating thickness inside the membrane pores (as characterized by pore size changes from MWCO) initially increased at low initial dopamine concentration or deposition time and then reached a plateau. A possible explanation for this phenomenon is that the membrane pore size cannot decrease without limit (i.e., if PDA fills a pore, there can be no further deposition), whereas PDA deposition on the membrane surface is not subject to such a limitation. However, further study is needed to completely understand this phenomenon.

5.2.4 Selectivity and Permeability Tradeoff

To gauge the impact of PDA deposition on the separation properties of membranes coated under various conditions, PEG rejection was measured as a function

of PDA coating conditions. In our study, PEG of very low molecular weight (i.e., 4 kDa PEG) was poorly rejected by the membranes at all coating conditions. PEG samples of high molecular weight were almost completely rejected by PDA-modified membranes (e.g., 35 kDa PEG), and even by uncoated membranes (e.g., 100 and 200 kDa PEGs). Thus, at the extremes of the PEG molecular weight range studied, there was relatively little change in rejection with coating conditions. From Figure 5.3 and Figure 5.4, large changes in rejection as a function of coating conditions were observed for intermediate PEG samples (i.e., 12 and 20 kDa PEG). The separation factor, α, which represents the retention capability of the membranes, was calculated for the 12 and 20 kDa PEG samples according to [42]:

$$\alpha = \frac{1}{S_a} = \frac{1}{(1 - R_a)} \tag{5.1}$$

Separation factors of unmodified and PDA-modified membranes are presented as a function of membrane hydraulic permeability (i.e., pure water permeance) in Figure 5.7. These plots show a correlation between membrane hydraulic permeability and separation factor. Membranes with a higher hydraulic permeability had a lower separation factor, and vice versa. Regardless of the modification conditions, PDA-modified membranes with similar hydraulic permeabilities had similar separation factors. Additionally, among the 12 and 20 kDa PEG molecules, the larger PEG probe molecule showed a greater change in rejection properties with changes in hydraulic permeability brought about by PDA deposition. The separation properties of large solutes should be more sensitive to changes in pore size than those of small solutes as long as the large solutes are not completely excluded from the pores. Generally, the ratio of solute size to membrane pore size governs membrane separation properties [43, 44].

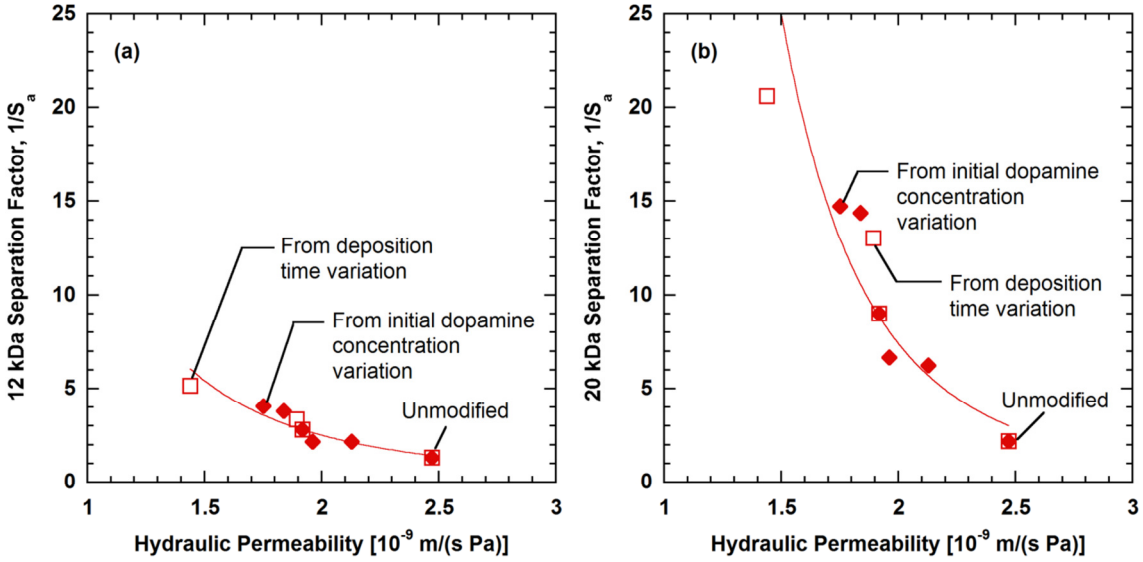

Figure 5.7: Effect of PDA deposition conditions on separation factor and hydraulic permeability of PS-20 UF membranes modified with PDA at various initial dopamine concentrations (♦) and deposition times (□). The solutes used to calculate the separation factor were (a) 12 kDa PEG and (b) 20 kDa PEG. The lines are drawn to guide the eye.

In a related correlation, Figure 5.8 presents pure water permeance and hydraulic permeability as a function of MWCO for unmodified and PDA-modified PS-20 membranes. Figure 5.8 provides another illustration of the tradeoff between water permeation and rejection properties. Generally, a reduction in membrane pore size leads to higher solute retention (i.e., higher separation factor due to lower MWCO) but reduced water transport. A similar effect of membrane permeability on separation properties of a variety of UF membranes was reported by Mehta and Zydney [42]. This tradeoff is at least qualitatively reminiscent of those observed for RO membranes [45] and gas separation membranes [46, 47].

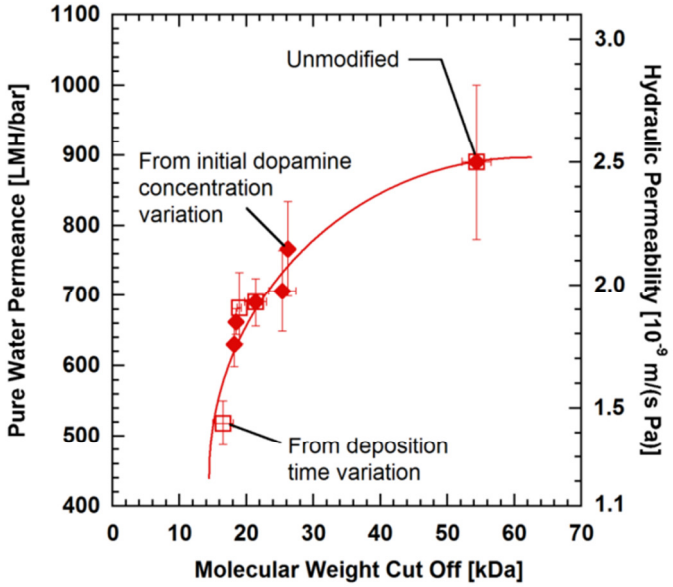

Figure 5.8: Effect of change in molecular weight cutoff of PS-20 UF membranes modified with PDA at various initial dopamine concentrations (♦) and deposition times (□) on pure water permeance (hydraulic permeability). The lines are to guide the eye.

5.2.5 Data Fitting to Determine $\bar{r}$, $\sigma/\bar{r}$, and ε/δ_m Parameters

In the MWCO experiments, the observed sieving coefficient, S_o, was measured for each solute molecular weight (i.e., PEG in this study) in each membrane considered. The hydraulic permeability (i.e., pure water permeance), $\overline{L}_p$, of each membrane was measured using dead-end filtration. These experimental $\overline{L}_p$ and S_o values were used to estimate $\bar{r}$, $\sigma/\bar{r}$, and ε/δ_m for each membrane by fitting the experimental S_o values to the theoretical S_o values calculated using the water and solute transport models.

The data fitting strategy is first described for the case when J_v and k are allowed to vary with r_c. For a particular membrane, the model calculations were started by choosing $\bar{r}$ and $\sigma/\bar{r}$ values that were reasonable (e.g., $\bar{r}$ = 4 nm, $\sigma/\bar{r}$ = 0.25) and using the pure water permeance, $\overline{L}_p$, to estimate ε/δ_m from Equation (2.8). This procedure

established an initial set of $\bar{r}$, $\sigma/\bar{r}$, and ε/δ_m parameters for further calculations. For a given PEG molecular weight, a corresponding molecular size, a, was calculated using Equation (2.22), and the diffusion coefficient was calculated using Equation (2.15). A radially-dependent permeate flux, $J_v(r_c)$, was estimated from Equation (2.26) using experimentally measured $\overline{J}_v$ and $\overline{L}_p$ values. For a particular membrane pore size, r, and a PEG molecular size, a, an asymptotic sieving coefficient, $S_\infty(r, a)$, was calculated using Equation (2.20), and a $Pe_m(r, a, r_c)$ was calculated from Equation (2.14). The calculated $S_\infty(r, a)$ and $Pe_m(r, a, r_c)$ were then inserted into Equation (2.13) to calculate $S_a(r, a, r_c)$. The average actual sieving coefficient for a certain membrane with a given PEG molecular weight, $\overline{S}_a(a, r_c)$, was then calculated by integrating $S_a(r, a, r_c)$ over the membrane pore size distribution using Equation (2.27). Afterwards, S_o value was evaluated from $\overline{S}_a(a, r_c)$ using the stagnant film model, Equation (2.30), where $k(r_c)$ was calculated for a given PEG molecular weight using Equation (2.29).

S_o values were calculated for all PEG molecular weights used in the MWCO tests for each membrane by repeating the calculation steps described above. For each membrane, calculated S_o values were fit to the experimental S_o values. The $\bar{r}$ and $\sigma/\bar{r}$ values were varied, and a goodness-of-fit parameter, χ^2 [35], between the experimental and calculated S_o values was computed. Best fit values of $\bar{r}$ and $\sigma/\bar{r}$ for each membrane were determined by minimizing χ^2. A grid-search method for nonlinear least-squares fitting, as explained by Bevington and Robinson [35], was used to identify optimum $\bar{r}$ and $\sigma/\bar{r}$ values having a minimum χ^2 value. Wolfram Mathematica 10.0 software was used for all calculations, and the NIntegrate command was used for numerical integration. The range of $\bar{r}$ used in the model fitting was selected based on the nominal pore radii of all membranes. A range of $\sigma/\bar{r}$ was chosen based, in part, on previously reported $\sigma/\bar{r}$ values of UF membranes (e.g., $\sigma/\bar{r}$ = 0.2 and 0.25 [41, 42]). Here, a broader

$\sigma/\bar{r}$ range than that of the literature-reported $\sigma/\bar{r}$ values was investigated. In our study, $\bar{r}$ was varied from 1 – 10 nm, and $\sigma/\bar{r}$ was varied from 0.05 – 1. The optimum ε/δ_m value of each membrane was that calculated from Equation (2.8) corresponding to the best fit $\bar{r}$ and $\sigma/\bar{r}$ values for a particular membrane.

For the case where J_v and k do not depend on r_c, $J_v(r_c)$ in Equation (2.14) was replaced by $\overline{J}_v$, which was the value set during the MWCO experiments. For each PEG molecular weight, the resulting expression for $Pe_m(r, a)$ was used in Equation (2.13) to calculate $S_a(r, a)$ of a particular membrane pore size r. The $S_a(r, a)$ was then integrated over the pore size distribution, $n(r)$, in Equation (2.27) to calculate $\overline{S}_a(a)$ of a given membrane. Subsequently, S_o for each membrane and each PEG molecular weight was calculated from this $\overline{S}_a(a)$ value using a stagnant film model, Equation (2.12), where $\overline{k}$ was calculated using Equation (2.28). S_o values were calculated for all PEG molecular weights studied for each membrane. Afterwards, the same strategy for minimizing χ^2 explained earlier was used to identify the best $\bar{r}$ and $\sigma/\bar{r}$ values for each membrane.

5.2.6 Mean Pore Size and Pore Size Distribution Analysis

The effect of PDA deposition conditions on mean pore size and pore size distribution of PDA-modified PS-20 UF membranes was further explored via modeling as described in the Background and Theory section. The S_o values calculated using the radially-dependent mass transfer coefficient, $k(r_c)$, and permeate flux, $J_v(r_c)$, were compared with those estimated using average parameters $\overline{k}$ and $\overline{J}_V$. The best fit $\bar{r}$ and σ parameters from model calculation using $k(r_c)$ and $J_v(r_c)$ are presented later in this section, and results based on $\overline{k}$ and $\overline{J}_V$ are presented in Appendix B (cf., Figure B.1). These two approaches provided very similar absolute values and trends for $\bar{r}$ and σ. In addition, these different approaches provided nearly identical fits of calculated S_o values

to experimental S_o values at PEG molecular weights of 4 – 35 kDa. However, the use of $k(r_c)$ led to improved S_o data fitting at higher PEG molecular weights (i.e., 100 and 200 kDa) compared to fits using $\overline{k}$. This result was perhaps due to a better prediction of concentration polarization when using $k(r_c)$ compared to using $\overline{k}$ for molecules with a high potential for concentration polarization, such as high molecular weight PEGs. Other modelling results presented in this section are based on the model calculations using $k(r_c)$ and $J_v(r_c)$.

Figure 5.9 presents calculated and experimental S_o values of membranes modified with PDA at various initial dopamine concentrations, and Figure 5.10 presents similar data for membranes modified with PDA at different deposition times. The solid curves in Figure 5.9 and Figure 5.10 represent S_o profiles from the model. The model fits in Figure 5.9 and Figure 5.10 are considered to be in good agreement with the experimental data. The experimental and calculated S_o values of unmodified and PDA-modified membranes are also recorded in Table B.1 and Table B.2 in Appendix B. However, for some PDA-modified membranes (not presented in this main study), some deviations in the experimental and modeled S_o from the data fitting were observed at large PEG molecules (i.e., 100 and 200 kDa). These membranes were those modified with PDA at low initial dopamine concentration (i.e., 0.1 mg/mL, using a 60-minute deposition time) and at short coating times (i.e., 15 and 30 minutes, using a 2 mg/mL initial dopamine concentration). The results are presented and discussed in Appendix B, and they were not included in this main study.

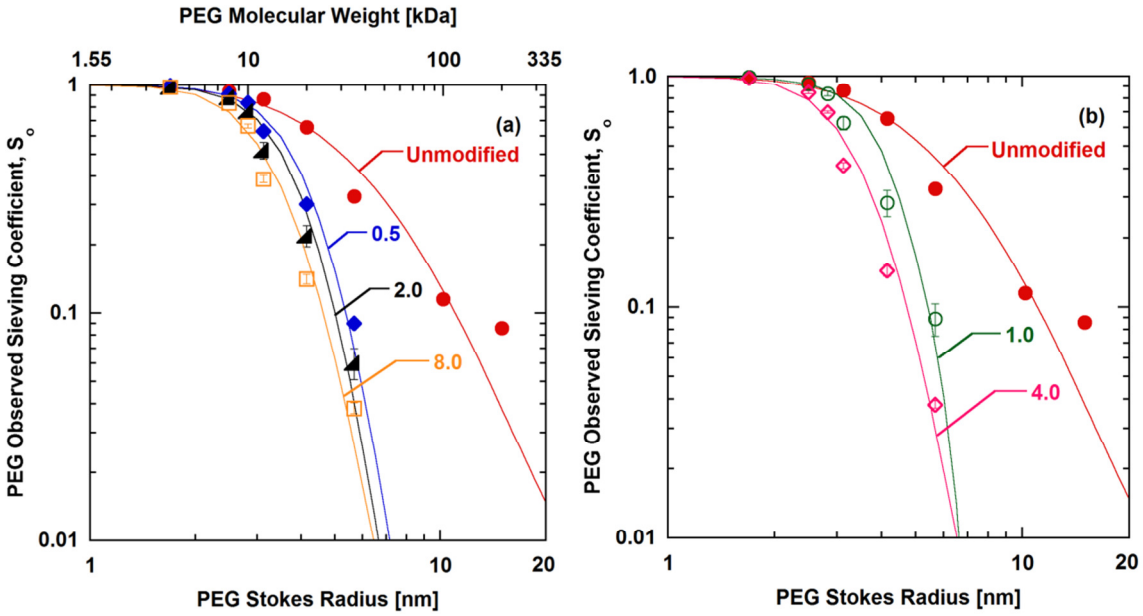

Figure 5.9: Effect of initial dopamine concentration on observed PEG sieving coefficient of unmodified and PDA-modified PS-20 UF membranes. Discrete data points show experimental data and solid curves show corresponding model calculations. ε/δ_m was used as a fitted parameter, and $k(r_c)$ and $J_v(r_c)$ were employed in the model calculations. The numbers in (a) and (b) represent initial dopamine concentration in mg/mL. A deposition time of 60 minutes was used.

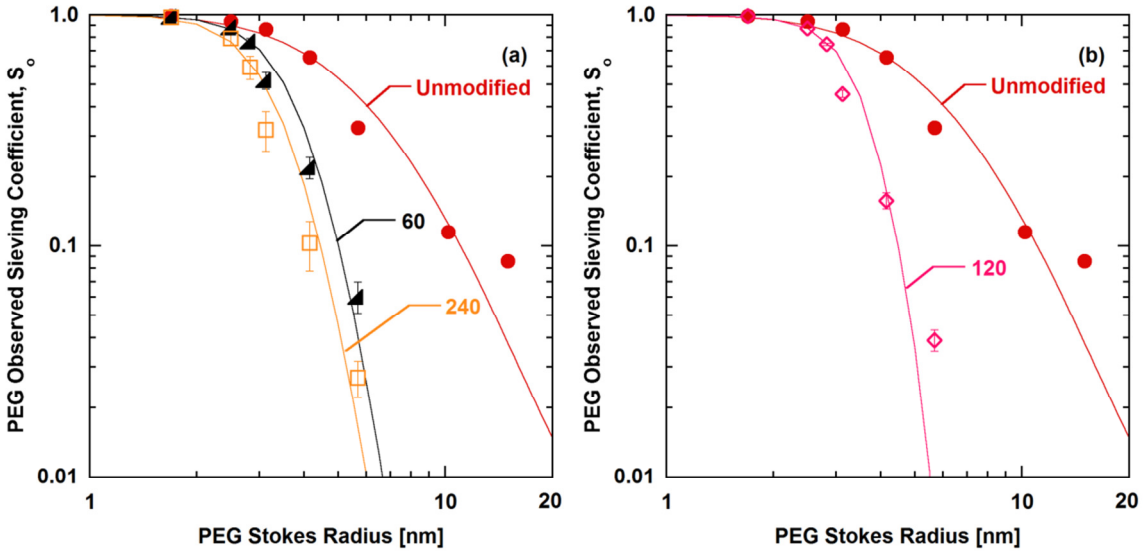

Figure 5.10: Effect of PDA deposition time on observed PEG sieving coefficient of unmodified and PDA-modified PS-20 UF membranes. Discrete data points show experimental data and solid curves show corresponding model calculations. ε/δ_m was used as a fitted parameter, and $k(r_c)$ and $J_v(r_c)$ were employed in the model calculations. The numbers in (a) and (b) represent PDA deposition time in minutes. An initial dopamine concentration of 2 mg/mL was used.

Figure 5.11 presents best fit values of $\bar{r}$ and σ for membranes modified with PDA at various conditions. These $\bar{r}$ and σ values represent the arithmetic (not geometric) mean and standard deviation of the membrane pore radius, r, respectively [48]. The uncertainties in $\bar{r}$ were estimated by varying $\bar{r}$ about its minimum χ^2 to increase χ^2 by 1 as explained in Bevington and Robinson [35]. Uncertainties in $\bar{r}$ calculated in this manner were less than 0.1 nm, so they are not apparent in Figure 5.11. The best fit values of $\bar{r}$ and $\sigma/\bar{r}$ for unmodified and PDA-modified membranes are also tabulated in Table B.3 and Table B.4 in Appendix B.

All PDA modification conditions led to an increase in membrane mean pore radius relative to that of unmodified membranes. At low initial dopamine concentrations (i.e., $\leq$ 1 mg/mL), $\bar{r}$ increased with increasing initial dopamine concentration (cf., Figure

5.11(a)). Similarly, at short deposition times (i.e., ≤ 120 minutes), $\bar{r}$ increased as the membranes were coated with PDA for longer times (cf., Figure 5.11(b)). An increase in mean pore radius with increasing initial dopamine concentration or deposition time could be caused by blockage of the smallest pores due to PDA deposition. Such low concentrations or short deposition times may not coat bigger pores sufficiently to significantly reduce their pore sizes, resulting in an overall increase in mean pore radius, basically shifting the pore size distribution to higher average pore sizes. Plots of the pore size distribution from the model reflect this trend (cf., Figure B.4 and Figure B.5 in Appendix B). In addition, this increase in mean pore radius might also be influenced by a membrane pore wetting due to PDA modification as observed in other studies [49].

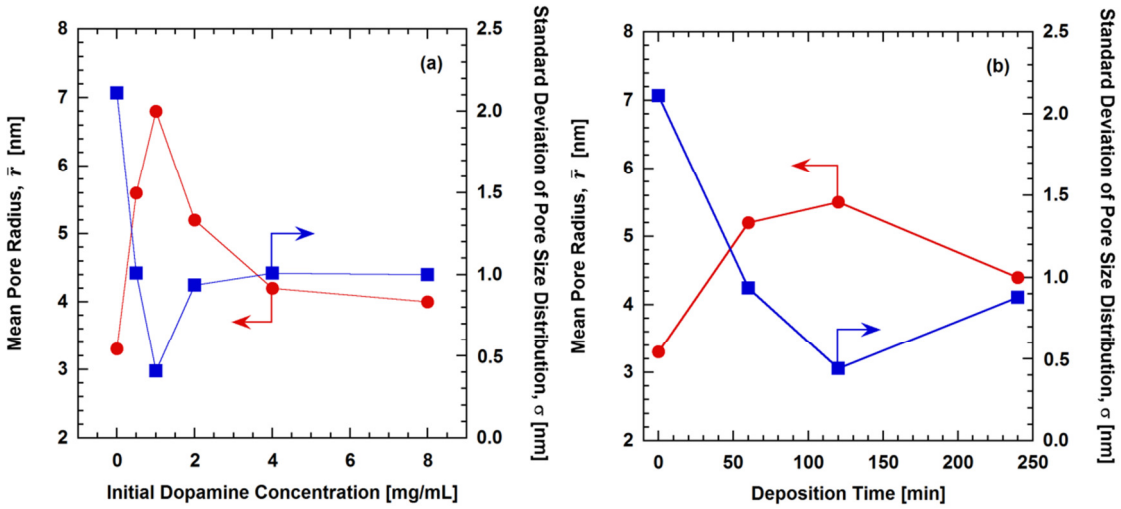

Figure 5.11: Effect of PDA deposition conditions on mean pore radius ($\bar{r}$) and standard deviation (σ) of pore size distribution of PS-20 UF membranes modified with PDA at various: (a) initial dopamine concentrations and (b) deposition times. ε/δ_m was used as a fitted parameter, and $k(r_c)$ and $J_v(r_c)$ were employed in the model calculations. A deposition time of 60 minutes was used in (a), and an initial dopamine concentration of 2 mg/mL was used in (b).

In contrast, at higher initial dopamine concentrations (i.e., > 1 mg/mL) or longer deposition times (i.e., > 120 minutes), $\bar{r}$ decreased with increasing initial dopamine concentration or increasing deposition time. At these more aggressive coating conditions, the PDA coating presumably blocked small pores and also reduced the size of large pores, decreasing the average pore radius (cf., Figure B.4 and Figure B.5). At the highest initial dopamine concentration (i.e., 8 mg/mL) or longest deposition time (i.e., 240 minutes), the mean pore radius was still somewhat higher than that of the unmodified membranes. In these cases, the size reduction of large pores and small pore blockage may both contribute to changes in the mean pore size of PDA-modified membranes, resulting in only modest increases in $\bar{r}$ from that of the unmodified membranes. The mean pore radii of unmodified and PDA-modified membranes were compared to their nominal pore radii, which were determined from MWCO experiments. This comparison is presented in Table B.3 and Table B.4, and a detailed discussion regarding the nominal and mean pore radii comparison is included in Appendix B.

From Figure 5.11, σ of membranes modified with PDA at all deposition conditions decreased relative to that of unmodified membranes. This finding is consistent with the reduction in the width of the pore size distribution inferred from the enhanced steepness of the PEG rejection curves due to PDA coating (cf., Figures 5.3, 5.4, B.4, and B.5). The PDA coating appears to reduce the size of the largest pores and block the smallest pores, which narrows the pore size distribution, leading to lower σ values. At initial dopamine concentrations lower than 1 mg/mL or deposition times shorter than 120 minutes, σ decreased with increasing initial dopamine concentration or deposition time, and reached minimum values. The σ value increased and approached a plateau at higher initial dopamine concentrations (i.e., > 1 mg/mL). Similarly, the σ value did not decrease further at longer deposition times (i.e., > 120 minutes), but instead increased. Perhaps

there were a limited number of small pores that could be completely blocked by PDA coating, resulting in minimum σ values of the pore size distribution of PDA-modified membranes. Extensive PDA modifications at high initial dopamine concentrations or long coating times might further decrease the overall pore sizes, leading to increased number of small pores (i.e., converting larger pores to small pores due to coating) and broader pore size distribution.

As discussed earlier, several correlations relating PEG Stokes radius to PEG molecular weight, such that similar to Equation (2.22), have been reported in the literature [32-34]. The correlation used in the model calculations can influence the values of $\bar{r}$ and σ, but it has no influence on the relative trends in these parameters among various PDA coating conditions. Thus, the reported fitted parameter values should only be used to provide a qualitative comparison among unmodified and different PDA-modified membranes. However, they should not be taken to represent absolute values, given the approximations inherent in both the modeling and the PEG molecule size estimations.

Figure 5.12 presents the influence of initial dopamine concentration (Figure 5.12(a)) and deposition time (Figure 5.12(b)) on ε/δ_m estimated from the model calculations. The values of ε/δ_m of unmodified and PDA-modified membranes are also tabulated in Table B.3 and Table B.4 in Appendix B. Changes in ε/δ_m describe changes in membrane porosity, tortuosity, and selective layer thickness, all of which could influence water and solute transport through membranes. From Figure 5.12(a), ε/δ_m of PDA-modified membranes tended to increase with increasing dopamine concentration initially, but it reached a plateau as dopamine concentration was increased above 4 mg/mL. Speculatively, the PDA coating inside the pores may open pores that may have been initially inaccessible due to wettability issues by increasing the hydrophilicity of the pore

walls, which would increase membrane porosity [49]. The plateau in ε/δ_m values could exist because all accessible pores had been opened. Although the PDA coating might increase membrane porosity in some cases, the pure water permeance of all PDA-modified membranes decreased relative to that of unmodified membranes (cf., Figure 5.2), suggesting that the pore size and distribution changes discussed above were responsible for the pure water permeance decrease. Any potential increase in porosity from pore opening in this study has a very minor influence on changes in pure water permeance relative to that caused by pore size and distribution changes.

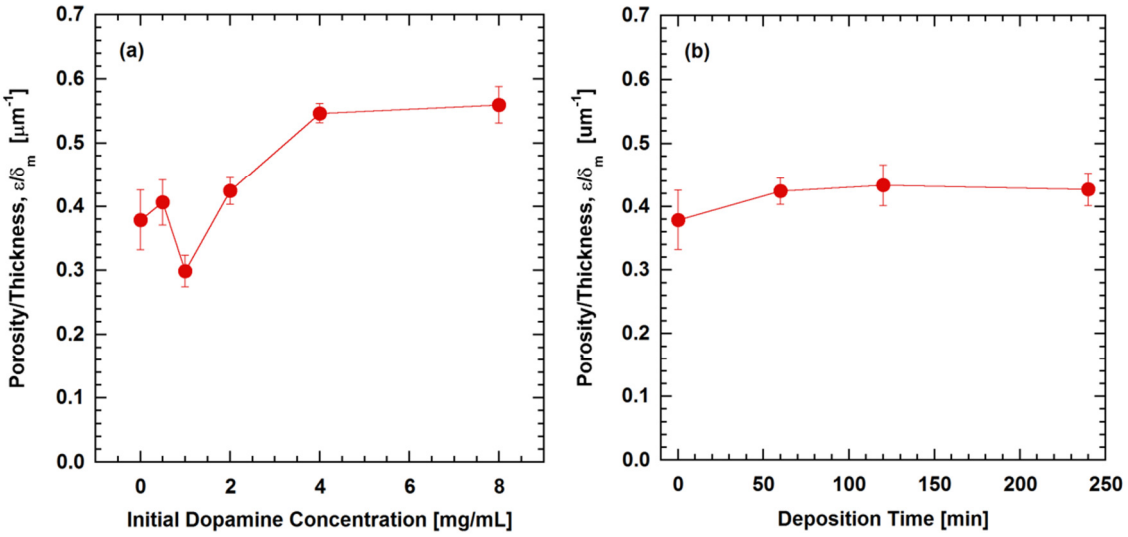

Figure 5.12: Effect of PDA deposition conditions on porosity to thickness ratio, ε/δ_m, of PS-20 UF membranes modified with PDA at various: (a) initial dopamine concentrations and (b) deposition times. ε/δ_m was used as a fitted parameter, and $k(r_c)$ and $J_v(r_c)$ were employed in the model calculations. A deposition time of 60 minutes was used in (a), and an initial dopamine concentration of 2 mg/mL was used in (b).

On the other hand, from Figure 5.12(b), ε/δ_m did not significantly change when the membranes were modified with PDA for longer deposition times. Another hypothesis is that the PDA modification did not significantly influence ε/δ_m values. In other studies,

ε/δ_m was chosen to be a constant value for modelling solute and solvent transport through different UF membranes [42]. Although Figure 5.12 shows some variation in ε/δ_m values at different PDA modification conditions, most of the ε/δ_m values were close to an average value of 0.4 μm^{-1}. Thus, we also modeled the membrane pore size distribution (i.e., $\bar{r}$ and σ parameters) using a constant ε/δ_m value of 0.4 μm^{-1}. For membranes modified with PDA at each modification condition, the Hagen-Poiseuille equation (cf., Equation (2.5)) was used to correlate $\bar{r}$ and σ values to achieve calculated $\overline{L}_p$ values equal to experimental pure water permeance values. The $\bar{r}$ and corresponding σ values were varied (keeping ε/δ_m fixed), and the calculated S_o values were computed using the hindered solute transport model (cf., Equations (2.13), (2.14), (2.20), and (2.27)) and stagnant film model (cf., Equation (2.30)) as explained earlier. The best fit $\bar{r}$ and σ values for each membrane were determined by minimizing the χ^2 between the modeled and experimental S_o data.

The best fit $\bar{r}$ and σ values from the model calculations using a fixed value of ε/δ_m (0.4 μm^{-1}) are presented in Figure B.2 in Appendix B. The influence of initial dopamine concentration or PDA deposition time on these $\bar{r}$ and σ values remained qualitatively similar to that reported earlier (cf., Figure 5.11).

5.3 CONCLUSIONS

PDA was deposited from aqueous solution onto PSf flat dense films and PS-20 UF membranes. As initial dopamine coating solution concentration or deposition time increased, the PDA surface coating thickness increased, and pure water permeance of PDA-modified PSf UF membranes decreased. MWCO, used to determine nominal pore size of the membranes, decreased with increasing initial dopamine concentration or longer deposition time. The decrease in MWCO was consistent with PDA coating inside

the membrane pores, and the coating reduced the membrane nominal pore size. In addition, PDA modification led to a tradeoff in hydraulic permeability and selectivity. A hindered solute transport model was used to characterize more completely the influence of PDA deposition conditions on mean pore size and pore size distribution, as well as the ratio of porosity to selective layer thickness of the membranes. When the membranes were coated at low initial dopamine concentrations or short deposition times, the mean pore radius increased relative to that of the unmodified membranes, possibly due to the blockage of small pores by PDA coating. At higher initial dopamine coating solution concentrations or longer deposition times, the mean pore size of PDA-modified membranes was somewhat higher than that of unmodified membranes. Perhaps large pores were coated sufficiently that the sizes of large pores were reduced. With contributions from the reduction in large pore sizes and blockage of small pores, there was only a moderate change in the mean pore radius of membranes modified with extensive PDA modification (i.e., at high dopamine concentration or long deposition time). The pore size distribution of all PDA-modified membranes was narrower than that of the unmodified membranes.

5.4 REFERENCES

[1] H. Lee, S.M. Dellatore, W.M. Miller, P.B. Messersmith, Mussel-inspired surface chemistry for multifunctional coatings, Science 318 (2007) 426–430.

[2] B.D. McCloskey, H.B. Park, H. Ju, B.W. Rowe, D.J. Miller, B.J. Chun, K. Kin, B.D. Freeman, Influence of polydopamine deposition conditions on pure water flux and foulant adhesion resistance of reverse osmosis, ultrafiltration, and microfiltration membranes, Polymer 51 (2010) 3472–3485.

[3] C. Cheng, S. Li, W. Zhao, Q. Wei, S. Nie, S. Sun, C. Zhao, The hydrodynamic permeability and surface property of polyethersulfone ultrafiltration membranes with mussel-inspired polydopamine coatings, Journal of Membrane Science 417–418 (2012) 228–236.

[4] R.A. Zangmeister, T.A. Morris, M.J. Tarlov, Characterization of polydopamine thin films deposited at short times by autoxidation of dopamine, Langmuir 29 (2013) 8619–8628.

[5] V. Ball, D.D. Frari, V. Toniazzo, D. Ruch, Kinetics of polydopamine film deposition as a function of pH and dopamine concentration: Insights in the polydopamine deposition mechanism, Journal of Colloid and Interface Science 386 (2012) 366–372.

[6] J. Jiang, L. Zhu, L. Zhu, B. Zhu, Y. Xu, Surface characteristics of a self-polymerized dopamine coating deposited on hydrophobic polymer films, Langmuir 27 (2011) 14180–14187.

[7] K. Kang, I.S. Choi, Y. Nam, A biofunctionalization scheme for neural interfaces using polydopamine polymer, Biomaterials 32 (2011) 6374–6380.

[8] J. Ou, J. Wang, S. Liu, J. Zhou, S. Ren, S. Yang, Microtribological and electrochemical corrosion behaviors of polydopamine coating on APTS-SAM modified Si substrate, Applied Surface Science 256 (2009) 894–899.

[9] F. Pan, H. Jia, S. Qiao, Z. Jiang, J. Wang, B. Wang, Y. Zhong, Bioinspired fabrication of high performance composite membranes with ultrathin defect-free skin layer, Journal of Membrane Science 341 (2009) 279–285.

[10] B. Li, W. Liu, Z. Jiang, X. Dong, B. Wang, Y. Zhong, Ultrathin and stable active layer of dense composite membrane enabled by poly(dopamine), Langmuir 25 (2009) 7368–7374.

[11] F. Bernsmann, A. Ponche, C. Ringwald, J. Hemmerle, J. Raya, B. Bechinger, J.-C. Voegel, P. Schaaf, V. Ball, Characterization of dopamine – melanin growth on silicon oxide, Journal of Physical Chemistry 113 (2009) 8234–8242.

[12] Y. Liu, K. Ai, L. Lu, Polydopamine and its derivative materials: Synthesis and promising applications in energy, environmental, and biomedical fields, Chemical Reviews 114 (2014) 5057–5115.

[13] N.F. Della Vecchia, R. Avolio, M. Alfè, M.E. Errico, A. Napolitano, M. d'Ischia, Building-block diversity in polydopamine underpins a multifunctional eumelanin-type platform tunable through a quinone control point, Advanced Functional Materials 23 (2013) 1331–1340.

[14] D.R. Dreyer, D.J. Miller, B.D. Freeman, D.R. Paul, C.W. Bielawski, Perspectives on poly(dopamine), Chemical Science 4 (2013) 3796–3802.

[15] H.W. Kim, B.D. McCloskey, T.H. Choi, C. Lee, M.J. Kim, B.D. Freeman, H.B. Park, Oxygen concentration control of dopamine-induced high uniformity surface coating chemistry, Applied Materials and Interfaces 5 (2013) 233–238.

[16] D.R. Dreyer, D.J. Miller, B.D. Freeman, D.R. Paul, C.W. Bielawski, Elucidating the structure of poly(dopamine), Langmuir 28 (2012) 6428–6435.

[17] D.J. Miller, D.R. Paul, B.D. Freeman, An improved method for surface modification of porous water purification membranes, Polymer 55 (2014) 1375–1383.

[18] ASTM Standard E1343 – 90, 1996 (2001), "Standard Test Method for Molecular Weight Cutoff Evaluation of Flat Sheet Ultrafiltration Membranes," ASTM International, West Conshohocken, PA, 2001, DOI: 10.1520/E1343-90R01, www.astm.org.

[19] C. Causserand, P. Aimar, Characterization of Filtration Membranes, in: E. Drioli, L. Giorno (Eds.) Comprehensive Membrane Science and Engineering, 1st ed., Elsevier, Kidlington, United Kingdom, 2010.

[20] M. Cheryan, Ultrafiltration and Microfiltration Handbook, Technomic Publishing Co., Inc., Lancaster, PA, 1998.

[21] W.S.W. Ho, K.K. Sirkar, Membrane Handbook, Van Nostrand Reinhold, New York, NY, 1992.

[22] M. Mulder, Basic Principles of Membrane Technology, Kluwer Academic Publishers, Dordrecht, The Netherlands, 1991.

[23] C. Causserand, S. Rouaix, A. Akbari, P. Aimar, Improvement of a method for the characterization of ultrafiltration membranes by measurements of tracers retention, Journal of Membrane Science 238 (2004) 177–190.

[24] S. Platt, M. Mauramo, S. Butylina, M. Nystrom, Retention of pegs in cross-flow ultrafiltration through membranes, Desalination 149 (2002) 417–422.

[25] S. Mochizuki, A.L. Zydney, Theoretical analysis of pore size distribution effects on membrane transport, Journal of Membrane Science 82 (1993) 211–227.

[26] P. Aimar, M. Meireles, V. Sanchez, A contribution to the translation of retention curves into pore size distributions for sieving membranes, Journal of Membrane Science 54 (1990) 321–338.

[27] L. Zeman, M. Wales, Polymer Solute Rejection by Ultrafiltration Membranes, in: A.F. Turbak (Ed.) ACS Symposium Series 154 (Synthetic Membranes: Volume II Hyper- and Ultrafiltration Uses), American Chemical Society, Washington, DC, 1981, pp. 411–434.

[28] A.S. Michaels, Analysis and prediction of sieving curves for ultrafiltration membranes: A universal correlation?, Separation Science and Technology 15 (1980) 1305–1322.

[29] D.J. Miller, S. Kasemset, L. Wang, D.R. Paul, B.D. Freeman, Constant flux crossflow filtration evaluation of surface-modified fouling-resistant membranes, Journal of Membrane Science 452 (2014) 171–183.

[30] B. Schlichter, V. Mavrov, H. Chmiel, Comparative characterisation of different commercial UF membranes for drinking water production, Journal of Water Supply: Research and Technology–AQUA 49 (2000) 321–328.

[31] M.C. Porter, Handbook of Industrial Membrane Technology, Noyes Publications, Park Ridge, NJ, 1990.

[32] S. Gaches, Application de la Viscosimetrie a la Determination du Rayon de Giration de Macromolecules, DEA Génie des Procédés, Université Paul Sabatier, 1991.

[33] C.M. Tam, A.Y. Tremblay, Membrane pore characterization – comparison between single and multicomponent solute probe techniques, Journal of Membrane Science 57 (1991) 271–287.

[34] S. Singh, K.C. Khulbe, T. Matsuura, P. Ramamurthy, Membrane characterization by solute transport and atomic force microscopy, Journal of Membrane Science 142 (1998) 111–127.

[35] P.R. Bevington, D.K. Robinson, Data Reduction and Error Analysis for the Physical Sciences, 3rd ed., The McGraw-Hill Companies, Inc., New York, NY, 2003.

[36] D.P. O'Shea, Ultura (formerly Sepro Membranes, Inc.), Personal Communication, 2013.

[37] G. Schock, A. Miquel, R. Birkenberger, Characterization of ultrafiltration membranes: Cut-off determination by gel permeation chromatography, Journal of Membrane Science 41 (1989) 55–67.

[38] G. Trägårdh, Characterization methods for ultrafiltration membranes, Desalination 53 (1985) 25–35.

[39] P. Prádanos, J.I. Arribas, A. Hernández, Mass transfer coefficient and retention of PEGs in low pressure cross-flow ultrafiltration through asymmetric membranes, Journal of Membrane Science 99 (1995) 1–20.

[40] S. Mochizuki, A.L. Zydney, Dextran transport through asymmetric ultrafiltration membranes: Comparison with hydrodynamic models, Journal of Membrane Science 68 (1992) 21–41.

[41] A.L. Zydney, A. Xenopoulos, Improving dextran tests for ultrafiltration membranes: Effect of device format, Journal of membrane Science 291 (2007) 180–190.

[42] A. Mehta, A.L. Zydney, Permeability and selectivity analysis for ultrafiltration membranes, Journal of Membrane Science 249 (2005) 245–249.

[43] W.S. Opong, A.L. Zydney, Diffusive and convective protein transport through asymmetric membranes, AIChE Journal 37 (1991) 1497–1510.

[44] L.J. Zeman, A.L. Zydney, Microfiltration and Ultrafiltration: Principles and Applications, Marcel Dekker, Inc., New York, NY, 1996.

[45] G.M. Geise, H.B. Park, A.C. Sagle, B.D. Freeman, J.E. McGrath, Water permeability and water/salt selectivity tradeoff in polymers for desalination, Journal of Membrane Science 369 (2011) 130–138.

[46] R.W. Baker, B.T. Low, Gas separation membrane materials: A perspective, Macromolecules 47 (2014) 6999–7013.

[47] D.F. Sanders, Z.P. Smith, R. Guo, L.M. Robeson, J.E. McGrath, D.R. Paul, B.D. Freeman, Energy-efficient polymeric gas separation membranes for a sustainable future: A review, Polymer 54 (2013) 4729–4761.

[48] A.L. Zydney, P. Aimar, M. Meirele, J.M. Pimbley, G. Belfort, Use of the log-normal probability density function to analyze membrane pore size distributions: Functional forms and discrepancies, Journal of Membrane Science 91 (1994) 293–298.

[49] J.T. Arena, B.D. McCloskey, B.D. Freeman, J.R. McCutcheon, Surface modification of thin film composite membrane support layers with polydopamine: Enabling use of reverse osmosis membranes in pressure retarded osmosis, Journal of Membrane Science 375 (2011) 55–62.

Chapter 6: Effect of Polydopamine Deposition Conditions on Polysulfone Ultrafiltration Membrane Properties and Threshold Flux During Oil/Water Emulsion Filtration

6.1 SUMMARY

Polysulfone ultrafiltration membranes were modified with polydopamine (PDA) at different initial dopamine concentrations and deposition times. Membrane properties, including surface hydrophilicity, roughness, and zeta potential, were characterized. PDA coatings significantly increased surface hydrophilicity, but they did not clearly change the surface roughness or zeta potential. The influence of PDA modification conditions on membrane threshold flux during oil/water emulsion fouling was investigated. Threshold flux increased when PDA was deposited at low initial dopamine concentrations or short coating times. However, PDA deposition at high initial dopamine concentrations or long coating times decreased threshold flux. These trends reflect a balance between increased hydrophilicity and modification of membrane pore size due to PDA deposition. An increase in membrane surface hydrophilicity was observed at all PDA deposition conditions. However, extensive PDA coating significantly decreased membrane pure water permeance, which may have narrowed or blocked some membrane pores, and in turn, increased local permeate flux through the remaining pores in the PDA-modified membranes. This higher local flux likely led to a more severe fouling and decreased the threshold flux. When unmodified and PDA-modified membranes began with similar pure water permeance, the PDA-modified membranes had higher threshold flux than the unmodified membranes.

6.2 RESULTS AND DISCUSSION

6.2.1 Membrane Surface Roughness

The root-mean-square surface roughness (R_{rms}) values of membranes modified with PDA at different initial dopamine concentrations and deposition times are recorded in Table 6.1 and Table 6.2, respectively. The surface roughness values of most PDA-modified membranes were statistically identical to that of the unmodified membranes. Thus, there was no obvious trend in the roughness values when initial dopamine concentration or PDA deposition time was varied. The large uncertainties in the roughness of some PDA-coated membranes could be due to deposition of PDA aggregates onto the membrane surfaces.

Table 6.1: Root-mean-square surface roughness (R_{rms}) of unmodified PS-20 UF membranes and membranes modified with PDA at various initial dopamine concentrations (60-minute deposition time).

Initial dopamine concentration (mg/mL)	**R_{rms} (nm)**
Unmodified	4.7±0.9
0.1	4.9±0.3
0.5	6±2
1	6±2
2	7±2
4	5.0±0.2
8	6.2±0.2

Table 6.2: Root-mean-square surface roughness (R_{rms}) of unmodified PS-20 UF membranes and membranes modified with PDA at various deposition times (2 mg/mL initial dopamine concentration).

Deposition time (minutes)	**R_{rms} (nm)**
Unmodified	4.7±0.9
15	5.4±0.2
30	5.7±0.4
60	7±2
120	7.5±0.6
240	5.3±0.5

In several previous studies, PDA modification increased surface roughness of various substrates due to the formation of PDA nanoaggregates on the surfaces [1-8]. Moreover, the roughness increased with increasing dopamine concentration [4] or coating time [1, 3-5, 8] perhaps because the size and number of PDA nanoparticles became larger [1, 4, 8]. Most of the substrates in the previous studies were flat, non-porous surfaces such as glass, Si wafers, and polymer films. For polymeric porous membranes, PDA modification has been reported to either increase or decrease surface roughness [2, 9]. The change in surface roughness could be influenced by a variation in the membrane pore size and porosity [2]. In our study, the native surface of PS-20 UF membranes was not smooth, so PDA coating led to essentially no significant change in membrane surface roughness.

6.2.2 Membrane Surface Hydrophilicity

Figure 6.1(a) and Figure 6.1(b) present contact angles of membranes modified with PDA at various initial dopamine concentrations and deposition times, respectively. From Figure 6.1(a), contact angle decreased with increasing initial dopamine concentration and plateaued at concentrations greater than 2 mg/mL. The PDA modification significantly increased membrane surface hydrophilicity (i.e., reduced contact angle) regardless of the initial dopamine concentration used, even for initial

dopamine concentrations as low as 0.1 mg/mL. The membranes coated at 2 mg/mL in our study may already be covered primarily with PDA on the surface, so any further increases in initial dopamine concentration did not change surface hydrophilicity (i.e., no reduction in contact angle value).

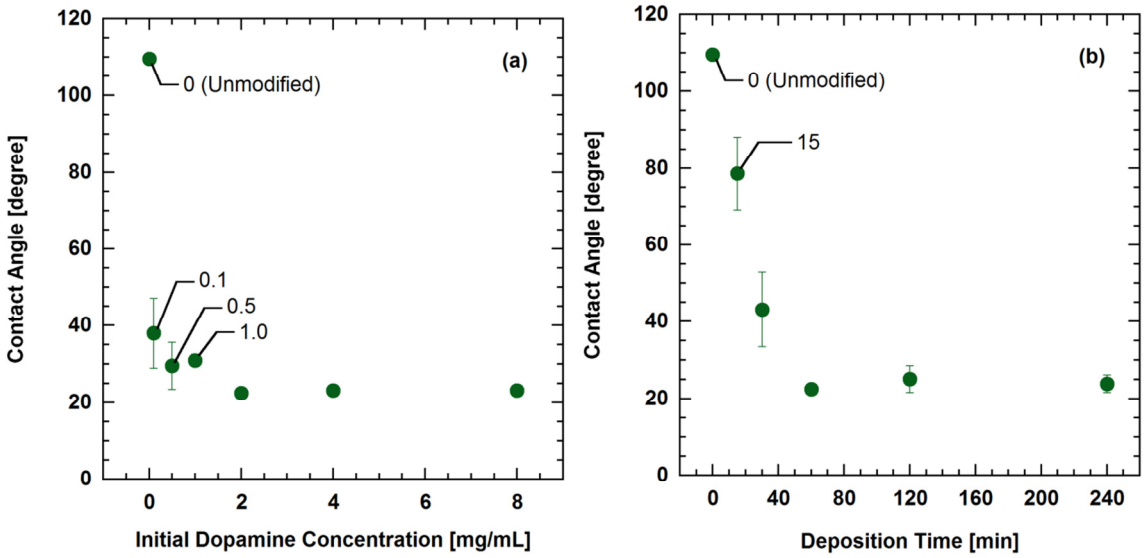

Figure 6.1: Influence of: (a) initial dopamine concentration and (b) PDA deposition time on contact angle (representing surface hydrophilicity) of unmodified and PDA-modified PS-20 UF membranes. The numbers in (a) and (b) represent initial dopamine concentration in mg/mL and deposition time in minutes, respectively. A deposition time of 60 minutes was used in (a), and an initial dopamine concentration of 2 mg/mL was used in (b).

From Figure 6.1(b), contact angle decreased continuously with increasing PDA deposition time until the coating time reached 60 minutes. Afterwards, the contact angle remained constant for coating times greater than 60 minutes. Membrane surface hydrophilicity moderately increased at short coating times of 15 and 30 minutes, suggesting that the membrane surface might only be partially coated with PDA at these conditions. Extending the coating time to 60 minutes increased surface hydrophilicity relative to 15-minute and 30-minute coatings. At longer coating times (i.e., greater than

60 minutes), the membranes could be covered with a higher amount of PDA and perhaps a more homogeneous coating than those coated at shorter deposition times.

Based on previous studies, as the PDA films grow on a surface, the contact angle of the surface usually converges to the same range regardless of the underlying substrate [10, 11]. As proposed in some studies, changes in contact angle induced by PDA deposition could also partly be due to changes in surface roughness [5, 6]. However, in our study, the membrane surface roughness was not obviously changed following PDA modification, so the decrease in contact angle was presumed to be primarily influenced by the increase in surface hydrophilicity. PDA is well-known for its hydrophilicity, and surface hydrophilicity increases of many substrates coated with PDA have been reported [1-6, 10-15]. Earlier literature studies on other substrates reported the influence of initial dopamine concentration [1, 2, 6] and PDA deposition time [1-3, 5, 6, 10] on surface hydrophilicity consistent with the trends observed in this study.

6.2.3 Membrane Zeta Potential

Figure 6.2 presents zeta potentials of unmodified and PDA-modified membranes as a function of pH. The zeta potential of the native polysulfone membranes in the pH range considered was negative, which is consistent with other literature reports [16-19]. Although polysulfone is non-ionizable and should be neutral, the negative surface charge is ascribed to adsorption of hydroxide ions (OH^-) from aqueous solution onto the membrane surface [16, 17, 19]. This phenomenon is regarded as the cause of apparent negative charges on many neutral hydrophobic surfaces, such as oil droplets and solid hydrophobic polymers [20-23].

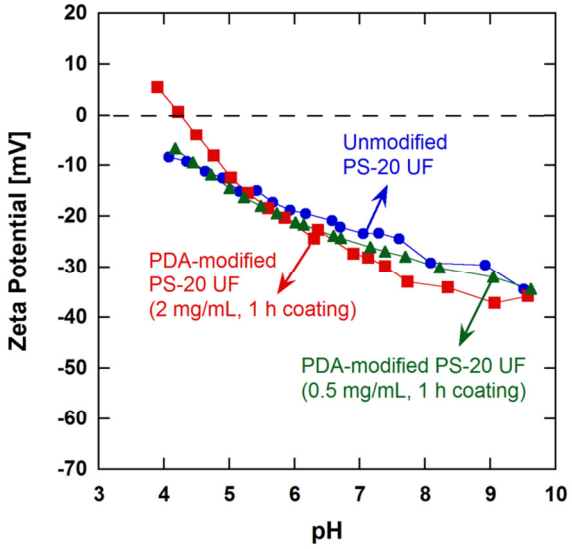

Figure 6.2: Influence of pH on zeta potential of unmodified PS-20 UF membranes and membranes modified with PDA at 0.5 and 2 mg/mL initial dopamine concentrations (1-hour deposition time).

PDA is believed to be an amphoteric material containing amine groups and phenolic hydroxyl groups [24-27]. At low pH, amine groups may be protonated from –NH to $-NH_2^+$, and at high pH, phenolic hydroxyl groups can dissociate from –OH to $-O^-$ [26]. At neutral pH, PDA exhibits a negative charge, possibly due to the deprotonation of phenolic hydroxyl groups [24, 28]. Several factors may influence the zeta potential of surface-modified membranes, including the chemical structure of the underlying membranes [25, 29], the functional (ionic) groups of the surface-modifying materials [29], and, in the case of polymeric coatings, the coating thickness [30] or grafting density [29, 31].

In our study, the zeta potential of membranes coated with PDA at 0.5 mg/mL was identical to that of unmodified membranes. This PDA coating condition may result in a coating layer too thin to influence the membrane zeta potential. In another study, a thin poly(ethylene glycol) (PEG) coating had no influence on the zeta potential of the coated

substrate, while the zeta potential changed more obviously as PEG coating thickness increased [30]. From Figure 6.2, the zeta potential profile of membranes coated with PDA at 2 mg/mL was only slightly different from that of unmodified membranes. The isoelectric point (IEP) of these PDA-modified membranes (2 mg/mL coating) was about pH 4.2. This value is similar to the IEP values of PDA coatings reported in the literature (i.e., pH 3.4 [32] and 4.0±0.5 [33]). The zeta potential profile of these PDA-coated membranes (2 mg/mL coating) qualitatively agrees with those reported in some other studies [9, 33]. However, in several other publications, the reported zeta potential values of PDA coatings are quite varied [24-26, 28, 32-36]. The variation in these values could be due to different substrates, PDA deposition conditions, or morphologies of the PDA layer (such as a flat film or a capsule). Different PDA coating concentrations or coating times could result in different PDA coating thicknesses and lead to variations in zeta potential [16]. Zeta potential values of PDA films at neutral pH from the literature were summarized and compared to results from our study in Table C.1 in Appendix C.

In this study, the membrane zeta potential was investigated to determine if the application of a PDA modification leads to any changes in membrane surface charge that could reduce oil fouling and possibly enhance the threshold flux. The oil/water emulsion used as a model foulant in this study had a pH of approximately 5 and a zeta potential of -13±0.9 mV at this pH. The negative charge on such emulsions is commonly observed (even if the oil/water emulsion is prepared with a non-ionic surfactant), due to OH^- ion adsorption at the oil/water interface [21]. Since oil droplets usually exhibit apparent negative surface charges, membranes may foul less if the membrane surface charge is more negative due to stronger electrostatic repulsion between the emulsion droplets and the membrane surface [37, 38]. At pH ~5, which was the pH of the oil/water emulsion used in our fouling experiments, the zeta potential values of unmodified and PDA-

modified membranes were approximately the same (cf., Figure 6.2). Since the zeta potential of the membranes at the conditions used for the fouling experiments was not influenced by PDA deposition, changes in membrane surface charge due to PDA modification were presumed to have little effect on fouling in this study.

6.2.4 Threshold Fluxes of PDA-Modified Membranes under Oil/Water Emulsion Filtration

6.2.4.1 Criteria for Threshold Flux Determination

The threshold fluxes of unmodified and PDA-modified PS-20 UF membranes during oil/water emulsion filtration were determined using the flux stepping method described earlier. The TMP and permeate flux profiles of a representative unmodified membrane during the flux stepping experiment are shown in Figure 6.3(a). Figure 6.3(b) and Figure 6.3(c) present TMP_{avg} and d(TMP)/dt, respectively, as a function of permeate flux of the unmodified membrane from the flux stepping test for threshold flux determinations.

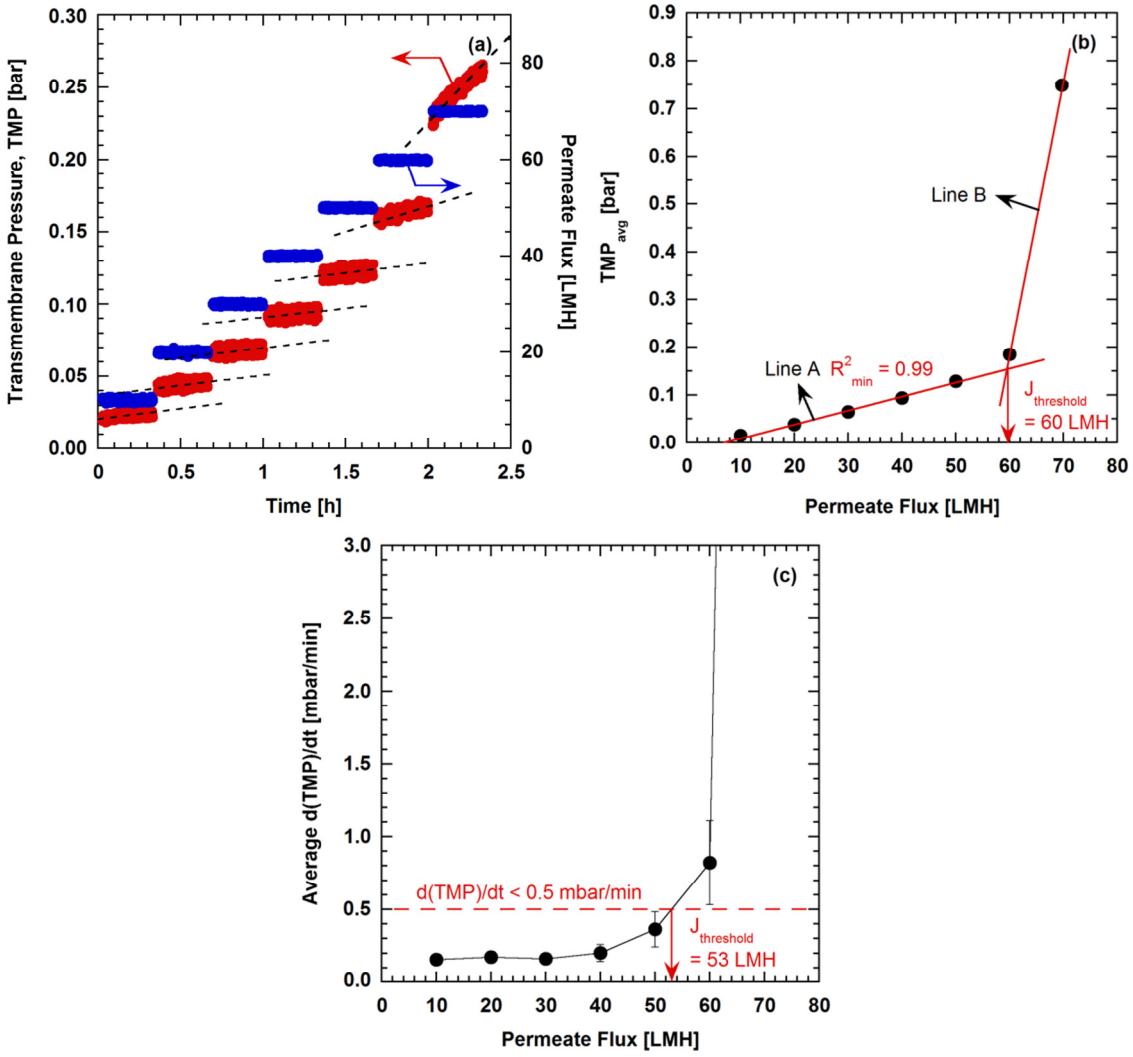

Figure 6.3: Threshold flux ($J_{threshold}$) determination of unmodified PS-20 UF membranes during oil/water emulsion filtration. (a) TMP and permeate flux profiles during the flux stepping experiment. (b) and (c) represent the threshold flux determination using the TMP_{avg} and d(TMP)/dt parameters, respectively. A minimum R^2 coefficient (R^2_{min}) of 0.99 was used to generate the linear regression line (line A) below the threshold flux in (b). Each plot is representative of at least three replicates. The line in (c) connects average d(TMP)/dt at each flux to guide the eye on changes in the d(TMP)/dt values.

In Figure 6.3(b), TMP_{avg} values were calculated from an average of TMP values recorded during each flux step. From this plot, the first linear regression line (i.e., line A)

of the data below the threshold flux ($J_{threshold}$) was established by requiring that the R^2 coefficient must not be less than 0.99. Above the threshold flux, the membrane fouls rapidly, and TMP usually does not increase linearly with increasing permeate flux [39-42]. The second linear regression line (i.e., line B) was then drawn from the first two data points beyond the threshold flux. The flux at the intersection of the first and second linear regression lines (i.e., lines A and B) was defined as the threshold flux. This flux divides the flux-independent fouling region (i.e., below $J_{threshold}$) from the flux-dependent fouling region (i.e., above $J_{threshold}$) [42]. When the minimum R^2 value (R^2_{min}) of 0.99 was used as shown in Figure 6.3(b), the threshold flux of the unmodified membrane was 60 LMH. This threshold flux value is in the same range as that observed in our previous study with the same membrane and model foulant system [43].

In many studies, a linear relationship of TMP_{avg} and permeate flux below the threshold flux was determined from visual observation of the linearity [44-48]. The linearity requirement of the regression line below the threshold flux (i.e., how well the experimental data fit with the line) was not reported quantitatively. Thus, an exact point where the non-linear behavior of the TMP_{avg} vs. flux profile started (i.e., the threshold flux) could be difficult to determine precisely [48]. The reported threshold flux value may vary according to how the regression at fluxes below the threshold flux (i.e., line A in Figure 6.3(b)) is drawn. The influence of the minimum R^2 value, which was used to establish line A in the TMP_{avg} vs. flux profile, on the estimated threshold flux was investigated in this study. In additional to Figure 6.3(b), where an R^2_{min} value of 0.99 was used, threshold flux determinations using the TMP_{avg} parameter with the R^2_{min} of 0.995 and 0.998 are presented in Figure C.1(a) and Figure C.1(b), respectively, in Appendix C. Three sets of the PDA-modified membrane threshold fluxes determined using R^2_{min} values of 0.99, 0.995 and 0.998 are compared in Figure C.2(a) and Figure C.2(b). Higher

R^2_{min} values led to somewhat lower threshold flux values. The R^2_{min} of 0.99 was chosen in this study because it provided threshold flux values most consistent with long-term filtration results presented in our earlier study [43]. More details about the selection of R^2_{min} criterion are provided in Appendix C. In addition, the regression lines below the threshold flux were established based on a statistical analysis using an F-test to estimate the threshold fluxes of unmodified and PDA-modified membranes. Details of this analysis are discussed in Appendix C.

In Figure 6.3(c), d(TMP)/dt values were calculated from the slope of a linear regression line (as shown with dashed lines in Figure 6.3(a)) of the TMP versus time during each flux step. The reported average d(TMP)/dt values at each flux step in Figure 6.3(c) is the arithmetic mean of d(TMP)/dt values from three membrane samples at that flux, and the error bars represent one standard deviation. At some permeate fluxes, the error bars are smaller than the symbols in the plot. The standard deviations typically increased in magnitude at fluxes above the threshold flux due to variations in the rate of fouling among different membrane coupons (also observed in other studies [45, 46]). In our study, the d(TMP)/dt limit used for the threshold flux determination was chosen to be 0.5 mbar/min. At this value, the d(TMP)/dt values of most membranes below and above the threshold fluxes were statistically different. The d(TMP)/dt values also started to obviously increase from those at lower fluxes using this d(TMP)/dt limit. Using this approach on the unmodified membrane as an example, Figure 6.3(c) gives a threshold flux of approximately 53 LMH determined by estimating, using linear interpolation, the flux at which the d(TMP)/dt reached the 0.5 mbar/min limit. This threshold flux value was somewhat lower than the value of 65 LMH determined using d(TMP)/dt in our previous study, possibly due to a membrane variability from different production batches [43]. Figure 6.3(c) shows d(TMP)/dt data at different permeate fluxes up to 60 LMH so

that the threshold flux determination at a d(TMP)/dt limit of 0.5 mbar/min limit can be seen more clearly. However, a full profile of the d(TMP)/dt vs. flux curve that includes d(TMP)/dt data at all permeate fluxes tested in the flux stepping experiments is shown in Figure C.3.

6.2.4.2 Threshold Fluxes of PDA-Modified Membranes

Figure 6.4(a) presents estimated threshold fluxes determined using the TMP_{avg} parameter for membranes modified with PDA at various initial dopamine concentrations. Figure 6.4(b) shows similar data for membranes modified with PDA at various deposition times. The TMP_{avg} vs. flux plots from the flux stepping experiments and the corresponding threshold flux from each plot for these membranes are presented in Figures C.4(a) – C.9(a) in the Appendix C. These threshold flux values are also tabulated in Table C.2 and Table C.3 in Appendix C. In addition, the threshold fluxes determined using the d(TMP)/dt approach are presented in Table C.2 and Table C.3 to compare with threshold fluxes estimated using the TMP_{avg} approach. Although the threshold flux values determined using these two approaches were not identical, they were in the same range and had similar trends when PDA modification conditions were changed. The d(TMP)/dt vs. flux plots of PDA-modified membranes are also shown in Figures C.4(b) – C.9(b), and their full profiles are presented in Figures C.4(c) – C.9(c).

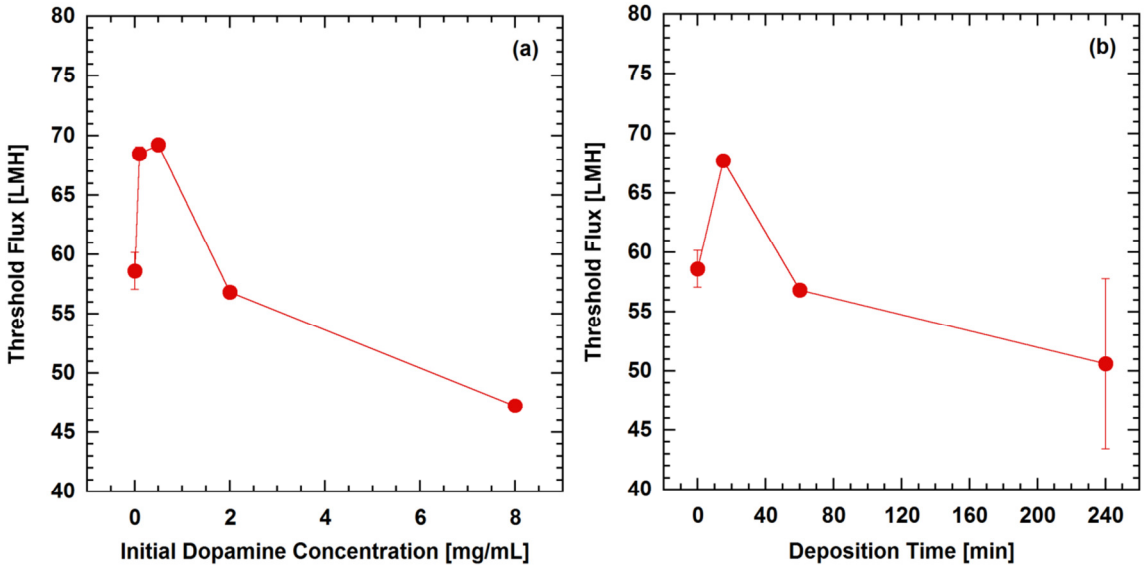

Figure 6.4: Influence of: (a) initial dopamine concentration and (b) PDA deposition time on the estimated threshold flux of PDA-modified PS-20 UF membranes during oil/water emulsion filtration. The threshold fluxes were determined using the TMP_{avg} parameter. A minimum R^2 coefficient (R^2_{min}) of 0.99 was used as a criterion to generate linear regression line below the threshold flux. A deposition time of 60 minutes was used in (a), and an initial dopamine concentration of 2 mg/mL was used in (b). The threshold flux of the unmodified membranes is shown in (a) as an initial dopamine concentration of zero mg/mL and in (b) as a deposition time of zero minute. At some PDA modification conditions, the error bars are smaller than the symbols in (a) and (b).

The threshold flux increased for membranes prepared using low initial dopamine concentrations or short PDA deposition times. As shown in Figure 6.4(a), a PDA coating deposited from 0.1 and 0.5 mg/mL initial dopamine concentration increased the threshold flux relative to that of unmodified membranes. Similarly, in Figure 6.4(b), coating the membrane with PDA for 15 minutes enhanced the membrane threshold flux relative to that of unmodified membranes. However, when membranes were coated with PDA using higher initial dopamine concentrations (≥ 2 mg/mL, cf., Figure 6.4(a)) or longer coating times (≥ 60 minutes, cf., Figure 6.4(b)), threshold flux decreased. Thus, the threshold flux

could be optimized when the membranes were modified with PDA using modification conditions giving low levels of surface modification. The threshold fluxes determined using the d(TMP)/dt approach, shown in Table C.2 and Table C.3, also provided a similar trend as discussed here when the initial dopamine concentration or PDA deposition time was varied.

As discussed earlier, PDA modification significantly increased the membrane surface hydrophilicity even at low initial dopamine concentrations or short deposition times (e.g., 15 minutes). However, PDA modification had a very minor effect on membrane surface roughness and surface charge (as characterized by zeta potential). For this reason, the observed threshold flux increase is attributed mainly to membrane surface hydrophilicity increase from PDA modification. Enhanced surface hydrophilicity helps reduce hydrophobic interactions between the emulsion droplets and the surface of the native polysulfone membranes, thereby reducing fouling. The threshold flux was reported to be higher for hydrophilic membranes than for hydrophobic membranes in several studies [42, 49, 50].

Despite the increase in surface hydrophilicity, the threshold flux decreased when the membranes were coated more extensively using high initial dopamine concentrations or long coating times. From our previous studies, the pure water permeance of these highly modified membranes was significantly lower than that of unmodified membranes (cf., Figure 5.2 and Figure 6.5) [14, 51]. During membrane modification, the PDA not only coats membrane surfaces, but it can also penetrate inside and coat membrane pores [51]. The pure water permeance decrease in highly modified membranes is attributed to membrane pore blockage and pore size reduction [52, 53]. The PDA coating, as a consequence, decreases the nominal pore size of UF membranes [51]. Furthermore, extensive PDA modification narrows the membrane pore size distribution, implying that

small pores may be blocked by PDA and large pores may become smaller [51]. These factors reduce pure water permeance (i.e., increase membrane hydraulic resistance to flow). While the macroscopic permeate flux over the entire membrane filtration area was maintained, the local permeate flux, which is the flux through individual open pores, was likely increased due to the decreased pore size and decreased number of open pores [54]. The higher local flux could lead to higher permeate drag forces on foulant particles approaching the membranes, leading to more severe fouling [54]. Thus, the higher local flux caused by PDA modification at extreme coating conditions (i.e., high initial dopamine concentration or long deposition time) is a likely cause of the threshold flux decrease observed in this study.

Figure 6.5 presents the threshold flux and pure water permeance of unmodified and PDA-modified membranes. The observed threshold flux appears to reflect a tradeoff between membrane surface hydrophilicity increase, which should increase threshold flux, and pure water permeance decrease, which should decrease threshold flux, due to PDA modification. The surface hydrophilicity of PDA-modified membranes (average contact angle, θ_{avg}, $\approx 30 - 40^{o}$) was significantly higher than that of unmodified membranes ($\theta_{UM} \approx 110^{o}$), even for those coated for 15 minutes. From our earlier studies, the membrane pure water permeance decreased with increasing initial dopamine concentration or coating time [14, 51, 55, 56]. However, the pure water permeance remained near that of unmodified membranes if low initial dopamine concentrations (such as 0.1 and 0.5 mg/mL) or short coating time (such as 15 minutes) were used.

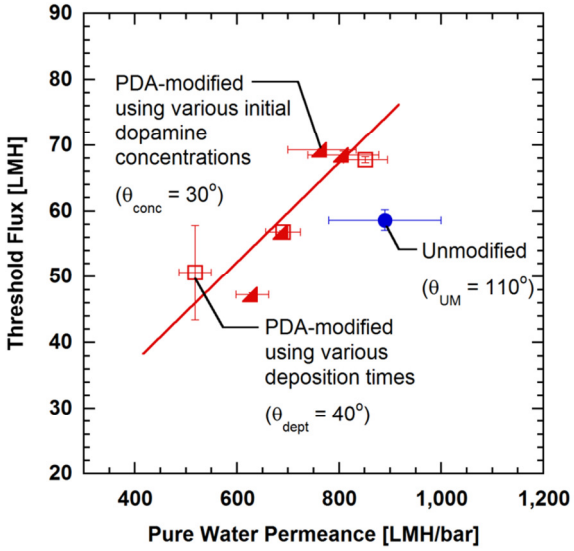

Figure 6.5: Correlation between pure water permeance and threshold flux of unmodified (●) and PDA-modified PS-20 UF membranes (◢, □). The membranes were modified with PDA at various initial dopamine concentrations (◢) of 0.1, 0.5, 2, and 8 mg/mL (60-minute deposition time) and at various deposition times (□) of 15, 60, and 240 minutes (2 mg/mL initial dopamine concentration). θ_{UM} represents the contact angle of unmodified membranes. θ_{conc} and θ_{dept} are average contact angles of membranes modified with PDA at various initial dopamine concentrations and various deposition times, respectively. The straight line is to guide the eye for the data trend of PDA-modified membranes. Pure water permeance values were taken from [51].

From Figure 6.5, comparing unmodified and PDA-modified membranes with pure water permeance in a similar range, the PDA-modified membranes had higher threshold flux than the unmodified membranes, presumably because of higher surface hydrophilicity. However, as pure water permeance of the PDA-modified membranes decreased substantially due to more extensive surface modification, the threshold flux of PDA-modified membranes became lower than that of unmodified membranes despite the higher surface hydrophilicity of the modified membranes. Membranes with low pure water permeance likely have smaller pore sizes and, therefore, higher local flux than membranes with high pure water permeance, leading to lower threshold flux values.

6.3 CONCLUSIONS

Polysulfone ultrafiltration membranes were modified with polydopamine (PDA) using various initial dopamine concentrations and deposition times. In this study, membrane properties related to fouling (i.e., surface hydrophilicity, roughness, and charge) of unmodified and PDA-modified membranes were investigated. PDA modification increased membrane surface hydrophilicity regardless of the modification conditions used. The membrane surface roughness or surface charge, as characterized by zeta potential, did not noticeably change following PDA modification. The threshold flux of membranes challenged with an oil/water emulsion increased when PDA modification was applied at optimum coating conditions. Changes in threshold flux were governed by a tradeoff between membrane surface hydrophilicity increase and pure water permeance decrease due to PDA modification. When low initial dopamine concentrations or short coating times were used, the threshold flux of PDA-modified membranes increased. In contrast, the threshold flux decreased when the membranes were modified with PDA at high initial dopamine concentrations or long coating times. With excessive PDA deposition, the membrane pure water permeance significantly decreased, and some membrane pores may have been blocked or the pore size may have been reduced. Thus, the local permeate flux was likely increased in highly modified membranes, leading to more severe fouling and a threshold flux decrease even though the surface hydrophilicity was improved.

6.4 REFERENCES

[1] C. Cheng, S. Li, W. Zhao, Q. Wei, S. Nie, S. Sun, C. Zhao, The hydrodynamic permeability and surface property of polyethersulfone ultrafiltration membranes with mussel-inspired polydopamine coatings, Journal of Membrane Science 417–418 (2012) 228–236.

[2] Z. Xi, Y. Xu, L. Zhu, Y. Wang, B. Zhu, A facile method of surface modification for hydrophobic polymer membranes based on the adhesive behavior of

poly(DOPA) and poly(dopamine), Journal of Membrane Science 327 (2009) 244–253.

[3] Y.M. Shin, Y.B. Lee, H. Shin, Time-dependent mussel-inspired functionalization of poly(L-lactide-co-ε-caprolactone) substrates for tunable cell behaviors, Colloids and Surfaces B: Biointerfaces 87 (2011) 79–87.

[4] V. Ball, D.D. Frari, V. Toniazzo, D. Ruch, Kinetics of polydopamine film deposition as a function of pH and dopamine concentration: Insights in the polydopamine deposition mechanism, Journal of Colloid and Interface Science 386 (2012) 366–372.

[5] J. Ou, J. Wang, S. Liu, J. Zhou, S. Ren, S. Yang, Microtribological and electrochemical corrosion behaviors of polydopamine coating on APTS-SAM modified Si substrate, Applied Surface Science 256 (2009) 894–899.

[6] J. Jiang, L. Zhu, L. Zhu, B. Zhu, Y. Xu, Surface characteristics of a self-polymerized dopamine coating deposited on hydrophobic polymer films, Langmuir 27 (2011) 14180–14187.

[7] Q. Wei, F. Zhang, J. Li, B. Li, C. Zhao, Oxidant-induced dopamine polymerization for multifunctional coatings, Polymer Chemistry 1 (2010) 1430–1433.

[8] R.A. Zangmeister, T.A. Morris, M.J. Tarlov, Characterization of polydopamine thin films deposited at short times by autoxidation of dopamine, Langmuir 29 (2013) 8619–8628.

[9] B.D. McCloskey, Novel surface modifications and materials for fouling resistant water purification membranes, PhD thesis, University of Texas at Austin, 2009.

[10] K. Kang, I.S. Choi, Y. Nam, A biofunctionalization scheme for neural interfaces using polydopamine polymer, Biomaterials 32 (2011) 6374–6380.

[11] Y. Liu, K. Ai, L. Lu, Polydopamine and its derivative materials: Synthesis and promising applications in energy, environmental, and biomedical fields, Chemical Reviews 114 (2014) 5057–5115.

[12] H. Lee, S.M. Dellatore, W.M. Miller, P.B. Messersmith, Mussel-inspired surface chemistry for multifunctional coatings, Science 318 (2007) 426–430.

[13] B.D. McCloskey, H.B. Park, H. Ju, B.W. Rowe, D.J. Miller, B.D. Freeman, A bioinspired fouling-resistant surface modification for water purification membranes, Journal of Membrane Science 413–414 (2012) 82–90.

[14] D.J. Miller, D.R. Paul, B.D. Freeman, An improved method for surface modification of porous water purification membranes, Polymer 55 (2014) 1375–1383.

[15] J. Jiang, L. Zhu, X. Li, Y. Xu, B. Zhu, Surface modification of PE porous membranes based on the strong adhesion of polydopamine and covalent immobilization of heparin, Journal of Membrane Science 364 (2010) 194–202.

[16] R. Blank, K.-H. Muth, S. Proske-Gerhards, E. Staude, Electrokinetic investigations of charged porous membranes, Colloids and Surfaces A: Physicochemical and Engineering Aspects 140 (1998) 3–11.

[17] D. Möckel, E. Staude, M. Dal-Cin, K. Darcovich, M. Guiver, Tangential flow streaming potential measurements: Hydrodynamic cell characterization and zeta potentials of carboxylated polysulfone membranes, Journal of Membrane Science 145 (1998) 211–222.

[18] X. Huang, D. Guduru, Z. Xu, J. Vienken, T. Groth, Blood compatibility and permeability of heparin-modified polysulfone as potential membrane for simultaneous hemodialysis and LDL removal, Macromolecular Bioscience 11 (2011) 131–140.

[19] K.J. Kim, A.G. Fane, M. Nystrom, A. Pihlajamaki, W.R. Bowen, H. Mukhtar, Evaluation of electroosmosis and streaming potential for measurement of electric charges of polymeric membranes, Journal of Membrane Science 116 (1996) 149–159.

[20] J.K. Beattie, The intrinsic charge on hydrophobic microfluidic substrates, Lab on a Chip 6 (2006) 1409–1411.

[21] K.G. Marinova, R.G. Alargova, N.D. Denkov, O.D. Velev, D.N. Petsev, I.B. Ivanov, R.P. Borwankar, Charging of oil−water interfaces due to spontaneous adsorption of hydroxyl ions, Langmuir 12 (1996) 2045-2051.

[22] R. Zangi, J.B.F.N. Engberts, Physisorption of hydroxide ions from aqueous solution to a hydrophobic surface, Journal of the American Chemical Society 127 (2005) 2272–2276.

[23] K.N. Kudin, R. Car, Why are water−hydrophobic interfaces charged?, Journal of the American Chemical Society 130 (2008) 3915–3919.

[24] B. Yu, J. Liu, S. Liu, F. Zhou, Pdop layer exhibiting zwitterionicity: a simple electrochemical interface for governing ion permeability, Chemical Communications 46 (2010) 5900–5902.

[25] H. Karkhanechi, R. Takagi, H. Matsuyama, Biofouling resistance of reverse osmosis membrane modified with polydopamine, Desalination 336 (2014) 87–96.

[26] M. Vaselbehagh, H. Karkhanechi, S. Mulyati, R. Takagi, H. Matsuyama, Improved antifouling of anion-exchange membrane by polydopamine coating in electrodialysis process, Desalination 332 (2014) 126–133.

[27] D.R. Dreyer, D.J. Miller, B.D. Freeman, D.R. Paul, C.W. Bielawski, Elucidating the structure of poly(dopamine), Langmuir 28 (2012) 6428–6435.

[28] K.Y. Kim, E. Yang, M.Y. Lee, K.J. Chae, C.M. Kim, I.S. Kim, Polydopamine coating effects on ultrafiltration membrane to enhance power density and mitigate biofouling of ultrafiltration microbial fuel cells (UF-MFCs), Water Research 54 (2014) 62–68.

[29] H. Susanto, M. Balakrishnan, M. Ulbricht, Via surface functionalization by photograft copolymerization to low-fouling polyethersulfone-based ultrafiltration membranes, Journal of Membrane Science 288 (2007) 157–167.

[30] Y.M. Chan, R. Schweiss, C. Werner, M. Grunze, Electrokinetic characterization of oligo- and poly(ethylene glycol)-terminated self-assembled monolayers on gold and glass surfaces, Langmuir 19 (2003) 7380–7385.

[31] H. Susanto, M. Ulbricht, Photografted thin polymer hydrogel layers on PES ultrafiltration membranes: Characterization, stability, and influence on separation performance, Langmuir 23 (2007) 7818–7830.

[32] Q. Liu, B. Yu, W. Ye, F. Zhou, Highly selective uptake and release of charged molecules by pH-responsive polydopamine microcapsules, Macromolecular Bioscience 11 (2011) 1227–1234.

[33] V. Ball, Impedance spectroscopy and zeta potential titration of dopa-melanin films produced by oxidation of dopamine, Colloids and Surfaces A: Physicochemical and Engineering Aspects 363 (2010) 92–97.

[34] R. Zhang, Y. Su, X. Zhao, Y. Li, J. Zhao, Z. Jiang, A novel positively charged composite nanofiltration membrane prepared by bio-inspired adhesion of polydopamine and surface grafting of poly(ethylene imine), Journal of Membrane Science 470 (2014) 9–17.

[35] S. Azari, L. Zou, Using zwitterionic amino acid L-DOPA to modify the surface of thin film composite polyamide reverse osmosis membranes to increase their fouling resistance, Journal of Membrane Science 401–402 (2012) 68–75.

[36] Y. Zhang, B.M. Teo, K.N. Goldie, B. Städler, Poly(N-isopropylacrylamide)/poly(dopamine) capsules, Langmuir 30 (2014) 5592−5598.

[37] J.S. Louie, I. Pinnau, I. Ciobanu, K.P. Ishida, A. Ng, M. Reinhard, Effects of polyether-polyamide block copolymer coating on performance and fouling of reverse osmosis membranes, Journal of Membrane Science 280 (2006) 762–770.

[38] P. Le-Clech, V. Chen, T.A.G. Fane, Fouling in membrane bioreactors used in wastewater treatment, Journal of Membrane Science 284 (2006) 17–53.

[39] P. Bacchin, P. Aimar, R.W. Field, Critical and sustainable fluxes: Theory, experiments and applications, Journal of Membrane Science 281 (2006) 42–69.

[40] D.J. Miller, S. Kasemset, D.R. Paul, B.D. Freeman, Comparison of membrane fouling at constant flux and constant transmembrane pressure conditions, Journal of Membrane Science 454 (2014) 505–515.

[41] R.W. Field, G.K. Pearce, Critical, sustainable and threshold fluxes for membrane filtration with water industry applications, Advances in Colloid and Interface Science 164 (2011) 38–44.

[42] J. Luo, S.T. Morthensen, A.S. Meyer, M. Pinelo, Filtration behavior of casein glycomacropeptide (CGMP) in an enzymatic membrane reactor: fouling control by membrane selection and threshold flux operation, Journal of membrane Science 469 (2014) 127–139.

[43] D.J. Miller, S. Kasemset, L. Wang, D.R. Paul, B.D. Freeman, Constant flux crossflow filtration evaluation of surface-modified fouling-resistant membranes, Journal of Membrane Science 452 (2014) 171–183.

[44] P. Le-Clech, B. Jefferson, I.S. Chang, S.J. Judd, Critical flux determination by the flux-step method in a submerged membrane bioreactor, Journal of Membrane Science 227 (2003) 81–93.

[45] K.Y. Choi, B.A. Dempsey, Bench-scale evaluation of critical flux and TMP in low-pressure membrane filtration, Journal of American Water Works Association 97 (2005) 134–143.

[46] S.P. Beier, G. Jonsson, Critical flux determination by flux-stepping, AIChE Journal 56 (2010) 1739–1747.

[47] S.S. Madaeni, A.G. Fane, D.E. Wiley, Factors influencing critical flux in membrane filtration of activated sludge, Journal of Chemical Technology and Biotechnology 74 (1999) 539–543.

[48] I.H. Huisman, E. Vellenga, G. Trägårdh, C. Trägårdh, The influence of the membrane zeta potential on the critical flux for crossflow microfiltration of particle suspensions, Journal of Membrane Science 156 (1999) 153–158.

[49] S. Metsämuuronen, J. Howell, M. Nyström, Critical flux in ultrafiltration of myoglobin and baker's yeast, Journal of Membrane Science 196 (2002) 13–25.

[50] L. Defrance, M.Y. Jaffrin, Comparison between filtrations at fixed transmembrane pressure and fixed permeate flux: application to a membrane bioreactor used for wastewater treatment, Journal of Membrane Science 152 (1999) 203–210.

[51] S. Kasemset, L. Wang, Z. He, D.J. Miller, A. Kirschner, B.D. Freeman, M.M. Sharma, Influence of polydopamine deposition conditions on permeability and sieving coefficient for a polysulfone ultrafiltration membrane, Journal of Membrane Science (2015), submitted.

[52] R.W. Baker, Membrane Technology and Applications, 2nd ed., John Wiley & Sons Ltd., West Sussex, England, 2004.

[53] L.J. Zeman, A.L. Zydney, Microfiltration and Ultrafiltration: Principles and Applications, Marcel Dekker, Inc., New York, NY, 1996.

[54] S. Ognier, C. Wisniewski, A. Grasmick, Membrane bioreactor fouling in sub-critical filtration conditions: A local critical flux concept, Journal of Membrane Science 229 (2004) 171–177.

[55] S. Kasemset, A. Lee, D.J. Miller, B.D. Freeman, M.M. Sharma, Effect of polydopamine deposition conditions on fouling resistance, physical properties, and permeation properties of reverse osmosis membranes in oil/water separation, Journal of Membrane Science 425–426 (2013) 208–216.

[56] B.D. McCloskey, H.B. Park, H. Ju, B.W. Rowe, D.J. Miller, B.J. Chun, K. Kin, B.D. Freeman, Influence of polydopamine deposition conditions on pure water flux and foulant adhesion resistance of reverse osmosis, ultrafiltration, and microfiltration membranes, Polymer 51 (2010) 3472–3485.

Chapter 7: Conclusions and Recommendations

A major challenge in membrane filtration is fouling. Polydopamine (PDA) surface modification can be used to increase membrane surface hydrophilicity [1-12]. Thus, it helps improve membrane fouling resistance towards various types of foulants, including organics such as oil/water emulsions [4, 5, 13, 14]. PDA modification conditions are important factors governing the reaction to form PDA and PDA deposition, which can directly influence PDA-modified membrane properties and fouling propensity. This dissertation presents systematic studies to determine the influence of PDA modification conditions on membrane properties (i.e., surface characteristics, permeability, and selectivity) and fouling behavior during oil/water emulsion filtration. The studies were conducted with both porous (UF) and non-porous (RO) membranes. A summary of the research studies discussed in Chapter 4 – 6 and recommendations for future work are presented in this chapter.

7.1 CONCLUSIONS

PDA surface modification of RO membranes is presented in Chapter 4. The RO membranes were surface-modified with PDA at various modification conditions, which include various initial dopamine concentrations, PDA deposition times, and pH values of dopamine coating solution. The pure water flux, permeate flux during oil/water emulsion filtration, and NaCl rejection of these PDA-modified membranes were determined and compared to those of unmodified membranes. The pure water flux of all membranes modified with PDA at alkaline conditions decreased relative to that of unmodified membranes, and it decreased with increasing initial dopamine concentration or PDA deposition time. This pure water flux decrease could be attributed to an increase in PDA coating thickness, which increased mass transfer resistance to water flow at higher initial

dopamine concentration or longer coating times. However, the pure water flux of membranes modified with PDA at acidic conditions (i.e., pH 5) remained the same as that of unmodified membranes, suggesting that PDA was not deposited onto the membranes at this modification condition. Fouling tests were performed under constant transmembrane pressure (TMP) filtration using oil/water emulsions as model foulants. All PDA-modified membranes except those coated at acidic conditions exhibited higher permeate flux than that of unmodified membranes during the fouling tests. Thus, PDA surface modification helped improve the fouling resistance of RO membranes to oil/water emulsions. For membranes modified with PDA at acidic conditions (i.e., pH 5), no difference in permeate flux was observed relative to that of unmodified membranes during the fouling tests, most likely because the PDA was not added to the membranes at acidic pH. The NaCl rejection of all PDA-modified membranes was maintained within the membrane manufacturer's specification. During the fouling test, enhanced permeate flux or improved fouling resistance of membranes modified with PDA at alkaline conditions (except those coated for 30 minutes) was similar regardless of the modification conditions. This result suggested that the mass transfer resistance during fouling due to PDA coating layer was less significant relative to that of fouling.

PDA surface modification studies on UF membranes are discussed in Chapters 5 and 6. Chapter 5 describes an investigation of PDA modification on the surface and inside the pores of UF membranes. The influence of PDA modification conditions on UF membrane pore characteristics is presented in detail in the same Chapter. The pore characteristics (e.g., pore size and pore size distribution) of porous membranes can influence several important membrane properties, including pure water permeance, solute selectivity, and fouling propensity [5, 15, 16]. For this reason, an understanding of

changes in membrane pore properties due to PDA modification is of interest in this research work.

Polysulfone (PSf) UF membranes were modified with PDA at various initial dopamine concentrations and PDA deposition times. Similarly, spin-coated PSf dense films were modified with PDA at these various PDA modification conditions. The PDA coating thickness on PSf dense films was determined and used to represent the PDA coatings on the membrane surface. Membrane pure water permeance was also determined. The PDA coating thickness increased and the pure water permeance decreased with increasing initial dopamine concentration or PDA deposition time. The pure water permeance decrease could be partly due to the increase in PDA coating thickness, which introduced higher mass transfer resistance to water flow. Molecular weight cut off (MWCO) values of unmodified and PDA-modified membranes were measured via poly(ethylene glycol) (PEG) rejection tests. The nominal pore radius of each membrane was then estimated from the Stokes radius of PEG molecules having a molecular weight that gave 90% rejection or was the same as the MWCO value. The MWCO (and in turn, the nominal pore radius) decreased with increasing initial dopamine concentration or PDA deposition time. The MWCO results suggested that PDA not only coated on the membrane surface, but also coated inside the pores, decreasing the membrane pore size. For PEGs that were not fully rejected by or completely passed through all membranes in this study, a tradeoff between permeability and selectivity was observed, similar to that reported in the literature for RO membranes [17] or gas separation membranes [18, 19]. More details of pore characteristics, such as pore size distribution, of PDA-modified membranes were investigated. UF membrane pore size is usually too small to be measured experimentally, by techniques such as porosimetry or bubble point tests for MF membranes. Thus, mathematical modelling using a hindered

solute transport model, proposed by Opong and Zydney [20], was employed to estimate membrane mean pore size and pore size distribution from the PEG rejection data. A log-normal pore size distribution was used to model UF membrane pores. The Hagen-Poiseuille equation and concentration polarization model were also used in this modelling work, and the details of model fitting are explained in Chapter 5. With increasing initial dopamine concentration or PDA deposition time, the PDA-modified membrane mean pore size increased for membranes with minimal PDA deposition, but it decreased for membranes with excessive PDA deposition. At minimal PDA deposition using low initial dopamine concentrations or short coating times, a significant increase in the mean pore size of PDA-modified membranes relative to unmodified membranes was observed, possibly due to small pore blockage by PDA coating. At excessive PDA deposition using high initial dopamine concentrations or long coating times, the mean pore size of PDA-modified membranes was still somewhat higher than that of unmodified membranes, but it was much closer to the value of unmodified membranes compared to the earlier case. In this latter case, the size of large pores could also be significantly reduced, and the contributions of both large pore size reduction and small pore blockage perhaps led to this moderate increase in the mean pore size. The pore size distribution of all PDA-modified membranes became narrower than that of unmodified membranes. Modeled pore size distributions of unmodified and PDA-modified membranes are presented in Appendix B. The porosity to selective layer thickness ratio of PDA-modified membranes slightly increased or remained similar relative to that of unmodified membranes.

Chapter 6 presents the influence of PDA modification conditions on surface properties and threshold flux of UF membranes. The PSf UF membranes were again modified with various initial dopamine concentrations and PDA deposition times. The membrane surface properties, including surface hydrophilicity, charge, and roughness

were characterized. The surface hydrophilicity of PDA-modified membranes was significantly higher than that of unmodified membranes. The surface hydrophilicity increased with increasing initial dopamine concentration or PDA deposition time, but then reached a constant at high initial dopamine concentration or long coating time. However, there was no noticeable change in surface roughness or zeta potential (i.e., representing surface charge) of PDA-modified membranes compared to those of unmodified membranes.

The threshold flux is the maximum permeate flux where fouling is low and stable membrane operation can be achieved [21]. Thus, the threshold flux can be used as an indicator of membrane fouling propensity. Membranes with higher threshold flux can be operated at higher permeate flux before fouling becomes significant, so they generally have lower fouling propensity. Chapter 6 discusses the threshold flux determination for PDA-modified membranes during oil/water emulsion filtration. PDA modification using low initial dopamine concentrations or short coating times increased the membrane threshold flux, presumably mainly due to surface hydrophilicity increase. With minimal PDA coating at these coating conditions, the membrane pure water permeance was still maintained near that of unmodified membranes. In contrast, the threshold flux of membranes modified with PDA using high initial dopamine concentrations or long coating times decreased relative to that of unmodified membranes, possibly due to significant decreases in membrane pure water permeance. A large decrease in pure water permeance of membranes modified extensively with PDA could be attributed to pore narrowing or blockage by PDA coating. Thus, these highly modified membranes likely had lower permeable open pore areas to permeate flow and, in turn, higher local permeate flux, thereby increasing the convective flow force acting to encourage foulant contact with the remaining open pores. The higher local permeate flux due to the extensive PDA

coating led to decreased threshold flux even though the membrane surface hydrophilicity was increased. In brief, changes in threshold flux due to PDA modification were influenced by a tradeoff between surface hydrophilicity increase and pure water permeance decrease. In addition, among PDA-modified membranes having similar surface hydrophilicity, the threshold flux decreased with decreasing pure water permeance. In summary, the membrane threshold flux may be increased via PDA surface modification using optimum coating conditions that help increase surface hydrophilicity, but still maintain high pure water permeance.

7.2 RECOMMENDATIONS FOR FUTURE WORK

7.2.1 MWCO Determination and UF Pore Size Modelling

7.2.1.1 Mass Transfer Coefficient (k) Determination

In this research, the mass transfer coefficient (k) was used in a concentration polarization model (i.e., film layer theory) to relate actual PEG sieving coefficients (or actual PEG rejections) and observed PEG sieving coefficients (or observed PEG rejections). The k values of different PEGs in the concentration boundary layer were determined using Equation (2.28) or Equation (2.29). The equation (2.28) was initially proposed by Smith et al. [22], and it has been widely-used to estimate k values in stirred filtration cells [20, 23]. However, these calculations and use of k value were based on several assumptions. For example, k was estimated as an average value (i.e., from Equation (2.28)) and used across an entire area over the stirred cell, while k in fact varies according to the radial position in the stirred cell [23]. Moreover, these calculations of k involved estimations of feed solution properties such as solute diffusivity, feed solution viscosity and density. These correlations could also depend on stirred cell geometry [22]. Although the estimation of k from the models has been widely acceptable, it may be

worthwhile to determine the *k* value experimentally, as conducted by some researchers [20]. The experimentally-determined *k* values should then be compared to the calculated *k* values from the models. The influence of different *k* values (i.e., those determined experimentally and from the models) on calculated actual PEG rejections (for MWCO determination) and on pore size modelling results should be investigated. It would also be interesting to check if *k* values determined from such experiments may help improve the model fitting of PEG sieving coefficient curves that are presented in Chapter 5 (cf., Figure 5.9 and Figure 5.10).

7.2.1.2 Modeled and Experimental Observed PEG Sieving Coefficient (S_o) Curve Fitting

As presented in Appendix B (cf., Figure B.6), the modeled S_o did not fit well with the experimental S_o values for 100 and 200 kDa PEGs for membranes modified with PDA at 0.1 mg/mL initial dopamine concentration (using 60 minutes coating time), and at 15 and 30 minutes coating time (using 2 mg/mL initial dopamine concentration). Although the cause of this deviation is not fully understood, several hypotheses are proposed. Some of these hypotheses include possible membrane defects (i.e., very large pores) that could have led to higher experimental S_o values than the predicted values [24, 25]. Different types of UF membranes (which are assumed to have different defects) with similar MWCO may be used in this PEG MWCO test and pore modelling analysis. It would be worthwhile to observe if the deviation between modeled and experimental S_o values of these PEGs (i.e., 100 and 200 kDa) is specific to only our membranes or if it may also exist in other types of UF membranes. In addition, some studies reported that such deviations could be due to an extensive concentration polarization in an actual stirred cell compared to that predicted by the models [23]. The experimentally-determined *k* values, as proposed in the earlier section, should be used for this model

calculation to best replicate the degree of concentration polarization occurred in the stirred cell. In addition, bulk properties of feed solution (e.g., viscosity and diffusivity) were used in our model calculations. However, the feed solution properties in the models are in fact those in the concentration boundary layer [26]. Thus, the effect of viscosity and diffusivity change due to higher solute concentration at the membrane wall (i.e., in the concentration boundary layer) relative to the bulk on the S_o prediction may be worth studying.

7.2.2 Threshold Flux Determination by Flux Stepping Experiments

The threshold flux was determined using a flux stepping method. In this work, the flux stepping experiments were conducted using an initial flux step of 10 LMH, a step height of 10 LMH, and a step length of 20 minutes for all membranes. These operational parameters were chosen based on convenience in performing the flux stepping experiments and the determined threshold flux values that were reasonable when compared to those determined from long term constant permeate flux filtration experiments. However, the initial flux step, step length, and step height have been reported to influence the estimated threshold flux values [27]. For this reason, the flux stepping experiments should also be conducted using different initial flux steps, step heights, and step lengths. The influence of these operational parameters on the determined threshold flux value should be systematically investigated for both unmodified and PDA-modified membranes. By using the most proper operational parameters, the accuracy of the threshold flux determined using this method might be enhanced. In addition, long term constant permeate flux filtration should be performed for each membrane to verify the threshold flux values determined from the flux stepping method, as recommended by some researchers [27].

7.2.3 Determination of Pore Characteristics of Fouled Membranes

Information related to pore characteristics of fouled membranes may help reveal fouling mechanisms during each stage of the filtration tests. For example, if MWCO and pore size of the fouled membranes are reduced from those of clean membranes, fouling may occur by pore blocking. The MWCO test and pore size modelling, presented in Chapter 5, should be used to determine the MWCO, mean pore size, and pore size distribution of unmodified and PDA-modified membranes after fouling. In addition, the pore characteristics of unmodified membranes after fouling should be compared with those of PDA-modified membranes to more clearly identify the fouling mechanisms in each membrane. Also, by using this approach, fouling propensity of the membranes may be determined more quantitatively than that from a conventional study.

7.3 REFERENCES

[1] C. Cheng, S. Li, W. Zhao, Q. Wei, S. Nie, S. Sun, C. Zhao, The hydrodynamic permeability and surface property of polyethersulfone ultrafiltration membranes with mussel-inspired polydopamine coatings, Journal of Membrane Science 417–418 (2012) 228–236.

[2] H. Lee, S.M. Dellatore, W.M. Miller, P.B. Messersmith, Mussel-inspired surface chemistry for multifunctional coatings, Science 318 (2007) 426–430.

[3] K. Kang, I.S. Choi, Y. Nam, A biofunctionalization scheme for neural interfaces using polydopamine polymer, Biomaterials 32 (2011) 6374–6380.

[4] B.D. McCloskey, H.B. Park, H. Ju, B.W. Rowe, D.J. Miller, B.D. Freeman, A bioinspired fouling-resistant surface modification for water purification membranes, Journal of Membrane Science 413–414 (2012) 82–90.

[5] D.J. Miller, D.R. Paul, B.D. Freeman, An improved method for surface modification of porous water purification membranes, Polymer 55 (2014) 1375–1383.

[6] Z. Xi, Y. Xu, L. Zhu, Y. Wang, B. Zhu, A facile method of surface modification for hydrophobic polymer membranes based on the adhesive behavior of poly(DOPA) and poly(dopamine), Journal of Membrane Science 327 (2009) 244–253.

[7] J. Jiang, L. Zhu, X. Li, Y. Xu, B. Zhu, Surface modification of PE porous membranes based on the strong adhesion of polydopamine and covalent immobilization of heparin, Journal of Membrane Science 364 (2010) 194–202.

[8] Y.M. Shin, Y.B. Lee, H. Shin, Time-dependent mussel-inspired functionalization of poly(L-lactide-co-ε-caprolactone) substrates for tunable cell behaviors, Colloids and Surfaces B: Biointerfaces 87 (2011) 79–87.

[9] Y. Liu, K. Ai, L. Lu, Polydopamine and its derivative materials: Synthesis and promising applications in energy, environmental, and biomedical fields, Chemical Reviews 114 (2014) 5057–5115.

[10] V. Ball, D.D. Frari, V. Toniazzo, D. Ruch, Kinetics of polydopamine film deposition as a function of pH and dopamine concentration: Insights in the polydopamine deposition mechanism, Journal of Colloid and Interface Science 386 (2012) 366–372.

[11] J. Ou, J. Wang, S. Liu, J. Zhou, S. Ren, S. Yang, Microtribological and electrochemical corrosion behaviors of polydopamine coating on APTS-SAM modified Si substrate, Applied Surface Science 256 (2009) 894–899.

[12] J. Jiang, L. Zhu, L. Zhu, B. Zhu, Y. Xu, Surface characteristics of a self-polymerized dopamine coating deposited on hydrophobic polymer films, Langmuir 27 (2011) 14180–14187.

[13] D.J. Miller, S. Kasemset, L. Wang, D.R. Paul, B.D. Freeman, Constant flux crossflow filtration evaluation of surface-modified fouling-resistant membranes, Journal of Membrane Science 452 (2014) 171–183.

[14] S. Kasemset, A. Lee, D.J. Miller, B.D. Freeman, M.M. Sharma, Effect of polydopamine deposition conditions on fouling resistance, physical properties, and permeation properties of reverse osmosis membranes in oil/water separation, Journal of Membrane Science 425–426 (2013) 208–216.

[15] L.J. Zeman, A.L. Zydney, Microfiltration and Ultrafiltration: Principles and Applications, Marcel Dekker, Inc., New York, NY, 1996.

[16] R.W. Baker, Membrane Technology and Applications, 2nd ed., John Wiley & Sons Ltd., West Sussex, England, 2004.

[17] G.M. Geise, H.B. Park, A.C. Sagle, B.D. Freeman, J.E. McGrath, Water permeability and water/salt selectivity tradeoff in polymers for desalination, Journal of Membrane Science 369 (2011) 130–138.

[18] R.W. Baker, B.T. Low, Gas separation membrane materials: A perspective, Macromolecules 47 (2014) 6999–7013.

[19] D.F. Sanders, Z.P. Smith, R. Guo, L.M. Robeson, J.E. McGrath, D.R. Paul, B.D. Freeman, Energy-efficient polymeric gas separation membranes for a sustainable future: A review, Polymer 54 (2013) 4729–4761.

[20] W.S. Opong, A.L. Zydney, Diffusive and convective protein transport through asymmetric membranes, AIChE Journal 37 (1991) 1497–1510.

[21] R.W. Field, G.K. Pearce, Critical, sustainable and threshold fluxes for membrane filtration with water industry applications, Advances in Colloid and Interface Science 164 (2011) 38–44.

[22] K.A. Smith, C.K. Colton, E.W. Merrill, L.B. Evans, Convective transport in a batch dialyzer: Determination of true membrane permeability from a single measurement, AIChE Symposium Series 64 (1968) 45–58.

[23] A.L. Zydney, A. Xenopoulos, Improving dextran tests for ultrafiltration membranes: Effect of device format, Journal of membrane Science 291 (2007) 180–190.

[24] L. Zeman, M. Wales, Polymer Solute Rejection by Ultrafiltration Membranes, in: A.F. Turbak (Ed.) ACS Symposium Series 154 (Synthetic Membranes: Volume II Hyper- and Ultrafiltration Uses), American Chemical Society, Washington, DC, 1981, pp. 411–434.

[25] T. Urase, K. Yamamoto, S. Ohgaki, Effect of pore size distribution of ultrafiltration membranes on virus rejection in crossflow conditions, Water Science and Technology 30 (1994) 199–208.

[26] S. Saksena, A.L. Zydney, Influence of protein–protein interactions on bulk mass transport during ultrafiltration, Journal of Membrane Science 125 (1997) 93–108.

[27] S.P. Beier, G. Jonsson, Critical flux determination by flux-stepping, AIChE Journal 56 (2010) 1739–1747.

Appendix A: List of Symbols

A.1 ENGLISH SYMBOLS

a	Solute or particle radius (m)
A	Effective membrane filtration area (m^2)
b	Membrane radius determined from effective membrane filtration area (m)
C_b	Bulk feed solute concentration (mg/L)
C_f	Filtrate solute concentration (mg/L)
C_m	Solute concentration at the membrane surface on feed side (mg/L)
D_∞	PEG diffusion coefficient in infinite dilute solution (m^2/s)
$\overline{J}_{pw}$	Average pure water flux (m/s)
$\overline{J}_v$	Average permeate flux from solute filtration test in the stirred cell (m/s)
$J_v(r_c)$	Local permeate flux from solute filtration test at any radial position r_c in the stirred cell (m/s)
K_c	Hindrance factor for solute convection
K_d	Hindrance factor for solute diffusion
$\overline{k}$	Average mass transfer coefficient (m/s)
$k(r_c)$	Local mass transfer coefficient at any radial position r_c in the stirred cell (m/s)
$\overline{L}_p$	Average membrane pure water permeance or hydraulic permeability (m/(s·Pa))
m	Permeate mass of pure water (kg)
M	PEG molecular weight (g/mol)
n_o	Total number of pores per unit membrane area
$n(r)$	Total number of pores of radius r per unit membrane area
Pe_m	Peclet number inside the membrane pores

$P_{feed}(r_c)$	Applied feed pressure at any radial position r_c in the stirred cell at the membrane surface (kg/(m·s^2))
P_f	Filtrate pressure (kg/(m·s^2))
P_o	Applied feed pressure at the central axis of the stirred cell at the membrane surface (kg/(m·s^2))
r	Membrane pore radius (m)
$\bar{r}$	Membrane mean pore radius (m)
r_c	Radial position from the center of the stirred cell (m)
R_a	Actual membrane retention coefficient
R_o	Observed membrane retention coefficient
Re	Reynolds number
S_a	Actual membrane sieving coefficient
S_o	Observed membrane sieving coefficient
$\overline{S}_a$	Averaged actual membrane sieving coefficient over all pore sizes (based on log-normal pore size distribution)
S_∞	Asymptotic sieving coefficient
Sc	Schmidt number
t	Pure water filtration time (s)
$TMP_{local}(r_c)$	Local transmembrane pressure at any radial position r_c in the stirred cell (kg/(m·s^2))
TMP_n	Nominal measured (average) transmembrane pressure (pressure difference between feed and permeate side of the membrane) (kg/(m·s^2))
z	Axial position away from the feed surface of the membrane (m)

A.2 GREEK SYMBOLS

α	Separation factor
α_{stir}	Constant based on filtration device geometry for $\bar{k}$ or $k(r_c)$ determination
χ^2	Chi-squared goodness-of-fit parameter
δ_c	Concentration boundary layer thickness (m)
δ_m	Membrane selective layer thickness (m)
ε	Porosity of membrane selective layer
μ	Dynamic viscosity of solvent (kg/(m·s))
ν	Kinematic viscosity of solvent (m^2/s)
ω	Stirring speed in the stirred filtration cell (radians/s)
ϕ	Equilibrium partition coefficient
ρ	Density of solvent (kg/m^3)
σ	Standard deviation of log-normal pore size distribution (m)

Appendix B: Supplementary Information for Chapter 5

B.1 Experimental and Calculated S_o Data

Table B.1: Comparison of observed PEG sieving coefficients, S_o, from experiments and model calculations of PS-20 UF membranes modified with PDA at various initial dopamine concentrations.

Initial dopamine concentration (mg/mL)	PEG Molecular weight (kDa)	PEG Stokes radius (nm)	Experimental S_o	Calculated S_o
Unmodified	4	1.7	0.985±0.003	0.975
	8	2.5	0.94±0.03	0.903
	12	3.1	0.866±0.006	0.816
	20	4.2	0.655±0.004	0.657
	35	5.7	0.33±0.01	0.444
	100	10.2	0.115±0.002	0.125
	200	15.0	0.086±0.003	0.038
0.5	4	1.7	0.995±0.005	0.983
	8	2.5	0.912±0.004	0.898
	10	2.8	0.836±0.004	0.821
	12	3.1	0.63±0.01	0.728
	20	4.2	0.301±0.008	0.360
	35	5.7	0.090±0.004	0.069
1	4	1.7	0.991±0.001	0.985
	8	2.5	0.925±0.005	0.926
	10	2.8	0.84±0.02	0.870
	12	3.1	0.63±0.04	0.796
	20	4.2	0.28±0.04	0.414
	35	5.7	0.09±0.01	0.069
2	4	1.7	0.979±0.001	0.978
	8	2.5	0.88±0.01	0.868
	10	2.8	0.77±0.02	0.770
	12	3.1	0.52±0.04	0.659
	20	4.2	0.22±0.02	0.274
	35	5.7	0.060±0.009	0.040
4	4	1.7	0.981±0.003	0.966
	8	2.5	0.85±0.01	0.787
	10	2.8	0.698±0.008	0.661
	12	3.1	0.41±0.01	0.537
	20	4.2	0.144±0.008	0.198
	35	5.7	0.038±0.001	0.029

Initial dopamine concentration (mg/mL)	PEG Molecular weight (kDa)	PEG Stokes radius (nm)	Experimental S_o	Calculated S_o
8	4	1.7	0.977±0.004	0.960
	8	2.5	0.83±0.02	0.760
	10	2.8	0.66±0.01	0.628
	12	3.1	0.39±0.01	0.502
	20	4.2	0.141±0.007	0.178
	35	5.7	0.038±0.002	0.026

Note: All samples (except unmodified membranes) were modified with PDA using a deposition time of 60 minutes. The PEG Stokes radius was calculated from Equation (2.22).

Table B.2: Comparison of observed PEG sieving coefficients, S_o, from experiments and model calculations of PS-20 UF membranes modified with PDA at various deposition times.

Deposition time (minutes)	PEG Molecular weight (kDa)	PEG Stokes radius (nm)	Experimental S_o	Calculated S_o
60	4	1.7	0.979±0.001	0.978
	8	2.5	0.88±0.01	0.868
	10	2.8	0.77±0.02	0.770
	12	3.1	0.52±0.04	0.659
	20	4.2	0.22±0.02	0.274
	35	5.7	0.060±0.009	0.040
120	4	1.7	0.988±0.003	0.980
	8	2.5	0.874±0.001	0.874
	10	2.8	0.746±0.008	0.768
	12	3.1	0.46±0.02	0.634
	20	4.2	0.16±0.01	0.173
	35	5.7	0.039±0.004	0.006
240	4	1.7	0.973±0.005	0.962
	8	2.5	0.79±0.05	0.765
	10	2.8	0.59±0.07	0.625
	12	3.1	0.32±0.06	0.489
	20	4.2	0.10±0.02	0.149
	35	5.7	0.027±0.005	0.016

Note: All samples were modified with PDA using an initial dopamine coating solution concentration of 2 mg/mL. The PEG Stokes radius was calculated from Equation (2.22).

B.2 A Comparison of Mean Pore Radii and Nominal Pore Radii of Unmodified and PDA-Modified UF Membranes

Table B.3 and Table B.4 present a comparison of nominal pore radii and mean pore radii of unmodified and PDA-modified membranes. Generally, the nominal pore radius (i.e., the radius of a solute molecule giving 90% rejection or the radius of a solute molecule with molecular weight the same as the MWCO) can be smaller or larger than the mean pore radius. The relationship of nominal and mean pore radii depends on the standard deviation of the pore size distribution [1]. In this study, the nominal pore radius of the unmodified membranes was larger than their mean pore radius. The unmodified membranes had a wide pore size distribution (i.e., high σ value), so there were presumably a relatively large number of big pores in this membrane. Other studies have shown that such a long tail-effect of big pores leads to high values of MWCO and, therefore, large nominal pore radii [1]. However, for PDA-modified membranes (as presented in Table B.3 and Table B.4), the nominal pore radii were smaller than their mean pore radii. The pore size distributions of these PDA-modified membranes were markedly narrower (i.e., have lower σ values) than that of the unmodified membranes. Consequently, the long-tail effect of big pores was not significant in these membranes while the sieving effect mainly controls MWCO, leading to smaller nominal pore radii than mean pore radii [1].

Table B.3: Mean pore radius, $\bar{r}$, ratio of standard deviation of pore size distribution to mean pore radius, $\sigma/\bar{r}$, and porosity to thickness ratio, ε/δ_m, of PS-20 UF membranes modified with PDA at various initial dopamine concentrations.

Initial dopamine concentration (mg/mL)	**MWCO (kDa)**	**Nominal pore radius from MWCO (nm)**	**Mean pore radius, $\bar{r}$ (nm)**	**$\sigma/\bar{r}$**	**ε/δ_m (μm^{-1})**
Unmodified	54±2	7.3±0.2	3.3	0.64	0.38±0.05
0.5	26.2±0.4	4.84±0.04	5.6	0.18	0.41±0.04
1	25±2	4.7±0.2	6.8	0.06	0.30±0.02
2	21±2	4.3±0.2	5.2	0.18	0.42±0.02
4	18.5±0.3	3.98±0.03	4.2	0.24	0.55±0.01
8	18.2±0.2	3.95±0.03	4	0.25	0.56±0.03

Note: All samples (except unmodified membranes) were modified with PDA using a deposition time of 60 minutes. Uncertainties in ε/δ_m represent one standard deviation and were calculated using propagation of errors [2].

Table B.4: Mean pore radius, $\bar{r}$, ratio of standard deviation of pore size distribution to mean pore radius, $\sigma/\bar{r}$, and porosity to thickness ratio, ε/δ_m, of PS-20 UF membranes modified with PDA at various PDA deposition times.

Deposition time (minutes)	**MWCO (kDa)**	**Nominal pore radius from MWCO (nm)**	**Mean pore radius, $\bar{r}$ (nm)**	**$\sigma/\bar{r}$**	**ε/δ_m (μm^{-1})**
Unmodified	54±2	7.3±0.2	3.3	0.64	0.38±0.05
60	21±2	4.3±0.2	5.2	0.18	0.42±0.02
120	19.0±0.3	4.04±0.04	5.5	0.08	0.43±0.03
240	17±2	3.7±0.2	4.4	0.2	0.43±0.03

Note: All samples (except unmodified membranes) were modified with PDA using an initial dopamine coating solution concentration of 2 mg/mL. Uncertainties in ε/δ_m represent one standard deviation and were calculated using propagation of errors [2].

B.3 Membrane Mean Pore Size and Pore Size Distribution Analysis

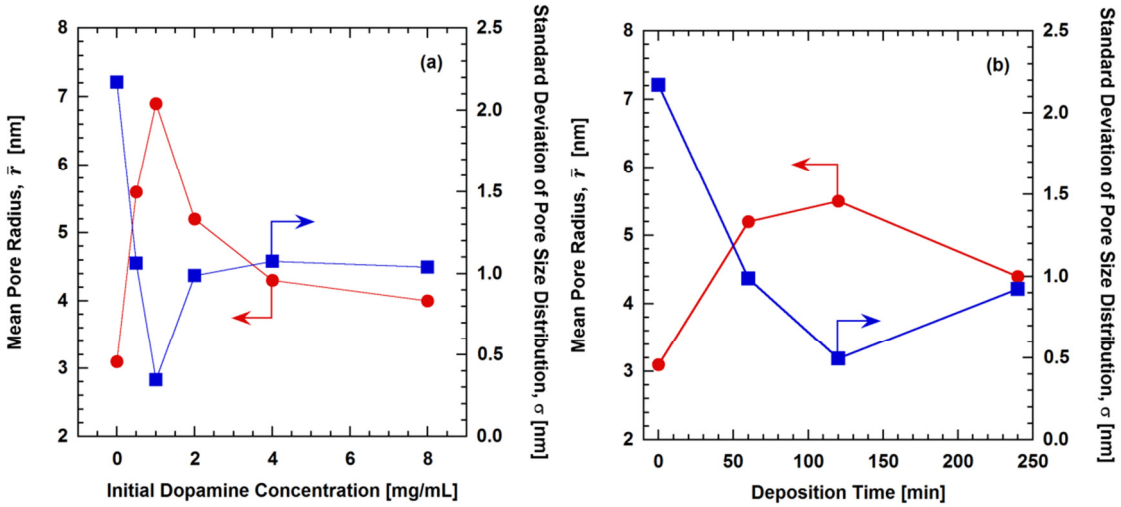

Figure B.1: Effect of PDA deposition conditions on mean pore radius ($\bar{r}$) and standard deviation (σ) of pore size distribution of PS-20 UF membranes modified with PDA at various: (a) initial dopamine concentrations and (b) deposition times. ε/δ_m was used as a fitted parameter, and $\overline{k}$ and $\overline{J}_V$ were employed in the model calculations. A deposition time of 60 minutes was used in (a), and an initial dopamine concentration of 2 mg/mL was used in (b).

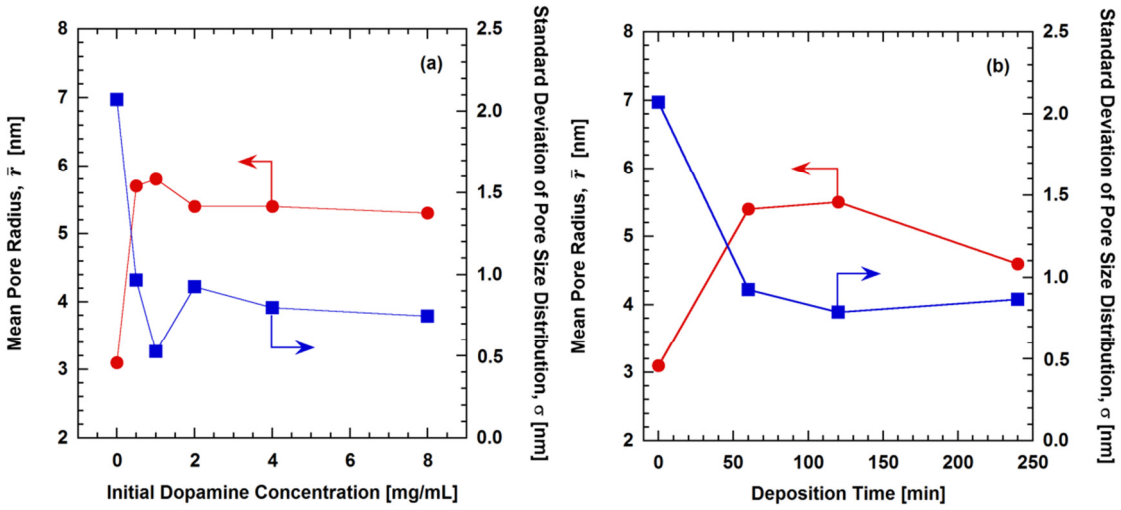

Figure B.2: Effect of PDA deposition conditions on mean pore radius ($\bar{r}$) and standard deviation (σ) of pore size distribution of PS-20 UF membranes modified with PDA at various: (a) initial dopamine concentrations and (b) deposition times. ε/δ_m was used as a constant value of 0.4 μm^{-1}, and $k(r_c)$ and $J_v(r_c)$ were employed in the model calculations. A deposition time of 60 minutes was used in (a), and an initial dopamine concentration of 2 mg/mL was used in (b).

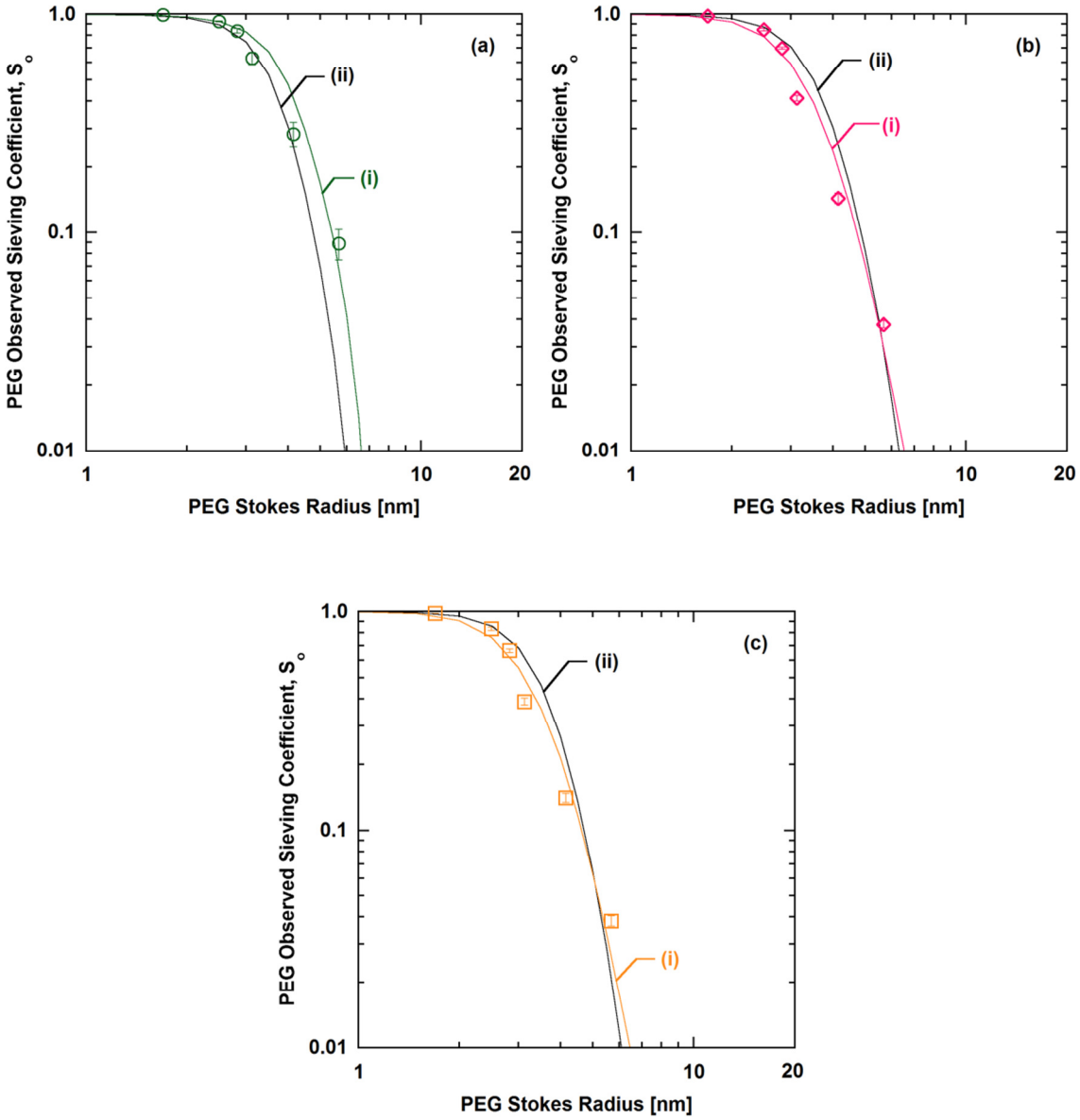

Figure B.3: S_o values from experiments (represented by discrete data points) and S_o from model calculations (represented by solid curves) using: (i) ε/δ_m as a fitted parameter and (ii) ε/δ_m as a constant value of 0.4 μm^{-1}. $k(r_c)$ and $J_v(r_c)$ were employed in the model calculations. The membranes were modified with PDA at initial dopamine concentrations of (a) 1 mg/mL, (b) 4 mg/mL, and (c) 8 mg/mL. A deposition time of 60 minutes was used.

B.4 A Comparison of Pore Size Distribution When ε/δ_m Is Treated as a Fitting Parameter and When ε/δ_m Is Set to a Constant Value for Model Calculations

When using ε/δ_m as a fitted parameter (cf., Figure S.4(a)), for membranes coated with PDA at 4 and 8 mg/mL initial dopamine concentrations, the distribution of pores shifted largely towards smaller pore sizes relative to those coated at lower initial dopamine concentrations. However, when using a fixed value of ε/δ_m as 0.4 μm^{-1} (cf., Figure B.4(b)), the pore size distribution of these membranes (i.e., coated with 4 and 8 mg/mL initial dopamine concentrations) remained closer to that of those coated at lower initial dopamine concentrations. Generally, the membrane pore size directly influences the pure water permeance [3]. The latter pore size distribution profiles, which were modeled using a fixed value of ε/δ_m, were more consistent with the experimental pure water permeance data. The pure water permeance only slightly decreased at high initial dopamine concentrations (i.e., 4 and 8 mg/mL) relative to that at low initial dopamine concentrations (i.e., 1 and 2 mg/mL) (cf., Figure 5.2(a)). The slight change in pure water permeance implies that there were only small changes in the membrane pore sizes at those coating conditions.

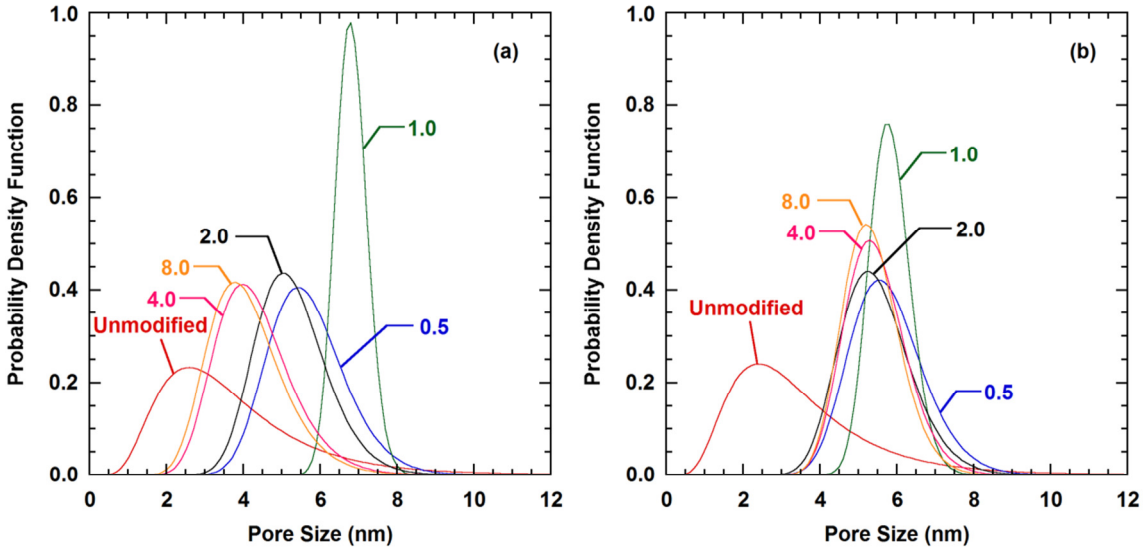

Figure B.4: Probability density function of pore size distributions, $n(r)/n_o$, calculated using the log-normal distribution, of unmodified membranes and membranes modified with PDA at various initial dopamine concentrations. The model calculations used (a) ε/δ_m as a fitted parameter and (b) ε/δ_m as a constant value of 0.4 μm^{-1}. $k(r_c)$ and $J_v(r_c)$ were employed in the model calculations. The numbers in plots (a) and (b) represent initial dopamine concentration in mg/mL. A deposition time of 60 minutes was used. $\bar{r}$ and σ values used to generate plots (a) and (b) are presented in Figure 5.11(a) (and Table B.3) and Figure B.2(a), respectively.

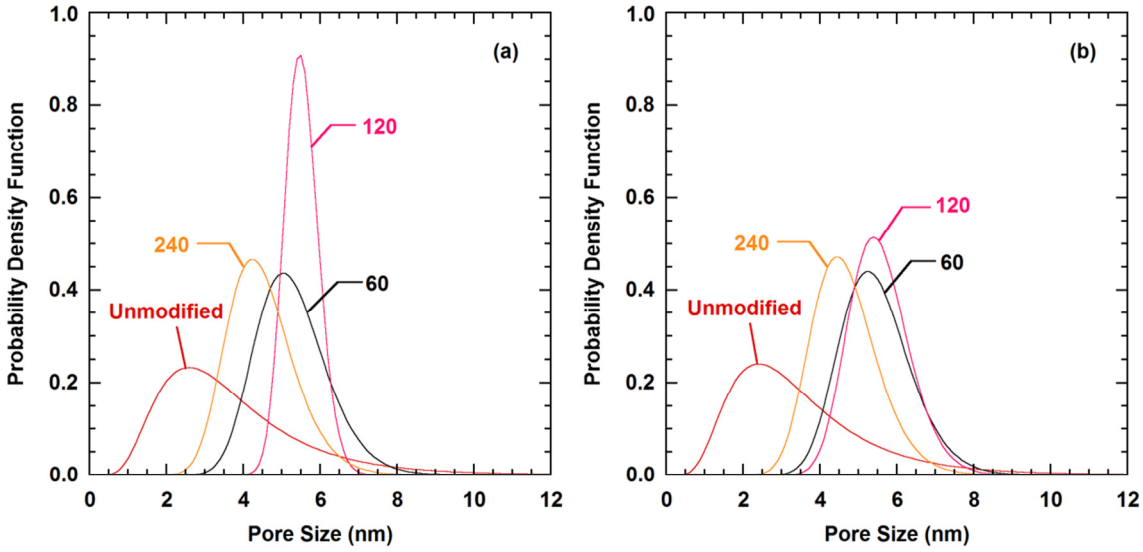

Figure B.5: Probability density function of pore size distributions, $n(r)/n_o$, calculated using the log-normal distribution, of unmodified membranes and membranes modified with PDA at various PDA deposition times. The model calculations used (a) ε/δ_m as a fitted parameter and (b) ε/δ_m as a constant value of 0.4 μm^{-1}. $k(r_c)$ and $J_v(r_c)$ were employed in the model calculations. The numbers in plots (a) and (b) represent PDA deposition time in minutes. An initial dopamine concentration of 2 mg/mL was used. $\bar{r}$ and σ values used to generate plots (a) and (b) are presented in Figure 5.11(b) (and Table B.4) and Figure B.2(b), respectively.

B.5 Deviation of Experimental and Modeled S_o from Data Fitting

Figure B.6 shows the modeled and experimental S_o values of membranes modified with PDA at the lowest initial dopamine concentration (i.e., 0.1 mg/mL, using 60 minutes coating time) and the shortest coating times (i.e., 15 and 30 minutes, using 2 mg/mL initial dopamine concentration) studied. For these PDA-modified membranes, high molecular weight PEGs, which were 100 and 200 kDa, were used for the MWCO tests. As shown in Figure B.6, the model did not capture S_o at the highest PEG molecular weights of 100 and 200 kDa, which corresponded to the largest PEG Stokes radii of 10 and 15 nm, respectively. The cause of this deviation is not fully understood. Zydney and Xenopoulos suggested that under-prediction of experimental S_o values from this model

could be due to more extensive concentration polarization in the experiment than predicted by the model [4]. Moreover, high molecular weight molecules could elongate under shear flow and pass through smaller pores than those predicted by the model, leading to higher observed sieving coefficients in the experiments than model values [5-7]. In addition, the actual membrane pore size distribution could deviate from the log-normal pore size distribution used here, leading to higher numbers of large pores than those predicted by the model. These membrane defects (i.e., large pores) could lead to increased membrane sieving coefficients relative to that of the defect-free membranes [8, 9]. Future studies aimed at clarifying the basis for such deviations would be helpful in understanding the limits of applicability of such modeling approaches and/or suggest experimental protocols to minimize such deviations.

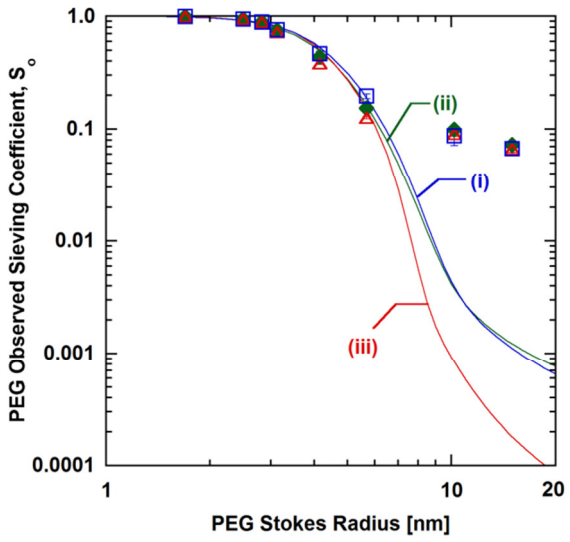

Figure B.6: Observed PEG sieving coefficients of PS-20 UF membranes modified with PDA at initial dopamine concentration ($C_{dopamine}$) and PDA deposition time ($t_{deposition}$) of (i) $C_{dopamine}$ = 0.1 mg/mL, $t_{deposition}$ = 60 minutes (□), (ii) $C_{dopamine}$ = 2 mg/mL, $t_{deposition}$ = 15 minutes (♦) and, and (iii) $C_{dopamine}$ = 2 mg/mL, $t_{deposition}$ = 30 minutes (Δ). Discrete data points show experimental data and solid curves show corresponding model calculations.

B.6 REFERENCES

[1] J. Ren, Z. Li, F.S. Wong, A new method for the prediction of pore size distribution and MWCO of ultrafiltration membranes, Journal of Membrane Science 279 (2006) 558–569.

[2] P.R. Bevington, D.K. Robinson, Data Reduction and Error Analysis for the Physical Sciences, 3rd ed., The McGraw-Hill Companies, Inc., New York, NY, 2003.

[3] L.J. Zeman, A.L. Zydney, Microfiltration and Ultrafiltration: Principles and Applications, Marcel Dekker, Inc., New York, NY, 1996.

[4] A.L. Zydney, A. Xenopoulos, Improving dextran tests for ultrafiltration membranes: Effect of device format, Journal of membrane Science 291 (2007) 180–190.

[5] D.R. Latulippe, J.R. Molek, A.L. Zydney, Importance of biopolymer molecular flexibility in ultrafiltration processes, Industrial and Engineering Chemistry Research 48 (2009) 2395–2403.

[6] D.P. Pope, A. Keller, Alignment of macromolecules in solution by elongational flow; a study of the effect of pure shear in a four roll mill, Colloid and Polymer Science 255 (1977) 633–643.

[7] D.G. Crowley, F.C. Frank, M.R. Mackley, R.G. Stephenson, Localized flow birefringence of polyethylene oxide solutions in a four roll mill, Journal of Polymer Science: Polymer Physics Edition 14 (1976) 1111–1119.

[8] L. Zeman, M. Wales, Polymer Solute Rejection by Ultrafiltration Membranes, in: A.F. Turbak (Ed.) ACS Symposium Series 154 (Synthetic Membranes: Volume II Hyper- and Ultrafiltration Uses), American Chemical Society, Washington, DC, 1981, pp. 411–434.

[9] T. Urase, K. Yamamoto, S. Ohgaki, Effect of pore size distribution of ultrafiltration membranes on virus rejection in crossflow conditions, Water Science and Technology 30 (1994) 199–208.

Appendix C: Supplementary Information for Chapter 6

C.1 Zeta Potentials of PDA Coating Films from Literature

Table C.1: Summary of literature zeta potentials of deposited PDA films at neutral pH.

Reference	Coated substrate	Initial dopamine concentration (mg/mL)	PDA deposition time (hours)	Tris buffer concentration (mM)	Tris buffer pH	Zeta potential (mV) at pH 7 [**]
This study	PSf UF	2	1	15	8.8	-28
Zhang et al. (2014) [1]	PES UF	2	2	50	8.5	-15.3 (pH 6)
Kim et al. (2014) [2]	Regenerated cellulose UF	2	12	15	8.5	-20.4
Azari and Zou (2012) [3]	SW30XLE RO	2 (using L-DOPA)	24	10	8.3	-21
Karkhanechi et al. (2014) [4]	ES20 RO	1.5	24	15	8.8	-8.9 (pH 5.9)
Vaselbehagh et al. (2014) [5]	Anion exchange membrane	0.5	24	15	8.8	-18 (pH 6.2)
		2				-15 (pH 6.2)
Ball (2010) [6]	Glass	2	12 immersions of 5 minutes each	50	8.5	-34 (from data interpolation)
Yu et al. (2010) [7]	PDA particles [*]	2	24	10	8.5	-2.26
Zhang et al. (2014) [8]	PDA capsules [*]	2	24	10	8.5	-7.9
		3				-14
Liu et al. (2011) [9]	PDA capsules [*]	0.2	24	N/A	8.5	-38 (from data interpolation)

Note: [*] Zeta potentials of PDA particles and capsules were measured using a Zetasizer.
[**] Zeta potential values are reported at pH 7 unless otherwise noted in the parenthesis.

C.2 THRESHOLD FLUX OF UNMODIFIED AND PDA-MODIFIED MEMBRANES

Table C.2: Threshold fluxes (determined from the TMP_{avg} and d(TMP)/dt estimates) of unmodified PS-20 UF membranes and membranes modified with PDA at various initial dopamine concentrations (60-minute deposition time).

Initial dopamine concentration (mg/mL)	**Threshold flux (LMH)**		**Nominal pore radius[**] (nm)**
	TMP_{avg}	**d(TMP)/dt**	
Unmodified	59±2	53	12.3
0.1	69±1	71	9.5
0.5	69[*]	70	5.6
2	57[*]	69	5.3
8	47[*]	51	4.7

Note: The threshold flux data from TMP_{avg} were determined using the R^2_{min} of 0.99, and the d(TMP)/dt value used to estimate threshold flux was 0.5 mbar/min.
[*] The uncertainties in these data were very small, so they are not presented here.
[**] The nominal pore radius values were taken from [10].

Table C.3: Threshold fluxes (determined from the TMP_{avg} and d(TMP)/dt estimates) of unmodified PS-20 UF membranes and membranes modified with PDA at various PDA deposition times (2 mg/mL initial dopamine concentration).

PDA deposition time (minutes)	**Threshold flux (LMH)**		**Nominal pore radius[**] (nm)**
	TMP_{avg}	**d(TMP)/dt**	
Unmodified	59±2	53	12.3
15	68[*]	61	10.2
60	57[*]	69	5.3
240	51±7	44	4.2

Note: The threshold flux data from TMP_{avg} were determined using the R^2_{min} of 0.99, and the d(TMP)/dt value used to estimate threshold flux was 0.5 mbar/min.
[*] The uncertainties in these data were very small, so they are not presented here.
[**] The nominal pore radius values were taken from [10].

C.3 Threshold Flux Determination of Unmodified and PDA-Modified Membranes Using Different R^2 Coefficients

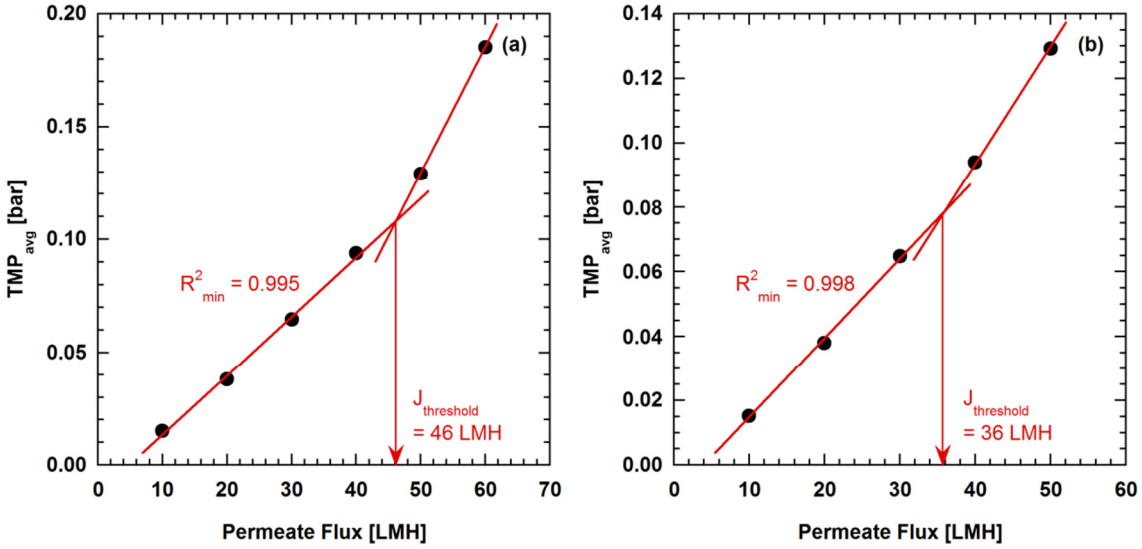

Figure C.1: Threshold flux ($J_{threshold}$) determination from TMP_{avg} vs. flux profile using different minimum R^2 coefficients (R^2_{min}): (a) R^2_{min} = 0.995 and (b) R^2_{min} = 0.998 for the linear regression of data below the threshold flux. Each plot is representative of at least three replicates.

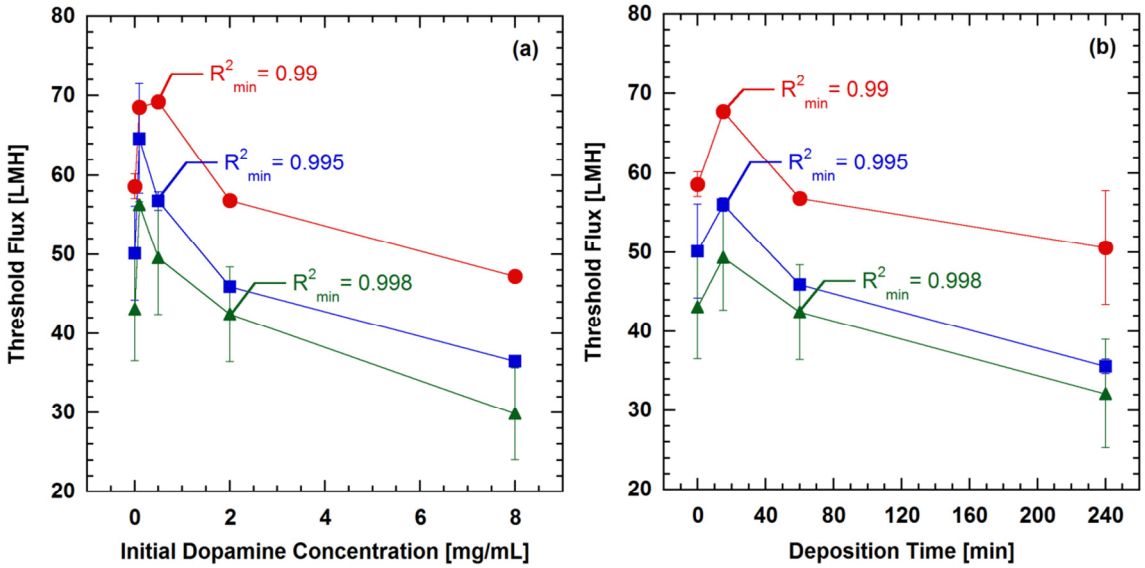

Figure C.2: A comparison of the threshold fluxes determined using the TMP_{avg} parameter with different R^2_{min} values: 0.99 (●), 0.995 (■), and 0.998 (▲) to generate linear regression lines below the threshold flux in TMP_{avg} vs. flux profiles of PS-20 UF membranes modified with PDA at various (a) initial dopamine concentrations and (b) deposition times. A deposition time of 60 minutes was used in (a) and an initial dopamine concentration of 2 mg/mL was used in (b).

To identify the most appropriate R^2_{min} used in this work, the threshold fluxes were verified with long-term constant flux filtration reported in our previous study [11]. From such constant flux filtration studies, the threshold flux of unmodified PS-20 UF membranes was in the range of 55 – 70 LMH [11]. Here, the average threshold fluxes (from three membrane samples) of unmodified PS-20 UF membranes using R^2_{min} values of 0.99, 0.995, and 0.998 were 59±2, 50±6, and 43±7 LMH, respectively. Since the R^2_{min} of 0.99 provided the most realistic threshold flux relative to that from the long-term filtration, the R^2_{min} of 0.99 was used as the criterion to estimate threshold fluxes for all membranes in this study.

In addition, we attempted to establish the regression line below the threshold flux based on a statistical analysis using the F-test [12]. The F-test was used to identify the maximum flux that changed the relationship of TMP_{avg} and flux from linear to non-linear (i.e., a quadratic polynomial). The analysis was performed based on confidence intervals of 95% and 99% (equivalent to levels of significance, α, of 0.05 and 0.01, respectively) [12]. For several membranes in this study, regardless of the confidence interval used, the threshold fluxes determined based on this analysis could not be identified. In these cases, the F-test analysis predicted threshold fluxes that were higher than the maximum fluxes tested in our flux stepping experiments. Thus, this approach could not provide reliable estimations of the threshold fluxes in our study.

C.4 THRESHOLD FLUX DETERMINATION

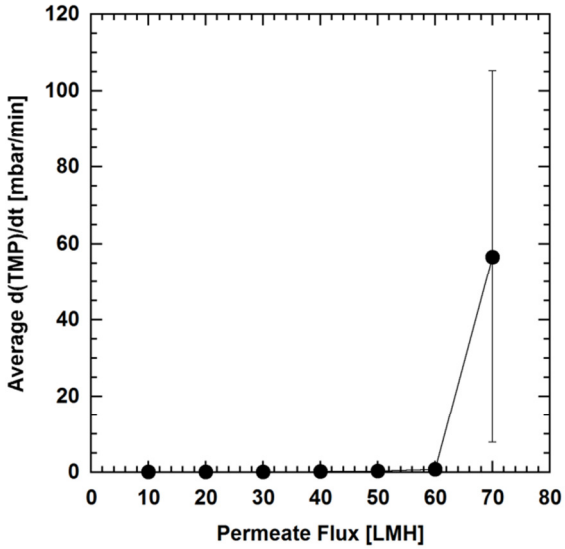

Figure C.3: A full profile of average d(TMP)/dt vs. permeate flux of unmodified PS-20 UF membranes from flux stepping experiments.

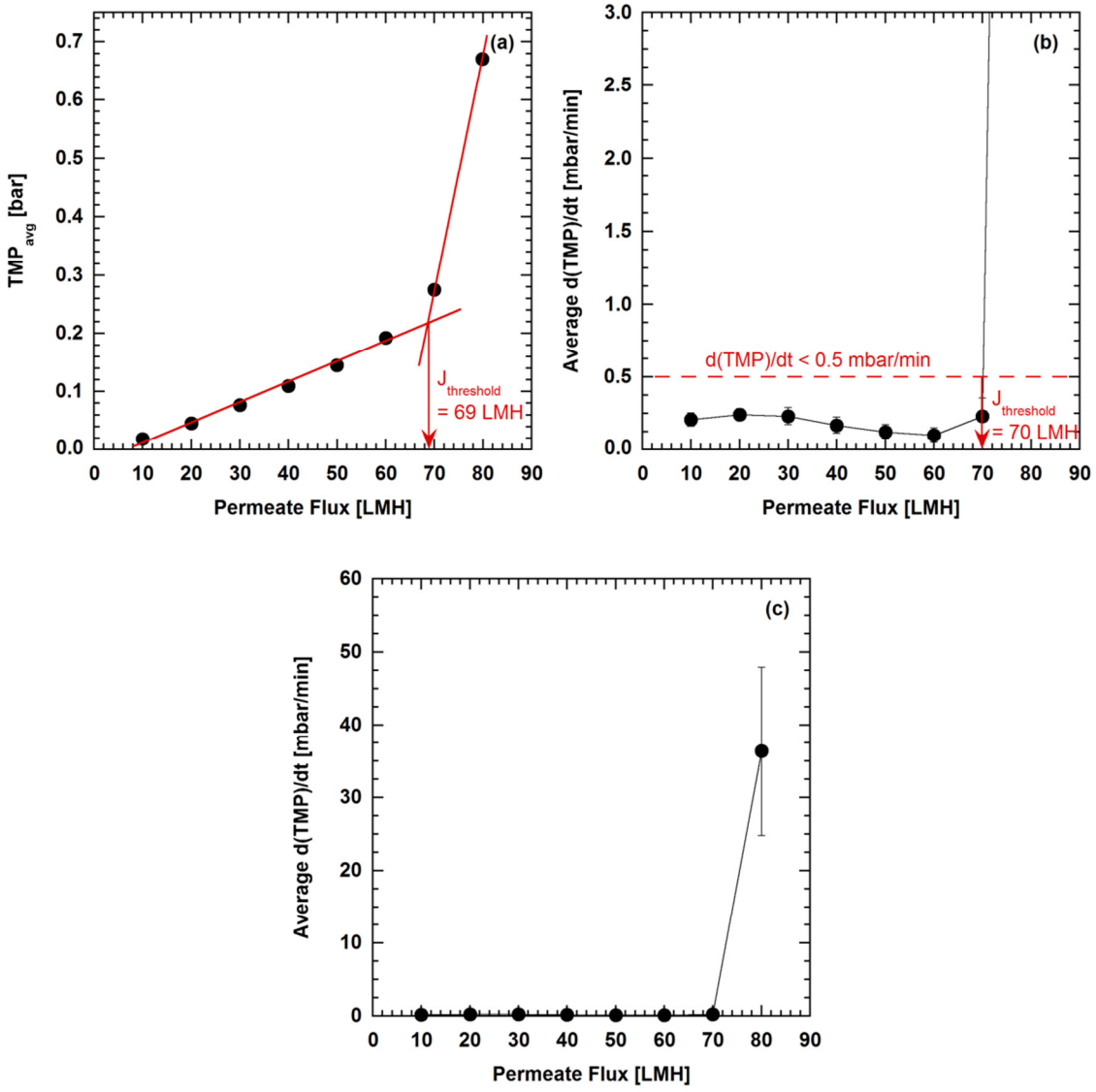

Figure C.4: Threshold flux ($J_{threshold}$) determination using: (a) TMP_{avg} and (b) d(TMP)/dt of PS-20 UF membranes modified with PDA at 0.1 mg/mL initial dopamine concentration (60-minute deposition time). (c) shows a full profile of average d(TMP)/dt vs. permeate flux from the flux stepping experiments. An R^2_{min} of 0.99 was used to generate linear regression line below the threshold flux in (a). The line in (b) connects average d(TMP)/dt at each flux to guide the eye on changes in the d(TMP)/dt values.

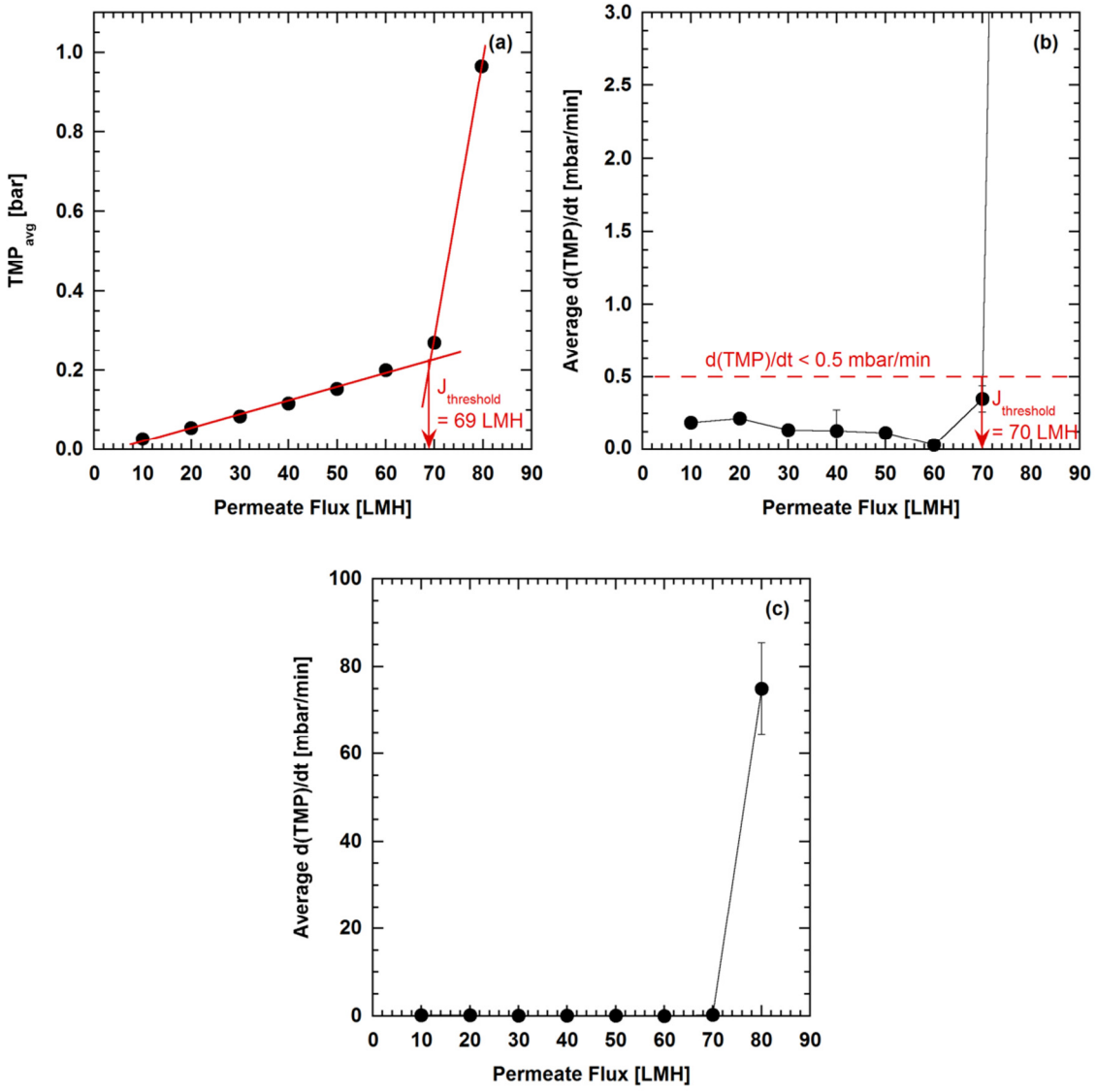

Figure C.5: Threshold flux ($J_{threshold}$) determination using: (a) TMP_{avg} and (b) d(TMP)/dt of PS-20 UF membranes modified with PDA at 0.5 mg/mL initial dopamine concentration (60-minute deposition time). (c) shows a full profile of average d(TMP)/dt vs. permeate flux from the flux stepping experiments. An R^2_{min} of 0.99 was used to generate linear regression line below the threshold flux in (a). The line in (b) connects average d(TMP)/dt at each flux to guide the eye on changes in the d(TMP)/dt values.

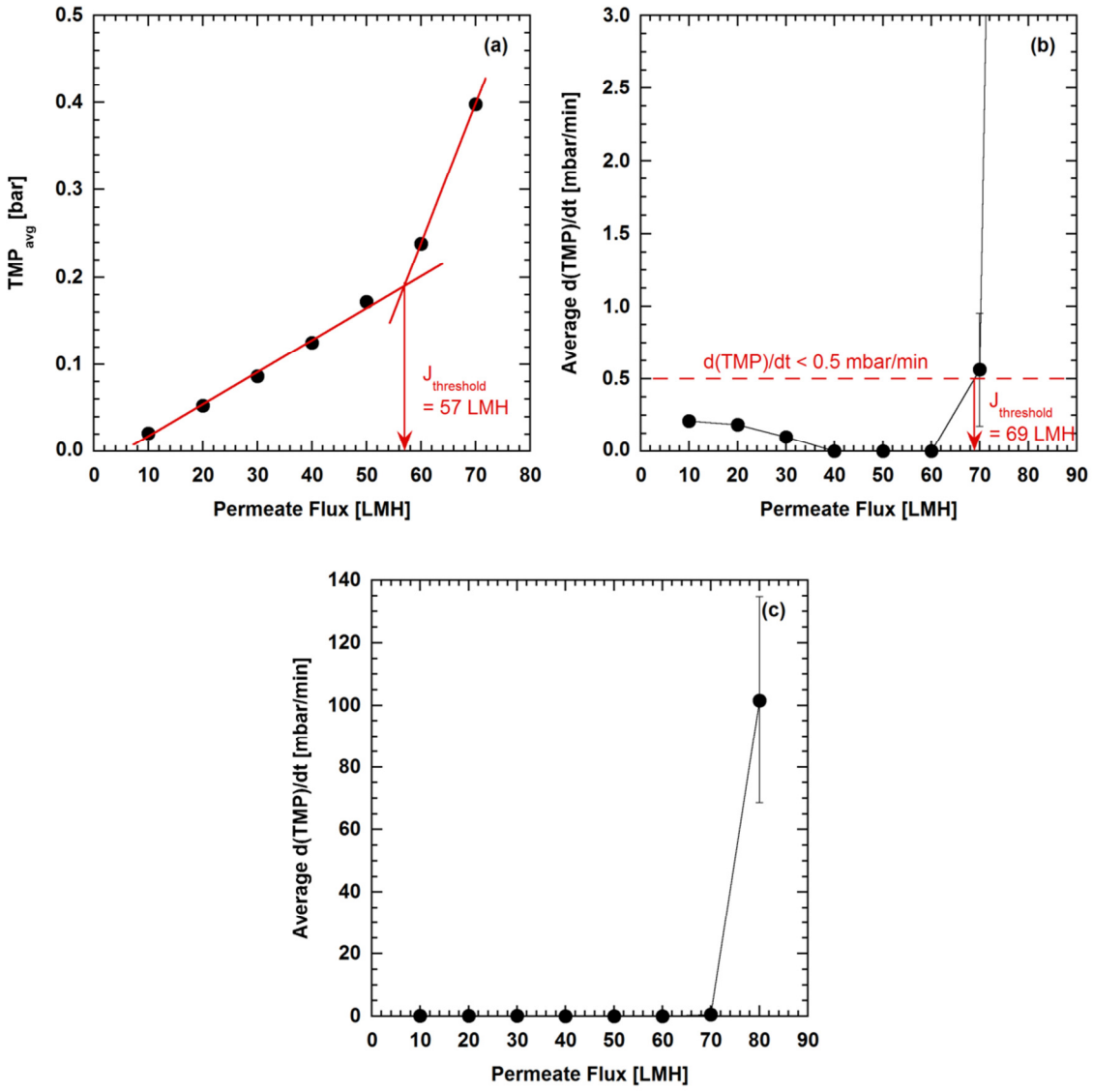

Figure C.6: Threshold flux ($J_{threshold}$) determination using: (a) TMP_{avg} and (b) d(TMP)/dt of PS-20 UF membranes modified with PDA at 2 mg/mL initial dopamine concentration (60-minute deposition time). (c) shows a full profile of average d(TMP)/dt vs. permeate flux from the flux stepping experiments. An R^2_{min} of 0.99 was used to generate linear regression line below the threshold flux in (a). The line in (b) connects average d(TMP)/dt at each flux to guide the eye on changes in the d(TMP)/dt values.

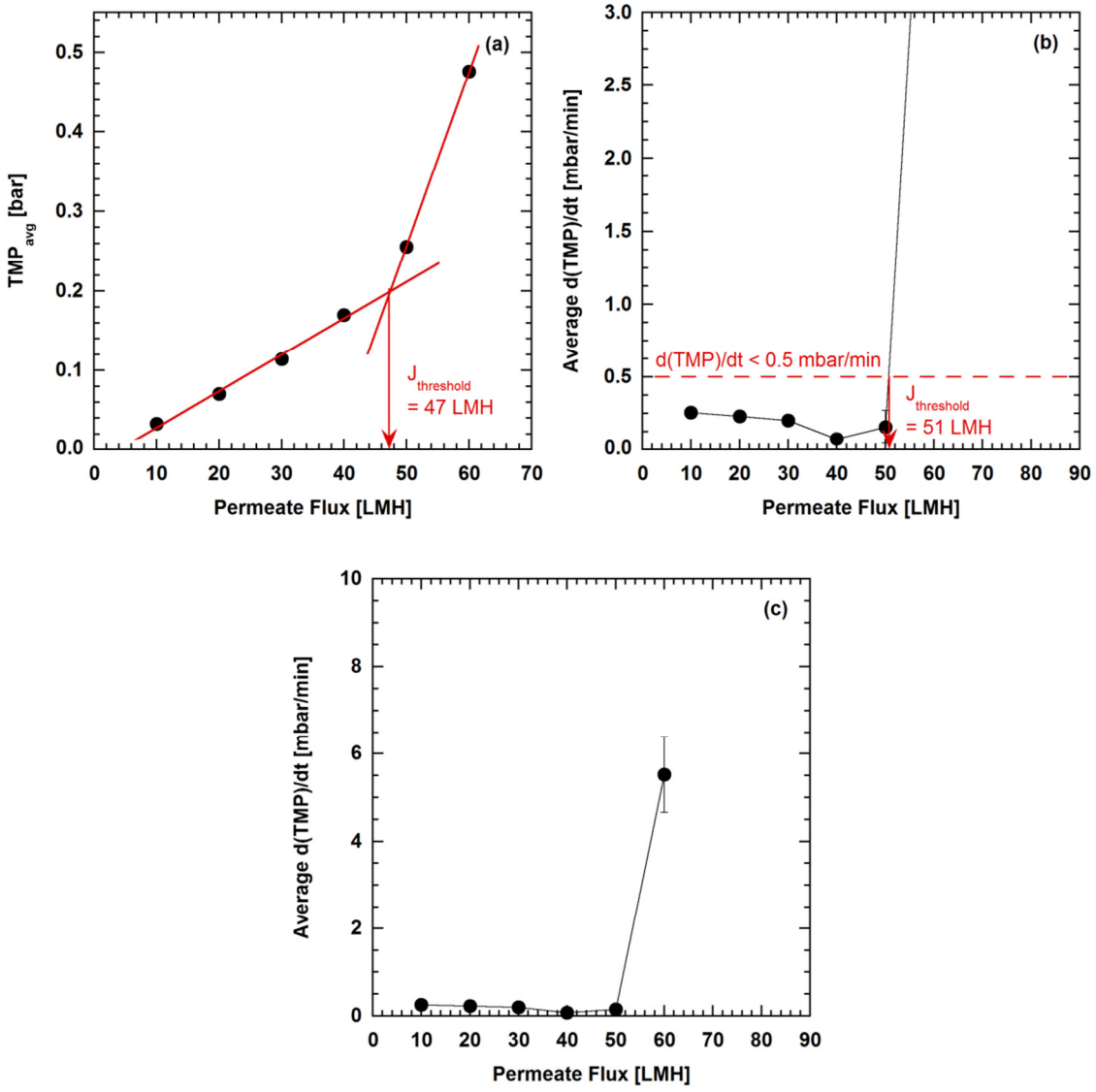

Figure C.7: Threshold flux ($J_{threshold}$) determination using: (a) TMP_{avg} and (b) d(TMP)/dt of PS-20 UF membranes modified with PDA at 8 mg/mL initial dopamine concentration (60-minute deposition time). (c) shows a full profile of average d(TMP)/dt vs. permeate flux from the flux stepping experiments. An R^2_{min} of 0.99 was used to generate linear regression line below the threshold flux in (a). The line in (b) connects average d(TMP)/dt at each flux to guide the eye on changes in the d(TMP)/dt values.

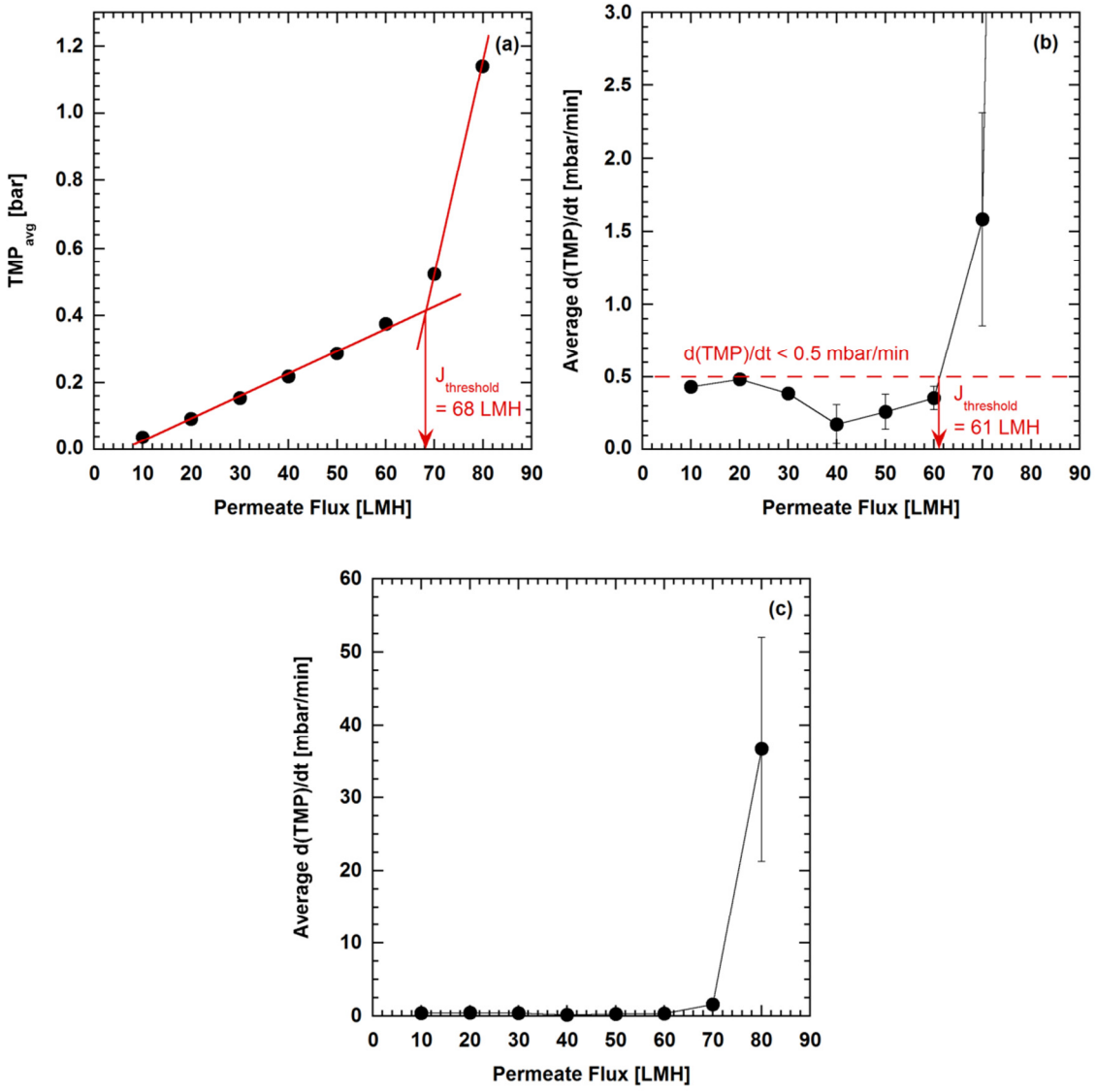

Figure C.8: Threshold flux ($J_{threshold}$) determination using: (a) TMP_{avg} and (b) d(TMP)/dt of PS-20 UF membranes modified with PDA at 15-minute deposition time (2 mg/mL initial dopamine concentration). (c) shows a full profile of average d(TMP)/dt vs. permeate flux from the flux stepping experiments. An R^2_{min} of 0.99 was used to generate linear regression line below the threshold flux in (a). The line in (b) connects average d(TMP)/dt at each flux to guide the eye on changes in the d(TMP)/dt values.

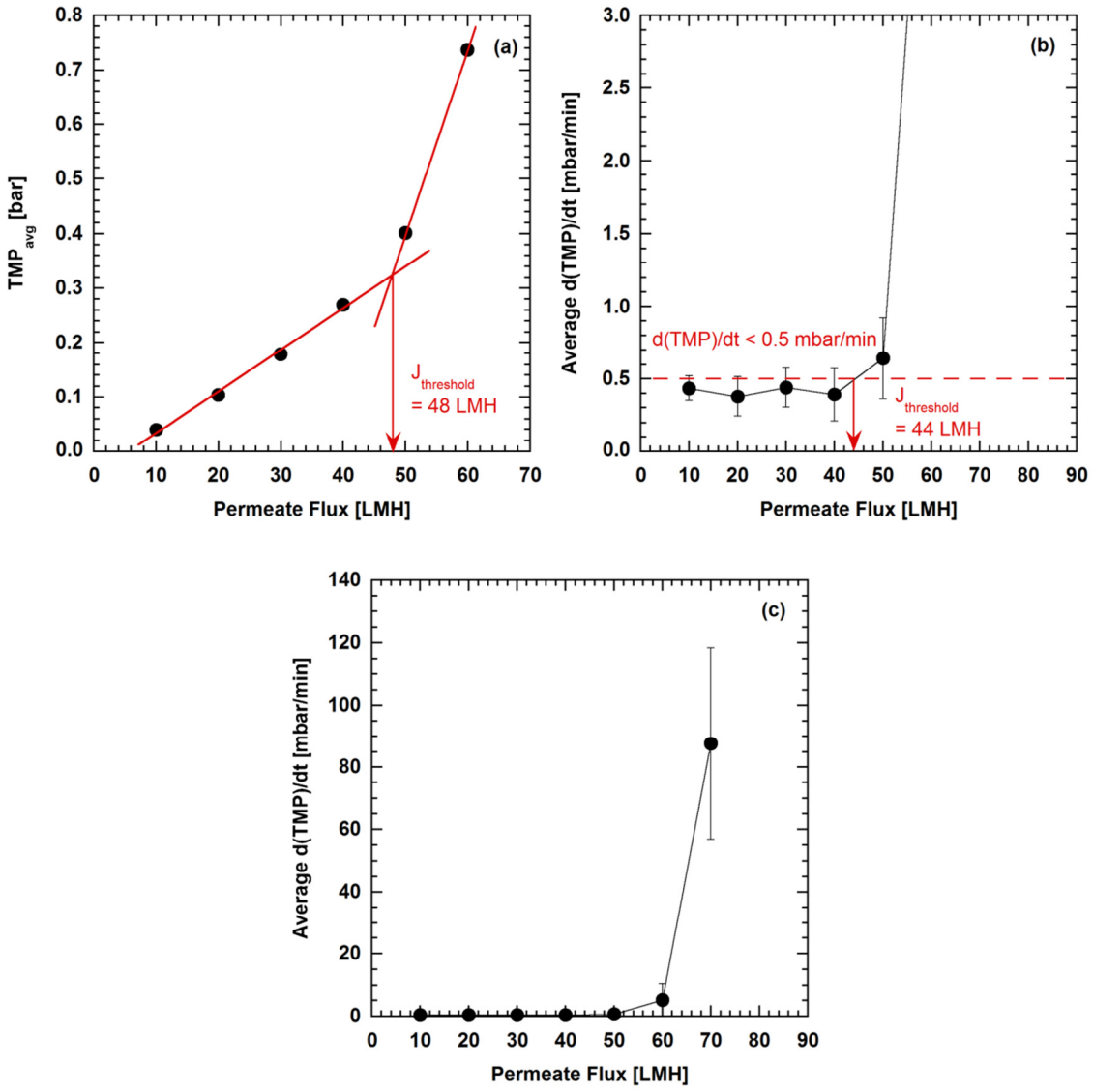

Figure C.9: Threshold flux ($J_{threshold}$) determination using: (a) TMP_{avg} and (b) d(TMP)/dt of PS-20 UF membranes modified with PDA at 240-minute deposition time (2 mg/mL initial dopamine concentration). (c) shows a full profile of average d(TMP)/dt vs. permeate flux from the flux stepping experiments. An R^2_{min} of 0.99 was used to generate linear regression line below the threshold flux in (a). The line in (b) connects average d(TMP)/dt at each flux to guide the eye on changes in the d(TMP)/dt values.

C.5 REFERENCES

[1] R. Zhang, Y. Su, X. Zhao, Y. Li, J. Zhao, Z. Jiang, A novel positively charged composite nanofiltration membrane prepared by bio-inspired adhesion of polydopamine and surface grafting of poly(ethylene imine), Journal of Membrane Science 470 (2014) 9–17.

[2] K.Y. Kim, E. Yang, M.Y. Lee, K.J. Chae, C.M. Kim, I.S. Kim, Polydopamine coating effects on ultrafiltration membrane to enhance power density and mitigate biofouling of ultrafiltration microbial fuel cells (UF-MFCs), Water Research 54 (2014) 62–68.

[3] S. Azari, L. Zou, Using zwitterionic amino acid L-DOPA to modify the surface of thin film composite polyamide reverse osmosis membranes to increase their fouling resistance, Journal of Membrane Science 401–402 (2012) 68–75.

[4] H. Karkhanechi, R. Takagi, H. Matsuyama, Biofouling resistance of reverse osmosis membrane modified with polydopamine, Desalination 336 (2014) 87–96.

[5] M. Vaselbehagh, H. Karkhanechi, S. Mulyati, R. Takagi, H. Matsuyama, Improved antifouling of anion-exchange membrane by polydopamine coating in electrodialysis process, Desalination 332 (2014) 126–133.

[6] V. Ball, Impedance spectroscopy and zeta potential titration of dopa-melanin films produced by oxidation of dopamine, Colloids and Surfaces A: Physicochemical and Engineering Aspects 363 (2010) 92–97.

[7] B. Yu, J. Liu, S. Liu, F. Zhou, Pdop layer exhibiting zwitterionicity: a simple electrochemical interface for governing ion permeability, Chemical Communications 46 (2010) 5900–5902.

[8] Y. Zhang, B.M. Teo, K.N. Goldie, B. Städler, Poly(N-isopropylacrylamide)/poly(dopamine) capsules, Langmuir 30 (2014) 5592−5598.

[9] Q. Liu, B. Yu, W. Ye, F. Zhou, Highly selective uptake and release of charged molecules by pH-responsive polydopamine microcapsules, Macromolecular Bioscience 11 (2011) 1227–1234.

[10] S. Kasemset, L. Wang, Z. He, D.J. Miller, A. Kirschner, B.D. Freeman, M.M. Sharma, Influence of polydopamine deposition conditions on permeability and sieving coefficient for a polysulfone ultrafiltration membrane, Journal of Membrane Science (2015), submitted.

[11] D.J. Miller, S. Kasemset, L. Wang, D.R. Paul, B.D. Freeman, Constant flux crossflow filtration evaluation of surface-modified fouling-resistant membranes, Journal of Membrane Science 452 (2014) 171–183.

[12] M.R. Spiegel, J. Schiller, R.A. Srinivasan, Schaum's Outlines Probability and Statistics, 3rd ed., McGraw-Hill, New York, NY, 2009.

Bibliography

Aimar, P., Meireles, M., & Sanchez, V. (1990). A contribution to the translation of retention curves into pore size distributions for sieving membranes. *Journal of Membrane Science, 54*, 321–338.

Arena, J. T., McCloskey, B. D., Freeman, B. D., & McCutcheon, J. R. (2011). Surface modification of thin film composite membrane support layers with polydopamine: Enabling use of reverse osmosis membranes in pressure retarded osmosis. *Journal of Membrane Science, 375*, 55–62.

Azari, S., & Zou, L. (2012). Using zwitterionic amino acid L-DOPA to modify the surface of thin film composite polyamide reverse osmosis membranes to increase their fouling resistance. *Journal of Membrane Science, 401–402*, 68–75.

Bacchin, P., Aimar, P., & Field, R. W. (2006). Critical and sustainable fluxes: Theory, experiments and applications. *Journal of Membrane Science, 281*, 42–69.

Bacchin, P., Aimar, P., & Sanchez, V. (1995). Model for colloidal fouling of membranes. *AIChE J., 41*, 368–376.

Baker, R. W. (2004). *Membrane Technology and Applications* (R. W. Baker Ed. 2nd ed.). West Sussex, England: John Wiley & Sons.

Baker, R. W., & Low, B. T. (2014). Gas separation membrane materials: A perspective. *Macromolecules, 47*, 6999–7013.

Ball, V. (2010). Impedance spectroscopy and zeta potential titration of dopa-melanin films produced by oxidation of dopamine. *Colloids and Surfaces A: Physicochemical and Engineering Aspects, 363*, 92–97.

Ball, V., Frari, D. D., Toniazzo, V., & Ruch, D. (2012). Kinetics of polydopamine film deposition as a function of pH and dopamine concentration: Insights in the polydopamine deposition mechanism. *Journal of Colloid and Interface Science, 386*, 366–372.

Beattie, J. K. (2006). The intrinsic charge on hydrophobic microfluidic substrates. *Lab on a Chip, 6*, 1409–1411.

Beier, S. P., & Jonsson, G. (2010). Critical flux determination by flux-stepping. *AIChE Journal, 56*(7), 1739–1747.

Belfort, G., Davis, R. H., & Zydney, A. L. (1994). The behavior of suspensions and macromolecular solutions in crossflow microfiltration. *Journal of Membrane Science, 96*, 1–58.

Bernsmann, F., Ponche, A., Ringwald, C., Hemmerle, J., Raya, J., Bechinger, B., Voegel, J.-C., Schaaf, P., & Ball, V. (2009). Characterization of dopamine – melanin growth on silicon oxide. *Journal of Physical Chemistry, 113*, 8234–8242.

Bevington, P. R., & Robinson, D. K. (2003). *Data Reduction and Error Analysis for the Physical Sciences* (3rd ed.). New York, NY: The McGraw-Hill Companies, Inc.

Bird, R. B., Stewart, W. E., & Lightfoot, E. N. (2002). *Transport Phenomena* (2nd ed.). New Jersey, NY: John Wiley & Sons, Inc.

Blank, R., Muth, K.-H., Proske-Gerhards, S., & Staude, E. (1998). Electrokinetic investigations of charged porous membranes. *Colloids and Surfaces A: Physicochemical and Engineering Aspects, 140*, 3–11.

Cakmakci, M., Kayaalp, N., & Koyuncu, I. (2008). Desalination of produced water from oil production fields by membrane processes. *Desalination, 222*, 176–186.

Causserand, C., & Aimar, P. (2010). Characterization of Filtration Membranes. In E. Drioli & L. Giorno (Eds.), *Comprehensive Membrane Science and Engineering* (1st ed.). Kidlington, United Kingdom: Elsevier.

Causserand, C., Rouaix, S., Akbari, A., & Aimar, P. (2004). Improvement of a method for the characterization of ultrafiltration membranes by measurements of tracers retention. *Journal of Membrane Science, 238*, 177–190.

Chan, R., & Chen, V. (2001). The effects of electrolyte concentration and pH on protein aggregation and deposition: critical flux and constant flux membrane filtration. *Journal of Membrane Science, 185*, 177–192.

Chan, Y. M., Schweiss, R., Werner, C., & Grunze, M. (2003). Electrokinetic characterization of oligo- and poly(ethylene glycol)-terminated self-assembled monolayers on gold and glass surfaces. *Langmuir, 19*, 7380–7385.

Chang, C. Y., Tsai, W. T., Ing, C. H., & Chang, C. F. (2003). Adsorption of polyethylene glycol (PEG) from aqueous solution onto hydrophobic zeolite. *Journal of Colloid and Interface Science, 260*, 273–279.

Chen, V. (1998). Performance of partially permeable microfiltration membranes under low fouling conditions. *Journal of Membrane Science, 147*, 265–278.

Cheng, C., Li, S., Zhao, W., Wei, Q., Nie, S., Sun, S., & Zhao, C. (2012). The hydrodynamic permeability and surface property of polyethersulfone ultrafiltration membranes with mussel-inspired polydopamine coatings. *Journal of Membrane Science, 417–418* 228–236.

Cheryan, M. (1986). *Ultrafiltration Handbook*. Lancaster, PA: Technomic Publishing Co., Inc.

Cheryan, M. (1998). *Ultrafiltration and Microfiltration Handbook*. Lancaster, PA: Technomic Publishing Co., Inc.

Cho, B. D., & Fane, A. G. (2002). Fouling transients in nominally sub-critical flux operation of a membrane bioreactor. *Journal of Membrane Science, 209*, 391–403.

Choi, K. Y., & Dempsey, B. A. (2005). Bench-scale evaluation of critical flux and TMP in low-pressure membrane filtration. *Journal of American Water Works Association, 97*, 134–143.

Clark, C. E., & Veil, J. A. (2009). Produced Water Volumes and Management Practices in the United States. U.S. Department of Energy: Office of Fossil Energy, National Energy Technology Laboratory.

CompleteEASE Data Analysis Manual. (2011). J.A. Woollam Co. Inc., Lincoln, NE.

Crowley, D. G., Frank, F. C., Mackley, M. R., & Stephenson, R. G. (1976). Localized flow birefringence of polyethylene oxide solutions in a four roll mill. *Journal of Polymer Science: Polymer Physics Edition, 14*, 1111–1119.

Defrance, L., & Jaffrin, M. Y. (1999). Comparison between filtrations at fixed transmembrane pressure and fixed permeate flux: application to a membrane bioreactor used for wastewater treatment. *Journal of Membrane Science, 152*, 203–210.

Della Vecchia, N. F., Avolio, R., Alfè, M., Errico, M. E., Napolitano, A., & d'Ischia, M. (2013). Building-block diversity in polydopamine underpins a multifunctional eumelanin-type platform tunable through a quinone control point. *Advanced Functional Materials, 23*, 1331–1340.

DOW Water & Process Solutions XLE-440 Product Specification. from http://www.dowwaterandprocess.com/products/membranes/xle_440.htm

Dreyer, D. R., Miller, D. J., Freeman, B. D., Paul, D. R., & Bielawski, C. W. (2012). Elucidating the structure of poly(dopamine). *Langmuir, 28*, 6428–6435.

Dreyer, D. R., Miller, D. J., Freeman, B. D., Paul, D. R., & Bielawski, C. W. (2013). Perspectives on poly(dopamine). *Chemical Science, 4*, 3796–3802.

Elimelech, M., Zhu, X., Childress, A. E., & Hong, S. (1997). Role of membrane surface morphology in colloidal fouling of cellulose acetate and composite aromatic polyamide reverse osmosis membranes. *Journal of Membrane Science, 127*, 101–109.

Field, R. W., & Pearce, G. K. (2011). Critical, sustainable and threshold fluxes for membrane filtration with water industry applications. *Advances in Colloid and Interface Science, 164*, 38–44.

Field, R. W., Wu, D., Howell, J. A., & Gupta, B. B. (1995). Critical flux concept for microfiltration fouling. *Journal of Membrane Science, 100*, 259–272.

Flinn, J. E. (1970). *Membrane Science and Technology: Industrial, Biological, and Waste Treatment Processes*. New York, NY: Plenum Press.

Foppoli, C., Coccia, R., Cini, C., & Rosei, M. A. (1997). Catecholamines oxidation by xanthine oxidase. *Biochimica et Biophysica Acta, 1334*, 200–206.

Gaches, S. (1991). *Application de la Viscosimetrie a la Determination du Rayon de Giration de Macromolecules, DEA Génie des Procédés.* Université Paul Sabatier, Toulouse, France.

Galusky, L. P. (2007). Fort Worth Basin/Barnett Shale Natural Gas Play: An Assessment of Present and Projected Fresh Water Use. Gas Technology Institute.

Geise, G. M., Lee, H., Miller, D. J., Freeman, B. D., McGrath, J. E., & Paul, D. R. (2010). Water purification by membranes: The role of polymer science. *Journal of Polymer Science: Part B: Polymer Physics, 48*, 1685–1718.

Geise, G. M., Park, H. B., Sagle, A. C., Freeman, B. D., & McGrath, J. E. (2011). Water permeability and water/salt selectivity tradeoff in polymers for desalination. *Journal of Membrane Science, 369*, 130–138.

Giglia, S., & Straeffer, G. (2012). Combined mechanism fouling model and method for optimization of series microfiltration performance. *Journal of Membrane Science, 417-418* 144–153.

Gilron, J., Belfer, S., Vaisanen, P., & Nystrom, M. (2001). Effects of surface modification on antifouling and performance properties of reverse osmosis membranes. *Desalination, 140*, 167–179.

Gleick, P. H. The changing water paradigm: A look at twenty-first century water resources development. *Water International, 25*(1), 127–138.

Gleick, P. H. (2000). The World's Water 2000-2001: The Biennial Report on Freshwater Resources. Island Press, Washington D.C.

Greenlee, L. F., Lawler, D. F., Freeman, B. D., Marrot, B., & Moulin, P. (2009). Reverse osmosis desalination: Water sources, technology, and today's challenges. *Water Research, 43*, 2317–2348.

Gregory, K. B., Vidic, R. D., & Dzombak, D. A. (2011). Water management challenges associated with the production of shale gas by hydraulic fracturing. *Elements, 7*, 181–186.

Guerra, K., Dahm, K., & Dundorf, S. (2011). Science and Technology Program Report No. 157: Oil and Gas Produced Water Management and Beneficial Use in the Western United States. U.S. Department of the Interior, Bureau of Reclamation, Denver, CO.

Harmant, P., & Aimar, P. (1998). Coagulation of colloids in a boundary layer during cross-flow filtration. *Colloids Surf. A, 138*, 217–230.

Hayes, T. D. (2009). Barnett and Appalachian Shale Water Management and Reuse Technologies, Gas Technology Institute (GTI) Proposal Number 70100 (Technical Volume). Des Plaines, IL.

Hermia, J. (1982). Constant pressure blocking filtration laws – Application to power-law non-Newtonian fluids. *Trans. Inst. Chem. E., 60*, 183–187.

Ho, W. S. W., & Sirkar, K. K. (1992). *Membrane Handbook*. New York, NY: Van Nostrand Reinhold.

Huang, X., Guduru, D., Xu, Z., Vienken, J., & Groth, T. (2011). Blood compatibility and permeability of heparin-modified polysulfone as potential membrane for simultaneous hemodialysis and LDL removal. *Macromolecular Bioscience, 11*, 131–140.

Huang, Y., & Paul, D. R. (2004). Experimental methods for tracking physical aging of thin glassy polymer films by gas permeation. *Journal of Membrane Science, 244*, 167–178.

Hughes, D., Taha, T., & Cui, Z. (2007). Chapter 5 Mass Transfer: Membrane Processes. In S. S. Sablani, A. K. Datta, M. S. Rahman & A. S. Mujumdar (Eds.), *Handbook of Food and Bioprocess Modeling Techniques*. Boca Raton, FL: CRC Press, Taylor & Francis Group.

Huisman, I. H., Vellenga, E., Trägårdh, G., & Trägårdh, C. (1999). The influence of the membrane zeta potential on the critical flux for crossflow microfiltration of particle suspensions. *Journal of Membrane Science, 156*, 153–158.

Jiang, J., Zhu, L., Li, X., Xu, Y., & Zhu, B. (2010). Surface modification of PE porous membranes based on the strong adhesion of polydopamine and covalent immobilization of heparin. *Journal of Membrane Science, 364*, 194–202.

Jiang, J., Zhu, L., Zhu, L., Zhu, B., & Xu, Y. (2011). Surface characteristics of a self-polymerized dopamine coating deposited on hydrophobic polymer films. *Langmuir, 27*, 14180–14187.

Johnston, S. T., Smith, K. A., & Deen, W. M. (2001). Concentration polarization in stirred ultrafiltration cells. *AIChE Journal, 47*(5), 1115–1125.

Ju, H. (2010). *Water transport study in crosslinked poly(ethyleneoxide) hydrogels as fouling-resistant membrane coating materials.* (PhD thesis), University of Texas at Austin.

Ju, H., & Freeman, B. D. (2008). Desalination and water purification research and development program report no. 129: Novel fouling-resistant membranes for water purification. Bureau of Reclamation, Denver, CO.

Kang, K., Choi, I. S., & Nam, Y. (2011). A biofunctionalization scheme for neural interfaces using polydopamine polymer. *Biomaterials, 32*, 6374–6380.

Karkhanechi, H., Takagi, R., & Matsuyama, H. (2014). Biofouling resistance of reverse osmosis membrane modified with polydopamine. *Desalination, 336*, 87–96.

Kasemset, S., Lee, A., Miller, D. J., Freeman, B. D., & Sharma, M. M. (2013). Effect of polydopamine deposition conditions on fouling resistance, physical properties, and permeation properties of reverse osmosis membranes in oil/water separation. *Journal of Membrane Science, 425–426*, 208–216.

Kasemset, S., Wang, L., He, Z., Miller, D. J., Kirschner, A., Freeman, B. D., & Sharma, M. M. (2015). Influence of polydopamine deposition conditions on hydraulic permeability and sieving coefficients for a polysulfone ultrafiltration membrane. *Journal of Membrane Science*, submitted.

Kim, H. W., McCloskey, B. D., Choi, T. H., Lee, C., Kim, M. J., Freeman, B. D., & Park, H. B. (2013). Oxygen concentration control of dopamine-induced high uniformity surface coating chemistry. *Applied Materials and Interfaces, 5*(2), 233−238.

Kim, K. J., Fane, A. G., Nystrom, M., Pihlajamaki, A., Bowen, W. R., & Mukhtar, H. (1996). Evaluation of electroosmosis and streaming potential for measurement of electric charges of polymeric membranes. *Journal of Membrane Science, 116*, 149–159.

Kim, K. Y., Yang, E., Lee, M. Y., Chae, K. J., Kim, C. M., & Kim, I. S. (2014). Polydopamine coating effects on ultrafiltration membrane to enhance power density and mitigate biofouling of ultrafiltration microbial fuel cells (UF-MFCs). *Water Research, 54*, 62–68.

Kudin, K. N., & Car, R. (2008). Why are water−hydrophobic interfaces charged? *Journal of the American Chemical Society, 130*(12), 3915–3919.

Kwon, D. Y., Vigneswaran, S., Fane, A. G., & Aim, R. B. (2000). Experimental determination of critical flux in cross-flow microfiltration. *Separation and Purification Technology, 19*, 169–181.

Latulippe, D. R., Molek, J. R., & Zydney, A. L. (2009). Importance of biopolymer molecular flexibility in ultrafiltration processes. *Industrial and Engineering Chemistry Research, 48*, 2395–2403.

Le-Clech, P., Chen, V., & Fane, T. A. G. (2006). Fouling in membrane bioreactors used in wastewater treatment. *Journal of Membrane Science, 284*, 17–53.

Le-Clech, P., Jefferson, B., Chang, I. S., & Judd, S. J. (2003). Critical flux determination by the flux-step method in a submerged membrane bioreactor. *Journal of Membrane Science, 227*, 81–93.

Lee, H., Dellatore, S. M., Miller, W. M., & Messersmith, P. B. (2007). Mussel-inspired surface chemistry for multifunctional coatings. *Science, 318*, 426–430.

Lee, H., Rho, J., & Messersmith, P. B. (2009). Facile conjugation of biomolecules onto surfaces via mussel adhesive protein inspired coatings. *Advanced Materials, 21*, 431–434.

Lee, H., Scherer, N. F., & Messersmith, P. B. (2006). Single-molecule mechanics of mussel adhesion. *Proceedings of the National Academy of Sciences of the United States of America, 103*, 12999–13003.

Li, B., Liu, W., Jiang, Z., Dong, X., Wang, B., & Zhong, Y. (2009). Ultrathin and stable active layer of dense composite membrane enabled by poly(dopamine). *Langmuir, 25*, 7368–7374.

Liu, Q., Yu, B., Ye, W., & Zhou, F. (2011). Highly selective uptake and release of charged molecules by pH-responsive polydopamine microcapsules. *Macromolecular Bioscience, 11*, 1227–1234.

Liu, Y., Ai, K., & Lu, L. (2014). Polydopamine and its derivative materials: Synthesis and promising applications in energy, environmental, and biomedical fields. *Chemical Reviews, 114*, 5057–5115.

Louie, J. S., Pinnau, I., Ciobanu, I., Ishida, K. P., Ng, A., & Reinhard, M. (2006). Effects of polyether-polyamide block copolymer coating on performance and fouling of reverse osmosis membranes. *Journal of Membrane Science, 280*, 762–770.

Luo, J., Ding, L., Wan, Y., & Jaffrin, M. Y. (2012). Threshold flux for shear-enhanced nanofiltration: Experimental observation in dairy wastewater treatment. *Journal of Membrane Science, 409–410*, 276–284.

Luo, J., Morthensen, S. T., Meyer, A. S., & Pinelo, M. (2014). Filtration behavior of casein glycomacropeptide (CGMP) in an enzymatic membrane reactor: fouling control by membrane selection and threshold flux operation. *Journal of Membrane Science, 469*, 127–139.

Madaeni, S. S., Fane, A. G., & Wiley, D. E. (1999). Factors influencing critical flux in membrane filtration of activated sludge. *Journal of Chemical Technology and Biotechnology, 74*, 539–543.

Mänttäri, M., & Nyström, M. (2000). Critical flux in NF of high molar mass polysaccharides and effluents from the paper industry. *Journal of Membrane Science, 170*, 257–273.

Marinova, K. G., Alargova, R. G., Denkov, N. D., Velev, O. D., Petsev, D. N., Ivanov, I. B., & Borwankar, R. P. (1996). Charging of oil−water interfaces due to spontaneous adsorption of hydroxyl ions. *Langmuir, 12*(8), 2045-2051.

Mauter, M. S., Alvarez, P. J. J., Burton, A., Cafaro, D. C., Chen, W., Gregory, K. B., Jiang, G., Li, Q., Pittock, J., Reible, D., & Schnoor, J. L. (2014). Regional variation in water-related impacts of shale gas development and implications for emerging international plays. *Environmental Science and Technology, 48*, 8298–8306.

McCloskey, B. D. (2009). *Novel surface modifications and materials for fouling resistant water purification membranes.* (PhD thesis), University of Texas at Austin.

McCloskey, B. D., Ju, H., & Freeman, B. D. (2010). Composite membranes based on a selective chitosan–poly(ethylene glycol) hybrid layer: Synthesis, characterization, and performance in oil-water purification. *Industrial and Engineering Chemistry Research, 49*, 366–373.

McCloskey, B. D., Park, H. B., Ju, H., Rowe, B. W., Miller, D. J., Chun, B. J., Kin, K., & Freeman, B. D. (2010). Influence of polydopamine deposition conditions on pure water flux and foulant adhesion resistance of reverse osmosis, ultrafiltration, and microfiltration membranes. *Polymer, 51*, 3472–3485.

McCloskey, B. D., Park, H. B., Ju, H., Rowe, B. W., Miller, D. J., & Freeman, B. D. (2012). A bioinspired fouling-resistant surface modification for water purification membranes. *Journal of Membrane Science, 413–414* 82–90.

Mehta, A., & Zydney, A. L. (2005). Permeability and selectivity analysis for ultrafiltration membranes. *Journal of Membrane Science, 249*, 245–249.

Metsämuuronen, S., Howell, J., & Nyström, M. (2002). Critical flux in ultrafiltration of myoglobin and baker's yeast. *Journal of Membrane Science, 196*, 13–25.

Michaels, A. S. (1980). Analysis and prediction of sieving curves for ultrafiltration membranes: A universal correlation? *Separation Science and Technology, 15*(6), 1305–1322.

Miller, D. J., Kasemset, S., Paul, D. R., & Freeman, B. D. (2014). Comparison of membrane fouling at constant flux and constant transmembrane pressure conditions. *Journal of Membrane Science, 454*, 505–515.

Miller, D. J., Kasemset, S., Wang, L., Paul, D. R., & Freeman, B. D. (2014). Constant flux crossflow filtration evaluation of surface-modified fouling-resistant membranes. *Journal of Membrane Science, 452*, 171–183.

Miller, D. J., Paul, D. R., & Freeman, B. D. (2013). A crossflow filtration system for constant permeate flux membrane fouling characterization. *Review of Scientific Instruments, 84*(3), 035003.

Miller, D. J., Paul, D. R., & Freeman, B. D. (2014). An improved method for surface modification of porous water purification membranes. *Polymer, 55*, 1375–1383.

Mochizuki, S., & Zydney, A. L. (1992). Dextran transport through asymmetric ultrafiltration membranes: Comparison with hydrodynamic models. *Journal of Membrane Science, 68*, 21–41.

Mochizuki, S., & Zydney, A. L. (1993). Theoretical analysis of pore size distribution effects on membrane transport. *Journal of Membrane Science, 82*, 211–227.

Möckel, D., Staude, E., Dal-Cin, M., Darcovich, K., & Guiver, M. (1998). Tangential flow streaming potential measurements: Hydrodynamic cell characterization and zeta potentials of carboxylated polysulfone membranes. *Journal of Membrane Science, 145*, 211–222.

Mulder, M. (1991). *Basic Principles of Membrane Technology*. Dordrecht, The Netherlands: Kluwer Academic Publishers.

Neumann, A. W., & Spelt, J. K. (1996). *Applied Surface Thermodynamics*. New York, NY: Marcel Dekkar, Inc.

Nunes, S. P., Sforça, M. L., & Peinemann, K.-V. (1995). Dense hydrophilic composite membranes for ultrafiltration. *Journal of Membrane Science, 106*, 49–56.

O'Shea, D. P. (2013). Ultura (formerly Sepro Membranes, Inc.), personal communication.

Ognier, S., Wisniewski, C., & Grasmick, A. (2004). Membrane bioreactor fouling in sub-critical filtration conditions: A local critical flux concept. *Journal of Membrane Science, 229*, 171–177.

Oki, T., & Kanae, S. (2006). Global hydrological cycles and world water resources. *Science, 313*, 1068–1072.

Opong, W. S., & Zydney, A. L. (1991). Diffusive and convective protein transport through asymmetric membranes. *AIChE Journal, 37*(10), 1497–1510.

Ou, J., Wang, J., Liu, S., Zhou, J., Ren, S., & Yang, S. (2009). Microtribological and electrochemical corrosion behaviors of polydopamine coating on APTS-SAM modified Si substrate. *Applied Surface Science, 256*, 894–899.

Pan, F., Jia, H., Qiao, S., Jiang, Z., Wang, J., Wang, B., & Zhong, Y. (2009). Bioinspired fabrication of high performance composite membranes with ultrathin defect-free skin layer. *Journal of Membrane Science, 341*, 279–285.

Platt, S., Mauramo, M., Butylina, S., & Nystrom, M. (2002). Retention of pegs in cross-flow ultrafiltration through membranes. *Desalination, 149*, 417–422.

Poling, B. E., Thomson, G. H., Friend, D. G., Rowley, R. L., & Wilding, W. V. (2008). Section 2 Physical and Chemical Data. In D. W. Green & R. H. Perry (Eds.), *Perry's Chemical Engineer's Handbook* (8th ed.). New York: McGraw-Hill.

Pope, D. P., & Keller, A. (1977). Alignment of macromolecules in solution by elongational flow; a study of the effect of pure shear in a four roll mill. *Colloid and Polymer Science, 255*, 633–643.

Porter, M. C. (1990). *Handbook of Industrial Membrane Technology*. Park Ridge, NJ: Noyes Publications.

Postel, S. L., Daily, G. C., & Ehrlich, P. R. (1996). Human appropriation of renewable fresh water. *Science, 271*, 785–788.

Prádanos, P., Arribas, J. I., & Hernández, A. (1995). Mass transfer coefficient and retention of PEGs in low pressure cross-flow ultrafiltration through asymmetric membranes. *Journal of Membrane Science, 99*, 1–20.

Rawn-Schatzinger, V., Arthur, D., & Langhus, B. (2003). Coalbed natural gas produced water: Water rights and treatment technologies. *GasTIPS, 9*, 13–18.

Ren, J., Li, Z., & Wong, F. S. (2006). A new method for the prediction of pore size distribution and MWCO of ultrafiltration membranes. *Journal of Membrane Science, 279*, 558–569.

Review of the Desalination and Water Purification Technology Roadmap. (2004). The National Academies Press, Washington, D.C.

Riley, R. L. (1990). Reverse Osmosis, Membrane Separation Systems — A Research & Development Needs Assessment, Publication Number DOE/ER/30133-H1-Vol. 2 (pp. 5(1)–5(53)). Department of Energy, Springfield, VA.

Rohani, R., Hyland, M., & Patterson, D. (2011). A refined one-filtration method for aqueous based nanofiltration and ultrafiltration membrane molecular weight cut-off determination using polyethylene glycols. *Journal of Membrane Science, 382*, 278–290.

Sagle, A. C., Van Wagner, E. M., Ju, H., McCloskey, B. D., Freeman, B. D., & Sharma, M. M. (2009). PEG-coated reverse osmosis membranes: Desalination properties and fouling resistance. *Journal of Membrane Science, 340*, 92–108.

Saksena, S., & Zydney, A. L. (1997). Influence of protein–protein interactions on bulk mass transport during ultrafiltration. *Journal of Membrane Science, 125*, 93–108.

Sanders, D. F., Smith, Z. P., Guo, R., Robeson, L. M., McGrath, J. E., Paul, D. R., & Freeman, B. D. (2013). Energy-efficient polymeric gas separation membranes for a sustainable future: A review. *Polymer, 54*, 4729–4761.

Schlichter, B., Mavrov, V., & Chmiel, H. (2000). Comparative characterisation of different commercial UF membranes for drinking water production. *Journal of Water Supply: Research and Technology–AQUA, 49*(6), 321–328.

Schock, G., Miquel, A., & Birkenberger, R. (1989). Characterization of ultrafiltration membranes: Cut-off determination by gel permeation chromatography. *Journal of Membrane Science, 41*, 55–67.

Service, R. F. (2006). Desalination freshens up. *Science, 313*, 1088–1090.

Shao, J., & Baltus, R. E. (2000). Hindered diffusion of dextran and polyethylene glycol in porous membranes. *AIChE Journal, 46*(6), 1149–1156.

Shin, Y. M., Lee, Y. B., & Shin, H. (2011). Time-dependent mussel-inspired functionalization of poly(L-lactide-co-ε-caprolactone) substrates for tunable cell behaviors. *Colloids and Surfaces B: Biointerfaces, 87*, 79–87.

Silva, J. M., Gettings, R. M., Kostedt, W. L., & Watkins, V. H. (2014). Produced water from hydrofracturing: Challenges and opportunities for reuse and recovery. In R. M. Latanision & C. H. Fletcher (Eds.), *The Bridge, Vol. 44, No. 2* (pp. 34–40). Washington D.C.: National Academy of Engineering.

Singh, S., Khulbe, K. C., Matsuura, T., & Ramamurthy, P. (1998). Membrane characterization by solute transport and atomic force microscopy. *Journal of Membrane Science, 142*, 111–127.

Smith, K. A., Colton, C. K., Merrill, E. W., & Evans, L. B. (1968). Convective transport in a batch dialyzer: Determination of true membrane permeability from a single measurement. *AIChE Symposium Series, 64*(84), 45–58.

Spiegel, M. R., Schiller, J., & Srinivasan, R. A. (2009). *Schaum's Outlines Probability and Statistics* (3rd ed.). New York, NY: McGraw-Hill.

Standard Test Method for Molecular Weight Cutoff Evaluation of Flat Sheet Ultrafiltration Membranes. (2001). West Conshohocken, PA: ASTM International.

Susanto, H., Balakrishnan, M., & Ulbricht, M. (2007). Via surface functionalization by photograft copolymerization to low-fouling polyethersulfone-based ultrafiltration membranes. *Journal of Membrane Science, 288*, 157–167.

Susanto, H., & Ulbricht, M. (2007). Photografted thin polymer hydrogel layers on PES ultrafiltration membranes: Characterization, stability, and influence on separation performance. *Langmuir, 23*, 7818–7830.

Sutzkover, I., Hasson, D., & Semiat, R. (2000). Simple technique for measuring the concentration polarization level in a reverse osmosis system. *Desalination, 131*, 117–127.

Tam, C. M., & Tremblay, A. Y. (1991). Membrane pore characterization – comparison between single and multicomponent solute probe techniques. *Journal of Membrane Science, 57*, 271–287.

Tao, F. T., Curtice, S., Hobbs, R. D., Sides, J. L., Wieser, J. D., Dyke, C. A., Tuohey, D., & Pilger, P. F. (1993). Reverse osmosis process successfully converts oil field brine into freshwater. *Oil and Gas Journal, 91*, 88–91.

Tarabara, V. V., Hovinga, R. M., & Wiesner, M. R. (2002). Constant transmembrane pressure vs. constant permeate flux: Effect of particle size on crossflow membrane filtration. *Environmental Engineering Science, 19*(6), 343–355.

Trägårdh, G. (1985). Characterization methods for ultrafiltration membranes. *Desalination, 53*, 25–35.

The United Nations World Water Development Report 3: Water in a Changing World. (2009). The United Nations Educational, Scientific, and Cultural Organization (UNESCO), Paris, France.

The United Nations World Water Development Report Volume 1: Water and Energy. (2014). The United Nations Educational, Scientific, and Cultural Organization (UNESCO), Paris, France.

Urase, T., Yamamoto, K., & Ohgaki, S. (1994). Effect of pore size distribution of ultrafiltration membranes on virus rejection in crossflow conditions. *Water Science and Technology, 30*(9), 199–208.

van der Marel, P., Zwijnenburg, A., Kemperman, A., Wessling, M., Temmink, H., & van der Meer, W. (2009). An improved flux-step method to determine the critical flux and the critical flux for irreversibility in a membrane bioreactor. *Journal of Membrane Science, 332*, 24–29.

Van Wagner, E. M. (2010). *Polyamide desalination membrane characterization and surface modification to enhance fouling resistance.* (PhD thesis), University of Texas at Austin.

Van Wagner, E. M., Sagle, A. C., Sharma, M. M., & Freeman, B. D. (2009). Effect of crossflow testing conditions, including feed pH and continuous feed filtration, on commercial reverse osmosis membrane performance. *Journal of Membrane Science, 345*, 97–109.

Van Wagner, E. M., Sagle, A. C., Sharma, M. M., La, Y.-H., & Freeman, B. D. (2011). Surface modification of commercial polyamide desalination membranes using poly(ethylene glycol) diglycidyl ether to enhance membrane fouling resistance. *Journal of Membrane Science, 367*, 273–287.

Vaselbehagh, M., Karkhanechi, H., Mulyati, S., Takagi, R., & Matsuyama, H. (2014). Improved antifouling of anion-exchange membrane by polydopamine coating in electrodialysis process. *Desalination, 332*, 126–133.

Vedavyasan, C. V. (2007). Pretreatment trends — an overview. *Desalination, 203*, 296–299.

Veil, J. A., Puder, M. G., Elcock, D., & Redweik, R. J. (2004). A White Paper Describing Produced Water from Production of Crude Oil, Natural Gas, and Coal Bed Methane. U.S. Department of Energy: National Energy Technology Laboratory.

Vengosh, A., Jackson, R. B., Warner, N., Darrah, T. H., & Kondash, A. (2014). A critical review of the risks to water resources from unconventional shale gas development and hydraulic fracturing in the United States. *Environmental Science and Technology, 48*, 8334–8348.

Vincent Vela, M. C., Blanco, S. Á., García, J. L., & Rodríguez, E. B. (2008). Analysis of membrane pore blocking models applied to the ultrafiltration of PEG. *Separation and Purification Technology, 62*, 489–498.

Vincent Vela, M. C., Blanco, S. Á., García, J. L., & Rodríguez, E. B. (2009). Analysis of membrane pore blocking models adapted to crossflow ultrafiltration in the ultrafiltration of PEG. *Chemical Engineering Journal, 149*, 232–241.

Vrijenhoek, E. M., Hong, S., & Elimelech, M. (2001). Influence of membrane surface properties on initial rate of colloidal fouling of reverse osmosis and nanofiltration membranes. *Journal of Membrane Science, 188*, 115–128.

Vyas, H. K., Bennett, R. J., & Marshall, A. D. (2002). Performance of crossflow microfiltration during constant transmembrane pressure and constant flux operations. *International Dairy Journal, 12*, 473–479.

Wei, Q., Zhang, F., Li, J., Li, B., & Zhao, C. (2010). Oxidant-induced dopamine polymerization for multifunctional coatings. *Polymer Chemistry, 1*, 1430–1433.

Wu, D., Howell, J. A., & Field, R. W. (1999). Critical flux measurement for model colloids. *Journal of Membrane Science, 152*, 89–98.

Wu, Y. H., Liu, Y. L., Chang, Y., Higuchi, A., & Freeman, B. D. (2010). Effect of UV intensity on structure, water sorption, and transport properties of crosslinked N-vinyl-2-pyrrolidone/N,N'-methylenebisacrylamide films. *Journal of Membrane Science, 348*, 47–55.

Wu, Z., Wang, Z., Huang, S., Mai, S., Yang, C., Wang, X., & Zhou, Z. (2008). Effects of various factors on critical flux in submerged membrane bioreactors for municipal wastewater treatment. *Separation and Purification Technology, 62*, 56–63.

Xi, Z., Xu, Y., Zhu, L., Wang, Y., & Zhu, B. (2009). A facile method of surface modification for hydrophobic polymer membranes based on the adhesive behavior of poly(DOPA) and poly(dopamine). *Journal of Membrane Science, 327*, 244–253.

Yu, B., Liu, J., Liu, S., & Zhou, F. (2010). Pdop layer exhibiting zwitterionicity: a simple electrochemical interface for governing ion permeability. *Chemical Communications, 46*, 5900–5902.

Yu, F., Chen, S., Chen, Y., Li, H., Yang, L., Chen, Y., & Yin, Y. (2010). Experimental and theoretical analysis of polymerization reaction process on the polydopamine membranes and its corrosion protection properties for 304 stainless steel. *Journal of Molecular Structure, 982*, 152–161.

Zangi, R., & Engberts, J. B. F. N. (2005). Physisorption of hydroxide ions from aqueous solution to a hydrophobic surface. *Journal of the American Chemical Society, 127*(7), 2272–2276.

Zangmeister, R. A., Morris, T. A., & Tarlov, M. J. (2013). Characterization of polydopamine thin films deposited at short times by autoxidation of dopamine. *Langmuir, 29*, 8619–8628.

Zeman, L., & Wales, M. (1981). Polymer Solute Rejection by Ultrafiltration Membranes. In A. F. Turbak (Ed.), *ACS Symposium Series 154 (Synthetic Membranes: Volume II Hyper- and Ultrafiltration Uses)* (pp. 411–434). Washington, DC: American Chemical Society.

Zeman, L. J., & Zydney, A. L. (1996). *Microfiltration and Ultrafiltration: Principles and Applications*. New York, NY: Marcel Dekker, Inc.

Zhang, J., Chua, H. C., Zhou, J., & Fane, A. G. (2006). Factors affecting the membrane performance in submerged membrane bioreactors. *Journal of Membrane Science, 284*, 54–66.

Zhang, R., Su, Y., Zhao, X., Li, Y., Zhao, J., & Jiang, Z. (2014). A novel positively charged composite nanofiltration membrane prepared by bio-inspired adhesion of polydopamine and surface grafting of poly(ethylene imine). *Journal of Membrane Science, 470*, 9–17.

Zhang, Y., Teo, B. M., Goldie, K. N., & Städler, B. (2014). Poly(N-isopropylacrylamide)/poly(dopamine) capsules. *Langmuir, 30*, 5592−5598.

Zhu, L., Yu, J., Xu, Y., Xi, Z., & Zhu, B. (2009). Surface modification of PVDF porous membranes via poly(DOPA) coating and heparin immobilization. *Colloids and Surfaces B: Biointerfaces, 69*, 152–155.

Zydney, A. L., Aimar, P., Meirele, M., Pimbley, J. M., & Belfort, G. (1994). Use of the log-normal probability density function to analyze membrane pore size distributions: Functional forms and discrepancies. *Journal of Membrane Science, 91*, 293–298.

Zydney, A. L., & Xenopoulos, A. (2007). Improving dextran tests for ultrafiltration membranes: Effect of device format. *Journal of Membrane Science, 291*, 180–190.

Vita

Sirirat Kasemset was born and raised in Bangkok, Thailand. She attended Chulalongkorn University (Bangkok, Thailand) and graduated with her Bachelor's degree in Chemical Engineering (with First-class Honors) in 2008. After she received her Bachelor's degree, she worked as a process engineer, supporting an offshore natural gas production platform in the Gulf of Thailand, at Chevron Thailand Exploration and Production, Ltd. Then, she was awarded a Fulbright Scholarship (Thailand-U.S. Educational Foundation) to pursue her graduate study in the U.S. She joined a graduate program in Chemical Engineering and worked under Prof. Benny D. Freeman at the University of Texas at Austin in 2009. She earned a Master of Science degree in Chemical Engineering in 2011 and a Ph.D. degree in Chemical Engineering in 2015. During the last stage of her Ph.D., she has started working at Evonik Corporation, based in Mobile, AL and will continue to work there upon a completion of her Ph.D. as a process engineer in Process Innovation team, focusing on applications of membrane technologies.

Permanent email: sirirat@utexas.edu

This dissertation was typed by the author.